

ADSORPTION OF CLOFIBRIC ACID AND NAPROXEN ON GRAPHENE OXIDE MODIFIED

SBA-15

Miss Wanchalach Sathienthamanee



จุฬาลงกรณ์มหาวิทยาลัย

CHULALONGKORN UNIVERSITY

บทคัดย่อและแฟ้มข้อมูลฉบับเต็มของวิทยานิพนธ์ตั้งแต่ปีการศึกษา 2554 ที่ให้บริการในคลังปัญญาจุฬาฯ (CUIR)
เป็นแฟ้มข้อมูลของนิสิตเจ้าของวิทยานิพนธ์ ที่ส่งผ่านทางบัณฑิตวิทยาลัย

The abstract and full text of theses from the academic year 2011 in Chulalongkorn University Intellectual Repository (CUIR)
are the thesis authors' files submitted through the University Graduate School.

A Thesis Submitted in Partial Fulfillment of the Requirements
for the Degree of Master of Science Program in Hazardous Substance and

Environmental Management

(Interdisciplinary Program)

Graduate School

Chulalongkorn University

Academic Year 2015

Copyright of Chulalongkorn University

การดูดซับกรดคลอไฟบริกและนาฟร็อกเซนบนเอสบีเอ-15ที่ตัดแปรด้วยกราฟีนออกไซด์



วิทยานิพนธ์นี้เป็นส่วนหนึ่งของการศึกษาตามหลักสูตรปริญญาวิทยาศาสตรมหาบัณฑิต

สาขาวิชาการจัดการสารอันตรายและสิ่งแวดล้อม (สหสาขาวิชา)

บัณฑิตวิทยาลัย จุฬาลงกรณ์มหาวิทยาลัย

ปีการศึกษา 2558

ลิขสิทธิ์ของจุฬาลงกรณ์มหาวิทยาลัย

Thesis Title	ADSORPTION OF CLOFIBRIC ACID AND NAPROXEN ON GRAPHENE OXIDE MODIFIED SBA-15
By	Miss Wanchalach Sathienthammanee
Field of Study	Hazardous Substance and Environmental Management
Thesis Advisor	Associate Professor Patiparn Punyapalakul, Ph.D.

Accepted by the Graduate School, Chulalongkorn University in Partial
Fulfillment of the Requirements for the Master's Degree

.....Dean of the Graduate School
(Associate Professor Sunait Chutintaranond, Ph.D.)

THESIS COMMITTEE

.....Chairman
(Assistant Professor Chantra Tongcumpou, Ph.D.)

.....Thesis Advisor
(Associate Professor Patiparn Punyapalakul, Ph.D.)

.....Examiner
(Doungkamon Pihusut, Ph.D.)

.....Examiner
(Pummarin Khamdahsag, Ph.D.)

.....External Examiner
(Panida Prarat, Ph.D.)

วรรณชลิช เสถียรธรรมณี : การดูดซับกรดคลอโรไฟบริกและนาพร็อกเซนบนเอสบีเอ-15 ที่ดัดแปรด้วยกราฟีนออกไซด์ (ADSORPTION OF CLOFIBRIC ACID AND NAPROXEN ON GRAPHENE OXIDE MODIFIED SBA-15) อ.ที่ปรึกษาวิทยานิพนธ์หลัก: รศ. ดร.ปฎิภาณ ปัญญาพลกุล, 171 หน้า.

งานวิจัยนี้มีวัตถุประสงค์เพื่อสังเคราะห์และศึกษาลักษณะสมบัติของเอสบีเอ-15 ที่ดัดแปรด้วยกราฟีนออกไซด์ (GO) รวมถึงศึกษากระบวนการดูดซับของกรดคลอโรไฟบริก (CFA) และนาพร็อกเซน (NAP) บนเอสบีเอ-15 ที่ดัดแปรด้วยกราฟีนออกไซด์โดยการทดลองแบบทีละเท และเพื่อศึกษากระบวนการดูดซับแบบคัดเลือกของ CFA และ NAP บนเอสบีเอ-15 ที่ดัดแปรด้วยกราฟีนออกไซด์ การทดลองนี้ได้ทำการสังเคราะห์เอสบีเอ-15 GO และ เอสบีเอ-15 ที่ดัดแปรด้วย GO จากนั้นทำการปรับปรุงผิวพื้นด้วยหมู่ฟังก์ชันเอมีนศึกษาผลกระทบของหมู่ฟังก์ชันเอมีนบนเอสบีเอ-15 กราฟีนออกไซด์ และเอสบีเอ-15 ที่ดัดแปรด้วยกราฟีนออกไซด์ต่อกลไกการดูดซับและประสิทธิภาพการดูดซับ

การดัดแปรเอสบีเอ-15 ด้วย GO สามารถเพิ่มประสิทธิภาพการดูดซับ CFA และ NAP การต่อติดหมู่ฟังก์ชันเอมีนบนเอสบีเอ-15 และ GO ทำให้อัตราเร็วในการดูดซับของ CFA และ NAP ลดลง แต่อย่างไรก็ตามการหมู่ฟังก์ชันเอมีนสามารถเพิ่มประสิทธิภาพของการดูดซับ CFA แต่ไม่พบการเปลี่ยนแปลงอย่างมีนัยสำคัญในกรณี NAP

ประสิทธิภาพของการดูดซับ CFA และ NAP ของเอสบีเอ-15 ที่ดัดแปรด้วย GO จะดีขึ้นเมื่ออยู่ในสภาวะกรดและจะลดลงเมื่อ pH เพิ่มขึ้น และพบว่าแรงดึงดูดทางประจุไฟฟ้าเป็นกลไกที่สำคัญในการดูดซับ นอกจากนี้การศึกษากการดูดซับที่ความเข้มข้นต่ำ (ไมโครกรัมต่อลิตร) พบว่าการดูดซับสอดคล้องกับไอโซเทอมแบบเส้นตรงสำหรับ CFA และสอดคล้องกับไอโซเทอมแบบแลงเมียร์สำหรับ NAP

จากข้อมูลการดูดซับแบบคัดเลือกสามารถระบุได้ว่าหมู่ฟังก์ชันเอมีนมีความสามารถในการดูดซับ CFA และพบว่าการดูดซับของ NAP บนเอสบีเอ-15 ที่ดัดแปรด้วย GO สามารถถูกรบกวนได้ง่ายจาก CFA

สาขาวิชา การจัดการสารอันตรายและ
สิ่งแวดล้อม

ลายมือชื่อนิสิต

ลายมือชื่อ อ.ที่ปรึกษาหลัก

ปีการศึกษา 2558

5787538820 : MAJOR HAZARDOUS SUBSTANCE AND ENVIRONMENTAL MANAGEMENT

KEYWORDS:

WANCHALACH SATHIENTHAMMANEE: ADSORPTION OF CLOFIBRIC ACID AND NAPROXEN ON GRAPHENE OXIDE MODIFIED SBA-15. ADVISOR: ASSOC. PROF. PATIPARN PUNYAPALAKUL, Ph.D., 171 pp.

The purposes in this study are to synthesize and characterize graphene oxide (GO) modified on mesoporous silica (SBA-15), to study the adsorptive information of clofibrilic (CFA) and naproxen (NAP) on GO modified SBA-15 by batch experiment, and to investigate selective adsorption of CFA and NAP on GO modified SBA-15. In this study, SBA-15, GO and GO modified SBA-15 were synthesized and functionalized with amine functional group to investigate the effect of amine functional group on adsorption capacity and mechanism.

GO modification on SBA-15 can increase the CFA and NAP adsorption capacity. Amine functional group on both SBA-15 and GO can decrease adsorption rate of CFA and NAP. But, the amine functional group can increase the adsorption capacities of CFA but did not change significantly for NAP.

CFA and NAP adsorption capacities on GO modified SBA-15 were more favor with acidic condition as pH 5 but decreased in higher pH. Electrostatic attraction can be concluded as an important adsorption mechanism. In addition, adsorption isotherms of CFA and NAP in low concentration (ppb level) were studied and compatible with Linear and Langmuir isotherm, respectively.

From adsorption selectivity, it can be confirmed that amine functional group showed the favor for CFA adsorption. And the adsorption of NAP was easily disturbed by CFA on GO modified SBA-15.

Field of Study: Hazardous Substance and Student's Signature
 Environmental Advisor's Signature
 Management

Academic Year: 2015

ACKNOWLEDGEMENTS

Firstly, I am pleased to express my thankfulness to my advisor, Assoc. Prof. Patiparn Punyapalakul, Ph.D. for his patience, support, and useful advices at all times of my thesis. I am highly obliged to Assist. Prof. Warinthorn Chavasiri, Ph.D. for his grateful guidance about the synthesis of A-GO-A-SBA-15 and invaluable discussions. I am grateful to Panida Prarat, Ph.D. for the synthesis of GO. I am also thankful to Doungkamon Pihusut, Ph.D. for the counsel of XPS drawing and results. I appreciate to take this opportunity to thank Assist. Prof. Chantra Tongcumpou as a chairman of committee, Doungkamon Pihusut, Ph.D., Pummarin Khamdahsag, Ph.D., and Panida Prarat, Ph.D. as members of thesis committee for their precious comments.

I would like to acknowledge the financial support from The Thailand Research Fund, Thailand under grant no. RSA5880018. This work was carried out as part of the research cluster “Hazardous Substance Management in Agricultural Industry” granted by the Center of Excellence for Hazardous Substance Management (HSM) and Research Unit Control of Emerging Micropollutants in Environment from Chulalongkorn University. This research has been supported by the Ratchadaphiseksomphot Endowment Fund (2015) Chulalongkorn University (CU-58-060-CC). The authors would like to thank the support from research grant of Kurita Water and Environment Foundation (2014). This research was also supported by 2013 Overseas Research Grants from the Asahi Glass Foundation. The Center of Excellence for Hazardous Substance Management (HSM), Graduate School, Chulalongkorn University for supplied the tuition, research grants, laboratory equipment, and research facilities.

Lastly, I am pleased to express my sincere gratitude to my beloved family and friends for their support and understanding.

CONTENTS

	Page
THAI ABSTRACT	iv
ENGLISH ABSTRACT	v
ACKNOWLEDGEMENTS	vi
CONTENTS	vii
LIST OF FIGURE.....	xiv
LIST OF TABLE	xviii
ABBREVIATION	xx
NOMENCLATURE	xxii
CHAPTER I INTRODUCTION.....	1
1.1 STATE OF PROBLEM.....	1
1.2 HYPOTHESIS.....	4
1.3 OBJECTIVES.....	4
1.4 SCOPES OF THE STUDY.....	4
1.4.1 Phase I: Synthesis of adsorbents	5
1.4.2 Phase II: Characterization.....	6
1.4.3 Phase III: Adsorption study.....	6
1.5 EXPECTED OUTCOME.....	6
CHAPTER II THERETICAL BACKGROUND AND LITERATURE REVIEWS.....	7
2.1 PHARMACEUTICALS AND PERSONAL CARE PRODUCTS (PPCPs).....	7
2.2 CLOFIBRIC (CFA).....	8
2.3 NAPROXEN (NAP).....	10
2.4 REMOVAL PROCESS.....	13

	Page
2.4.1 Biodegradation	13
2.4.2 Photodegradation	13
2.4.3 Ozonation.....	14
2.4.4 Advance oxidation processes (AOPs).....	15
2.4.5 Adsorption.....	16
2.4.5.1 Adsorption capacity.....	17
2.4.5.2 Adsorption kinetic.....	18
2.4.5.2.1 <i>Pseudo-first-order model</i>	18
2.4.5.2.2 <i>Pseudo-second order model</i>	18
2.4.5.3 Adsorption isotherm.....	19
2.4.5.3.1 <i>Linear adsorption model</i>	19
2.4.5.3.2 <i>Langmuir adsorption model</i>	19
2.4.5.3.3 <i>Freundlich adsorption model</i>	20
2.4.5.5 Materials of adsorbents.....	20
2.4.5.5.1 <i>Mesoporous silica adsorbent</i>	20
2.4.5.5.2 <i>Surface modification of mesoporous silica</i>	21
2.4.5.5.2.1 <i>Post- synthesis method</i>	21
2.4.5.5.2.2 <i>Direct co-condensation method</i>	22
2.4.5.5.3 <i>Graphene oxide (GO)</i>	22
2.4.5.5.4 <i>Surface modification of GO</i>	23
2.4.5.5.5 <i>Graphene oxide modified SBA-15</i>	24
2.4.5.5.6 <i>Surface functionalized graphene oxide modified SBA-15</i>	25

	Page
2.5 LITERATURE REVIEWS	25
CHAPTER III MATERIALS AND METHODOLOGY	29
3.1 MATERIALS	29
3.1.1 Chemical reagents.....	29
3.2 METHODOLOGY	31
3.2.1 Experimental framework.....	31
3.2.2 Preparation of CFA, and NAP stock solutions.....	32
3.2.3 Preparation of adsorbent.....	32
3.2.3.1 Synthesis Santa Brabara Acid-15 (SBA-15) (Hoffmann, Cornelius et al. 2006).....	32
3.2.3.2 Synthesis amino functionalized of SBA-15 (A-SBA-15)	33
3.2.3.3 Synthesis graphene oxide (GO).....	33
3.2.3.4 Synthesis amine functionalized graphene oxide (A-GO).....	34
3.2.3.5 Synthesis GO modified A-SBA-15 (GO-A-SBA-15).....	35
3.2.3.6 Synthesis amine functionalized of GO-A-SBA-15 (A-GO-A-SBA- 15)	36
3.2.4 Characterization of adsorbent.....	37
3.2.4.1 Structure	38
3.2.4.2 Surface area and pore size	38
3.2.4.3 Surface functional group.....	38
3.2.4.4 Elemental composite on surface	38
3.2.4.5 Point of zero charge (PZC).....	39
3.2.4.6 Amount of nitrogen.....	39
3.2.4.7 Material morphology.....	39

	Page
3.2.5 Adsorption experiments.....	39
3.2.5.1 Adsorption kinetic study	40
3.2.5.2 Adsorption isotherm study in high concentration at pH 7 (Single solute).....	40
3.2.5.3 Adsorption isotherm study in high concentration at vary pH (Single solute).....	41
3.2.5.4 Adsorption isotherm in low concentration level at pH 7 (Single solute).....	41
3.2.5.5 Adsorption selectivity in high concentration at pH 7 (Multi- solute).....	42
CHAPTER IV RESULTS AND DISCUSSION	43
4.1 CHARACTERIZATION OF SYNTHESIZED ADSORBENTS	43
4.1.1 X-ray diffraction (XRD)	43
4.1.2 N ₂ adsorption-desorption isotherms.....	44
4.1.3 Fourier Transform Infrared Spectrometer (FTIR).....	50
4.1.4 Point of zero charges (PZC).....	53
4.1.5 CHNS elemental analyzer	54
4.1.6 Scanning electron microscopy (SEM).....	55
4.1.7 Transmission electron microscopy (TEM)	57
4.1.8 X-ray photoelectron spectroscopy (XPS).....	59
4.2 ADSORPTION EXPERIMENT	66
4.2.1 Adsorption kinetic experiment	66
4.2.1.1 Adsorption kinetic of CFA at high concentration in pH 7	67
4.2.1.1.1 <i>Effect of surface functional group on silica materials ...</i>	67

	Page
4.2.1.1.2 Effect of surface functional group on graphene oxide materials	67
4.2.1.1.3 <i>Effect of GO on silica materials</i>	68
4.2.1.1.4 <i>Adsorption kinetic of PAC</i>	68
4.2.1.2 Adsorption kinetic of NAP on synthesized adsorbents at high concentration in pH 7.....	71
4.2.1.2.1 <i>Effect of surface functional group on silica materials</i> ...	72
4.2.1.2.2 <i>Effect of surface functional group on graphene oxide materials</i>	72
4.2.1.2.3 <i>Effect of GO on silica materials</i>	72
4.2.1.2.4 <i>Adsorption kinetic of PAC</i>	73
4.2.2 Intraparticle diffusion mechanism	75
4.2.2.1 Intraparticle diffusion of CFA.....	76
4.2.2.2 Intraparticle diffusion of NAP	80
4.2.3 Adsorption isotherms	83
4.2.3.1 Adsorption isotherms of CFA at high concentration in pH 7 (single solute)	84
4.2.3.1.1 <i>Effect of surface functional group on silica material</i>	84
4.2.3.1.2 <i>Effect of surface functional group on graphene oxide materials</i>	87
4.2.3.1.3 <i>Effect of GO modified silica materials</i>	91
4.2.3.1.4 <i>The adsorption capacity of PAC</i>	94
4.2.3.2 Comparison of adsorption isotherms for CFA on A-GO-A-SBA-15, 3N-SBA-15, 3N-HMS-SP, and NiAlOr-NaBt at high concentration	99

	Page
4.2.3.3 Adsorption isotherms of CFA on A-GO-A-SBA-15 at high concentration in pH 5-9 (single solute).....	99
4.2.3.4 Adsorption isotherms of CFA on A-GO-A-SBA-15 at low concentration in pH 7 (single solute)	101
4.2.3.5 Comparison of adsorption isotherms for CFA on A-GO-A-SBA-15, 3N-SBA-15, and 3N-HMS at low concentration.....	102
4.2.3.6 Adsorption isotherms of NAP at high concentration in pH 7 (single solute)	103
4.2.3.6.1 <i>Effect of surface functional group on silica material ...</i>	103
4.2.3.6.2 <i>Effect of surface functional group on graphene oxide materials</i>	104
4.2.3.6.3 <i>Effect of GO modified silica materials</i>	107
4.2.3.6.4 <i>The adsorption capacity of PAC</i>	110
4.2.3.7 Comparison of adsorption isotherms for NAP on GO-A-SBA-15, and 3N-HMS at high concentration	114
4.2.3.8 Adsorption isotherms of NAP on GO-A-SBA-15 at high concentration in pH 5-9 (single solute).....	114
4.2.3.9 Adsorption isotherms of NAP on GO-A-SBA-15 at low concentration in pH 7 (single solute)	116
4.2.4 Adsorption selectivity	118
4.2.4.1 Adsorption selectivity on GO-A-SBA-15 at high concentration in multi-solute	118
4.2.4.2 Adsorption selectivity on A-GO-A-SBA-15 at high concentration in multi-solute.....	122
CHAPTER V CONCLUSION AND RECOMMENDATIONS	125

	Page
5.1 CONCLUSION.....	125
5.2 RECOMMENDATIONS.....	127
REFERENCES	128
VITA.....	171



LIST OF FIGURE

Figure 1.1 Experimental framework.....	5
Figure 2.1 Origin and routes of PPCPs transfer	8
Figure 2.2 Degradation pathway and some intermediate compound of CFA.....	16
Figure 2.3 Degradation pathway and some intermediate compound of NAP	16
Figure 2.4 Three step of adsorption mechanism	17
Figure 2.5 Mesoporous silica	21
Figure 2.6 Post-grafting method and co-condensation method.....	22
Figure 2.7 Structure of graphene oxide (GO).....	23
Figure 2.8 Structure of surface modified GO.....	23
Figure 2.9 Structure of graphene oxide modified SBA-15	24
Figure 3.1 Experimental framework in this study.....	31
Figure 3.2 Synthesis of SBA-15.....	32
Figure 3.3 Synthesis of amine functionalized SBA-15 (A-SBA-15).....	33
Figure 3.4 Synthesis of graphene oxide (GO)	34
Figure 3.5 Synthesis of amine functionalized graphene oxide (A-GO)	35
Figure 3.6 Synthesis of graphene oxide modified A-SBA-15 (GO-A-SBA-15).....	36
Figure 3.7 Synthesis of amine functionalized GO-A-SBA-15 (A-GO-A-SBA-15).....	37
Figure 4.1 (a) XRD pattern of GO and GO-A-SBA-15 at high angle (5-40°), and (b) XRD pattern of A-SBA-15 and GO-A-SBA-15 at low angle (0.7-5°)	44
Figure 4.2 N ₂ adsorption-desorption isotherms of (a) A-SBA-15, (b) A-SBA-15, (c) GO-A-SBA-15, and (d) A-GO-A-SBA-15.....	46
Figure 4.3 Type of physisorption isotherms (Sing 1982)	47

Figure 4.4 Pore size distribution (BJH) of synthesized adsorbents (a) SBA-15, (b) A-SBA-15, (c) GO-A-SBA-15, and (d) A-GO-A-SBA-15.....	50
Figure 4.5 FTIR spectra of all synthesized adsorbents.....	52
Figure 4.6 Percentage of GO and A-GO in GO-A-SBA-15 and A-GO-A-SBA-15	55
Figure 4.7 Images x 5,000 of SEM (a) SBA-15, (b) A-SBA-15, (c) GO, (d) A-GO, (e) GO-A-SBA-15, and (f) A-GO-A-SBA-15.....	56
Figure 4.8 TEM images of a) SBA-15, b) A-SBA-15, c) GO, d) A-GO, e) GO-A-SBA-15, and f) A-GO-A-SBA-15.....	58
Figure 4.9 XPS spectra of a) A-SBA-15, b) GO, c) A-GO, d) GO-A-SBA-15, and e) A-GO-A-SBA-15.....	64
Figure 4.10 The kinetic curves of CFA on a) SBA-15, b) A-SBA-15, c) GO, d) A-GO, e) GO-A-SBA-15, f) A-GO-A-SBA-15, and g) PAC.....	70
Figure 4.11 The kinetic curves of NAP on a) SBA-15, b) A-SBA-15, c) GO, d) A-GO, e) GO-A-SBA-15, f) A-GO-A-SBA-15, and g) PAC.....	74
Figure 4.12 Plots of intraparticle diffusion model (Weber and Morris) for the adsorption of CFA on a) SBA-15, b) A-SBA-15, c) GO, d) A-GO, e) GO-A-SBA-15, f) A-GO-A-SBA-15, and g) PAC.	79
Figure 4.13 Plots of intraparticle diffusion model (Weber and Moris) for the adsorption of NAP on a) GO, b) A-GO, c) GO-A-SBA-15, d) A-GO-A-SBA-15, and e) PAC.....	82
Figure 4.14 Comparison of pristine functional group and amine functional group on mesoporous silica materials in adsorption capacity of CFA.....	85
Figure 4.15 Effect of the amount of nitrogen on mesoporous silica materials in adsorption capacity of CFA	85
Figure 4.16 Effect of surface area on mesoporous silica materials in adsorption capacity of CFA	86

Figure 4.17 Comparison of pristine functional group and amine functional group on GO materials in adsorption capacity of CFA.	89
Figure 4.18 XPS spectra of a) GO dispersed in phosphate buffer b) the adsorption for CFA on GO dispersed in phosphate buffer c) GO dispersed in DI d) the adsorption for CFA on GO dispersed in DI.....	91
Figure 4.19 Comparison of pristine functional group and amine functional group on GO modified A-SBA-15 materials in adsorption capacity of CFA.....	93
Figure 4.20 Adsorption isotherm of CFA on PAC a) per g of adsorbent and b) per m ² of surface area	96
Figure 4.21 The adsorption isotherm of CFA on a) SBA-15, b) A-SBA-15, c) GO, d) A-GO, e) GO-A-SBA-15, f) A-GO-A-SBA-15, and g) PAC	97
Figure 4.22 The comparison of A-GO-A-SBA-15, 3N-HMS-SP, 3N-SBA-15, and NiAlO _r -NaBt adsorption for CFA at high concentration.....	99
Figure 4.23 Effect of pH on A-GO-A-SBA-15 adsorbent materials in adsorption capacity of CFA	101
Figure 4.24 Adsorption isotherm of CFA on A-GO-A-SBA-15 at low concentration.....	102
Figure 4.25 The comparison of A-GO-A-SBA-15, 3N-HMS-SP, and 3N-SBA-15 adsorption for CFA at low concentration	103
Figure 4.26 Comparison of pristine functional group and amine functional group on mesoporous silica materials in adsorption capacity of NAP.	104
Figure 4.27 Comparison of pristine functional group and amine functional group on GO materials in adsorption capacity of NAP	105
Figure 4.28 XPS spectra of a) GO dispersed in phosphate buffer b) the adsorption for NAP on GO dispersed in phosphate buffer c) GO dispersed in DI d) the adsorption for NAP on GO dispersed in DI	107
Figure 4.29 Comparison of pristine functional group and amine functional group on GO modified A-SBA-15 materials in adsorption capacity of NAP.	108

Figure 4.30 Adsorption isotherm of NAP on PAC a) per g of adsorbent and b) per m^2 of surface area	111
Figure 4.31 The adsorption isotherm of NAP on a) GO, b) A-GO, c) GO-A-SBA-15, d) A-GO-A-SBA-15, and e) PAC	112
Figure 4.32 The comparison of GO-A-SBA-15, and P-HMS-SP adsorption for NAP at high concentration	114
Figure 4.33 Effect of pH on GO-A-SBA-15 adsorbent materials in adsorption capacity of NAP	116
Figure 4.34 Adsorption isotherm of CFA on A-GO-A-SBA-15 at low concentration.....	117
Figure 4.35 Adsorption isotherm of vary NAP and CFA on GO-A-SBA-15 in multi-solute	119
Figure 4.36 Adsorption isotherm of vary CFA and NAP on GO-A-SBA-15 in multi-solute	121
Figure 4.37 Adsorption isotherm of vary CFA and NAP on A-GO-A-SBA-15 in multi-solute	122
Figure 4.38 Adsorption isotherm of vary NAP and CFA on A-GO-A-SBA-15 in multi-solute	124

LIST OF TABLE

Table 2.1 Overview of physical and chemical characteristics of CFA.....	10
Table 2.2 The detection of CFA.....	10
Table 2.3 Overview of physical and chemical characteristics of NAP.....	12
Table 2.4 The detection of NAP	12
Table 4.1 Pore diameter, pore volume, and BET surface area of SBA-15, A-SBA-15, GO-A-SBA-15, and A-GO-A-SBA-15.....	48
Table 4.2 PZC of all synthesized adsorbents	53
Table 4.3 Elemental content of all synthesized adsorbents.....	54
Table 4. 4 Physiochemical characteristic of all synthesized adsorbents	65
Table 4.5 The adsorption kinetic parameters of CFA on SBA-15, A-SBA-15, GO, A-GO, GO-A-SBA-15, A-GO-A-SBA-15 and PAC after fitting with the pseudo-second order model and the Ritchie-second order model.....	71
Table 4.6 The adsorption kinetic parameters of NAP on SBA-15, A-SBA-15, GO, A-GO, GO-A-SBA-15, A-GO-A-SBA-15 and PAC after fitting with the pseudo-second order model and the Ritchie-second order model.....	75
Table 4.7 Intraparticle diffusion parameters of CFA adsorption on SBA-15, A-SBA-15, GO, A-GO, GO-A-SBA-15, A-GO-A-SBA-15, and PAC.....	80
Table 4.8 Intraparticle diffusion parameters of NAP adsorption on SBA-15, A-SBA-15, GO, A-GO, GO-A-SBA-15, A-GO-A-SBA-15, and PAC.....	83
Table 4.9 Percentage of A-SBA-15, GO, and A-GO in synthesized adsorbents for the adsorption capacity of CFA.....	94
Table 4.10 The adsorption isotherm parameters of CFA on SBA-15, A-SBA-15, GO, A-GO, GO-A-SBA-15, A-GO-A-SBA-15 and PAC at pH 7 after fitting with Linear, Langmuir, and Freundlich isotherm model.....	98

Table 4.11 The adsorption isotherm parameters of CFA on A-GO-A-SBA-15 at low concentration after fitting with Linear, Langmuir, and Freundlich isotherm model...	102
Table 4.12 Percentage of A-SBA-15, GO, and A-GO in synthesized adsorbents for the adsorption capacity of NAP	109
Table 4.13 The adsorption isotherm parameters of NAP on GO, A-GO, GO-A-SBA-15, A-GO-A-SBA-15 and PAC at pH 7 after fitting with Linear, Langmuir, and Freundlich isotherm model.	113
Table 4.14 The adsorption isotherm parameters of NAP on GO-A-SBA-15 at low concentration after fitting with Linear, Langmuir, and Freundlich isotherm model...	117
Table 4.15 The charge present, and pKa of CFA	117
Table 4.16 The charge present, and PZC of SBA-15, A-SBA-15, GO, A-GO, GO-A-SBA-15, and A-GO-A-SBA-15 at pH 7	118
Table 4.17 The adsorption isotherm data of vary NAP and CFA on GO-A-SBA-15 in multi-solute.	120
Table 4.18 The adsorption isotherm data of vary CFA and NAP on GO-A-SBA-15 in multi-solute.	121
Table 4.19 The adsorption isotherm data of vary CFA and NAP on A-GO-A-SBA-15 in multi-solute.....	123
Table 4.20 The adsorption isotherm data of vary NAP and CFA on A-GO-A-SBA-15 in multi-solute.....	124

ABBREVIATION

AOPs	=	Advance oxidation processes
APTES	=	3-aminopropyltriethoxysilane
A-GO	=	Amine functionalized graphene oxide
A-GO-A-SBA-15	=	Amine functionalized graphene oxide modified amine functionalized Santa Brabara Acid-15
A-SBA-15	=	Amine functionalized Santa Brabara Acid-15
BET	=	Brunner-Eller-Teller
BJH	=	Barret-Joyner-Halenda
C	=	Carbon
CFA	=	Clofibrlic acid
DAD	=	Diode array detector
DCC	=	N,N'-dicyclohexylcarbodiimide
DETA	=	Diethylenetriamine
DI	=	Deionized water
DMF	=	Dimethylformamide
FT-IR	=	Fourier transform infrared spectrometer
GO	=	Graphene oxide
GO-A-SBA-15	=	Graphene oxide modified amine functionalized Santa Brabara Acid-15
H	=	Hydrogen
HCl	=	Hydrochloric acid
HPLC	=	High Performance Liquid Chromatography
IS	=	Ionic strength
N	=	Nitrogen
NaOH	=	Sodium hydroxide
NAP	=	Naproxen
PAC	=	Powder activated carbon
PZC	=	Point of zero charge

S	=	Sulfur
SBA-15	=	Santa Brabara Acid-15
SEM	=	Scanning electron microscopy
TEM	=	Transmission electron microscopy
TEOS	=	Tetraethylorthosilicate or tetraethoxysilane
XPS	=	X-ray photoelectron spectroscopy
XRD	=	X-ray diffraction



NOMENCLATURE

C	=	Constant
C_0	=	Initial concentration (mg/L or $\mu\text{g/L}$)
C_e	=	Equilibrium concentration (mg/L or $\mu\text{g/L}$)
h	=	Initial adsorption rate (mg/g.h)
k_1	=	Pseudo-first-order rate constant (1/min)
k_2	=	Pseudo-second-order rate constant (g/mg.min)
k_r	=	Ritchie-second-order rate constant (1/min)
k_s	=	External diffusion rate constant (mg/g.min ^{1/2})
k_p	=	Intraparticle diffusion rate constant (mg/g.min ^{1/2})
M	=	Mass (g)
n	=	Adsorption intensity in Freundlich isotherm model
q_e	=	Adsorption capacity at equilibrium (mg/g or $\mu\text{g/g}$)
q_m	=	Maximum of adsorption capacity (mg/g)
q_t	=	Adsorption capacity at time (mg/g)
R^2	=	Correlation coefficient
S_{BET}	=	Specific surface area (m ² /g)
t	=	Time (min)
$t^{1/2}$	=	Time ^{1/2} (min ^{1/2})
T	=	Temperature ($^{\circ}\text{C}$)
V	=	Volume (L or mL)
V_p	=	Pore volume (mm ³ /g)

CHAPTER I

INTRODUCTION

1.1 STATE OF PROBLEM

At present, pharmaceuticals and personal care products (PPCPs) are widely used to cure the diseases and to improve human health; however, some PPCPs are toxic and resistant dissemination to aquatic environments. The results in the release of themselves through domestic waste water treatment plant have been concerned. During the past decade, their occurrences have been reported in many sources, e.g., soil, sediment and surface water, ground water, and drinking water. Potentially, fate of these residual PPCPs related to their persistence and bioaccumulation is not easy to determine and investigate. Besides, they cannot be completely degraded or eliminated by the nature owing to large and complicated structure. Consequently, they are emerging substances and may become the potential problems to the environment.

Clofibric acid (CFA) and Naproxen (NAP) are two of the most routine reported PPCPs found in the aqueous environments such as waste water treatment plant (WWTP), sewage treatment plant (STP), surface water, ground water, and drinking water. CFA is an intermediate compound of blood lipid regulator. It is a common form of a human metabolite clofibrate (its ethyl ester form) after excretion which has been frequently found in the aqueous environments, used as a blood lipid regulator. It can affect a reproductive toxicity on daphnia (Ferrari, Paxéus et al. 2003), and triglyceride accumulation in fish growth. For another potential residual, naproxen (NAP) is a non-steroidal anti-inflammatory drug (NSAIDs). It is normally used to treat pain or inflammation caused by arthritis, ankylosing spondylitis, tendinitis and gout. Due to lots of tons consumption in developed countries, it can be detected at high concentration

in pharmaceutical wastewater stream. In addition, it can affect the enzymes of fish and reproductive in rat. In addition, it is associated with cardiovascular risks (Trelle, Reichenbach et al. 2011). Besides, current STP was reported 51% and 40-66% mother compound removal for CFA and NAP, respectively; therefore, large amount of them can release to the environment.

Many researches have been studied the removal of these compounds from the environment; several methods have been used to treat the pharmaceutical compounds such as biodegradation, photodegradation, ozonation, advance oxidation processes (AOPs), and adsorption. In addition, biodegradation process was reported that it can remove PPCPs up to 95% in NAP (Marco-Urrea, Perez-Trujillo et al. 2010) and up to 51% in CFA (Salgado, Oehmen et al. 2012). The reported results of photodegradation showed degradation of CFA and NAP 99.3% and 90%, respectively (Kim, Yamashita et al. 2009, Li, Lu et al. 2009). Likewise, ozonation was reported the mineralized of CFA and NAP at 85% and 62%, respectively (Rosal, Rodriguez et al. 2008, Rosal, Gonzalo et al. 2009). AOPs was investigated the degradation of CFA and NAP. The results showed more than 99% degradation for CFA and completely degradation for NAP (Li, Lu et al. 2010, Kanakaraju, Motti et al. 2015). Nevertheless, some intermediate compounds are still unclear and might be more toxic than the original compounds. Thus, the adsorption method should be suitable for pharmaceutical compounds removal.

Recently, carbon-based materials have been studied to remove organic pollutant and metal with high adsorption capacity. Graphene oxide (GO) is one of the most interesting carbon-based materials because of chemical stability, large specific area, abundant pore size distribution, and feasibility of mass production. Previous studies have been shown that it can remove organic, inorganic, and metal compounds from the aqueous solution with vary high adsorption capacity which was reported the

maximum adsorption capacities for CFA was 994 mg/g (Zhang, Liu et al. 2014) and 11 mg/g for NAP (Asgharinezhad and Ebrahimzadeh 2016). In spite of physical characteristics, it's hardly recovered from water except using high-speed centrifugation that actually cannot be applied in the wastewater treatment plant (Zhang, Liu et al. 2014).

Currently, mesoporous silicate materials are developed and used as novel adsorbents to remove impurity in liquid phase. Santa Brabara Acid-15 (SBA-15) is the porous material which is commonly used in adsorption process because of high surface area, large pore volume, constant pore size, adjustable pore structure and good ability of separation from water. Additionally, it's already shown the potential for the removal of organic and inorganic pollutants from aqueous environment (Bui and Choi 2009).

The combination of GO and amine functionalized SBA-15 (A-SBA-15) as adsorbent material was synthesized by covalently binding to improve ability in separating from water and to increase adsorption selectivity (Li, Wang et al. 2015). In order to improve hydrophilicity, and adsorption efficiency, modification of functional group can be applied. According to recent studies, amine functional groups have high potential to interact with CFA by electronegativity and hydrophilic interaction, and aromatic ring can increase the adsorption efficiency of NAP by hydrophobicity and π - π interaction (Kaosaiphan 2013, Premrungruang 2013, Ruangtrakul 2010, Suriyanon, Premrungruang et al. 2015).

In this study, amine functionalized SBA-15 (A-SBA-15) will be used as based mesoporous silicates material of adsorbent combining with graphene oxide. Besides, modification of amine functional group on GO surface by post-grafting method was applied and expected to increase adsorption capacity of CFA and NAP by increasing of hydrophilicity, selectivity and positive charge property. Moreover, synthesized

adsorbent (GOs, SBA-15s and GOs modified SBA-15s) will be characterized the physical and chemical properties and discussed the adsorption mechanism. Adsorptive information was also studied, e.g. adsorption kinetics, adsorption isotherms, and the selective of adsorbents.

1.2 HYPOTHESIS

The adsorption efficiencies of CFA and NAP on GO modified SBA-15 will be higher than pristine functional group modified SBA-15 due to attractive electrostatic interaction (from amine functional group).

1.3 OBJECTIVES

1. To synthesize and characterize GO modified SBA-15.
2. To study the adsorptive information of CFA and NAP on GO modified SBA-15 by batch experiment.
3. To investigate selective adsorption of CFA and NAP on GO modified SBA-15

1.4 SCOPES OF THE STUDY

There are three phases in this study. The first phase is synthesis of adsorbents. The second phase is characterization and the last phase is adsorption study which can be divided as Figure 1.1

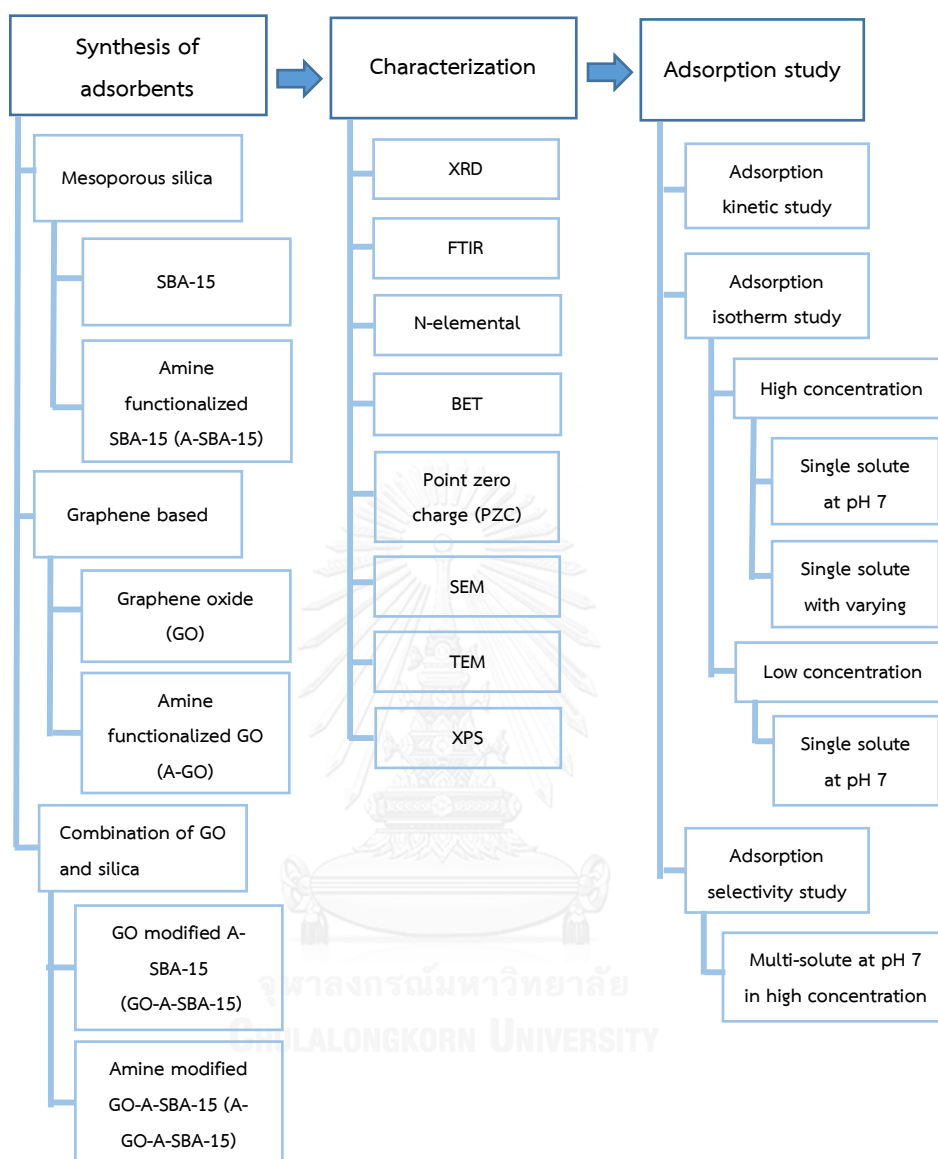


Figure 1.1 Experimental framework

1.4.1 Phase I: Synthesis of adsorbents

Six types of adsorbents were synthesized as followed:

1. SBA-15
2. Amine functionalized SBA-15 (A-SBA-15)
3. Graphene oxide (GO)

4. Amine functionalized GO (A-GO)
5. GO modified A-SBA-15 (GO-A-SBA-15)
6. Amine functionalized GO-A-SBA-15 (A-GO-A-SBA-15)

1.4.2 Phase II: Characterization

Synthesized adsorbents were characterized by XRD, TEM, SEM, FT-IR, N-elemental analysis, XPS, and nitrogen adsorption-desorption isotherm (BET).

1.4.3 Phase III: Adsorption study

Clofibric acid (CFA) and naproxen (NAP) were used as model of pharmaceutical compounds to study the adsorption capacity and mechanism. The adsorption was studied under batch experiment at high concentration level (ppm level). Additionally, adsorption kinetics were investigated by varying contact time from 0 to 10 hours. Adsorption isotherms were investigated in both single- and multi-solute solution and pH of the single solute was varied from 5 – 9 to study the effect of pH in the adsorption isotherms on the highest efficiency of adsorbent. Moreover, adsorption isotherms in low concentration level (ppb) were investigated just for the adsorbent that has the highest adsorption efficiency. CFA and NAP concentration were analyzed by HPLC-DAD.

1.5 EXPECTED OUTCOME

1. The adsorption efficiencies of CFA and NAP on GO modified SBA-15 will be higher than pristine functional group modified SBA-15

CHAPTER II

THERETICAL BACKGROUND AND LITERATURE REVIEWS

2.1 PHARMACEUTICALS AND PERSONAL CARE PRODUCTS (PPCPs)

PPCPs are widely used as human and veterinary application. Besides, they have become the essential element in our life. Due to rapid urbanization, improve standard of living, and increase world population, the demand of PPCPs is increasing every day starting from the early morning, coffee, soap, shampoo, lotion, fragrance, drug, etc.

However, PPCPs as pollutants basically contain chemical compounds or constituents so the results in the release of them can contaminate the aqueous environment. Figure 2.1 shows origin and routes of PPCPs transferring to the environment (Mompelat, Le Bot et al. 2009). Over the last decade, many studies reported the occurrence in aqueous environment up to $\mu\text{g/L}$ level in many countries, e.g. ofloxacin and a fluoroquinolone antibiotic were detected up to $35.5 \mu\text{g/L}$ in wastewater in U.S.A. (Brown, Kulis et al. 2006), paracetamol was detected up to 211 ng/L in ground water in French (Rabiet, Togola et al. 2006), and ibuprofen was detected in the local septic tank in Canada up to $2,150 \text{ ng/L}$ (Carrara, Ptacek et al. 2008). Besides, clofibric acid (CFA) was detected in the North Sea from $0.5\text{-}7.8 \text{ ng/L}$ (Buser, Müller et al. 1998) and naproxen was found in U.S. drinking water around 0.9 ng/L (Benotti, Trenholm et al. 2009). Due to their persistence, ecotoxicity, and complicated structure, these residues of PPCPs are emerging substance in the environment. Additionally, current wastewater treatment systems are not designed for PPCPs removal so that the release of them might become potential problems to the environment.

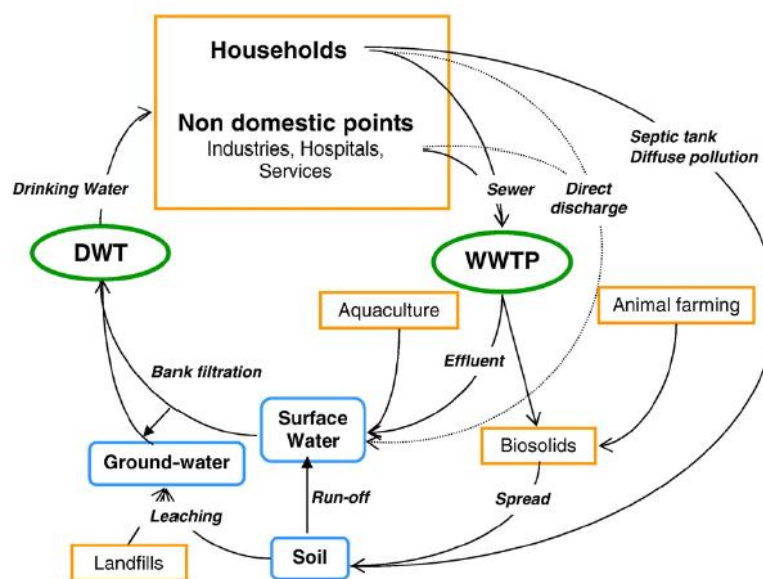


Figure 2.1 Origin and routes of PPCPs transfer

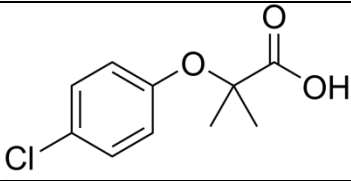
2.2 CLOFIBRIC (CFA)

Clofibric acid, i.e., an intermediate compound of an active metabolite in blood lipid regulator and the cholesterol lowering pharmaceutical drug, is one of the most routine reported PPCPs found in the wastewater treatment plant (WWTP), surface water, ground water, even drinking water in ppb-ppm range because of low degradation rate, high mobile, and prospective environmental persistence. The physical and chemical characteristics are shown in Table 2.1. Additionally, it was detected up to 4000 ng/L in sewage treatment plant (STP), 125 ng/L in ground water, 270 ng/L in drinking water in Germany (Heberer and Stan 1997, Heberer, Mechlinski et al. 2004), and up to 1600 ng/L in sewage treatment plant in Germany (Ternes 1998) as Table 2.2. It has an estimate persistent around 21 years (Winkler, Lawrence et al. 2001), some intermediate compounds are more toxic than the parent compound, and some pathways of degradation are still not clear (Liu, Zhou et al. 2013).

CFA has been considered by the effect in lipid metabolism of aquatic life. It normally has effects on cholesterol level of all sex steroid hormones. In previous study, it showed that chronic CFA exposure impacted triglyceride accumulation in muscle, fish growth, and development. All effects occurred with changes in gene level involved with lipid homeostasis, both in the exposed fish and epigenetic mechanism (Coimbra, Peixoto et al. 2015). The decreasing of total lipids, triglyceride, and cholesterol in crab was reported after exposure (Lautier, Chanal et al. 1986). Likewise, CFA has the effects on a direct indicator of the female reproductive on mRNA level in hepatocytes (Richert, Lambolely et al. 2003).

Particularly, CFA is an active derivative substance of clofibrate and fibrates. Clofibrate is the major metabolite of CFA and it may enhance the hormonal action of endogenous estradiol by stimulating the formation of estradiol fatty acid esters by liver microsomes. For another, fibrates mediate their peroxisome proliferator effects by operating specific transcription factors belonging to the nuclear hormone receptor known as peroxisome proliferator-activated receptors (Sovadinova, Liedtke et al. 2014).

Table 2.1 Overview of physical and chemical characteristics of CFA

Parameters	Clofibric acid (CFA)
CAS-number	882-09-7 ^a
Therapeutic class	Active metabolite (lipid regulator) ^a
Structure	
Molecular weight	214.6 ^a
Solubility (mg/L)	582.5 ^a
pK _a	2.84 ^b
Log K _{ow}	2.57 ^a

^a(Ferrari, Paxéus et al. 2003), and ^b(Sim, Lee et al. 2010),

Table 2.2 The detection of CFA

Country	Source	Concentration (ppt)
Germany	Sewage treatment plant	1,600 – 4,000 ^{a,b}
Germany	Drinking water	270 ^b
Detroit river (U.S.A. and Canada)	Surface water	103 ^c
Germany	Ground water	125 ^d

^a(Ternes 1998), ^b(Heberer and Stan 1997), ^c(Boyd, Reemtsma et al. 2003), and ^d(Heberer, Mechlinski et al. 2004)

2.3 NAPROXEN (NAP)

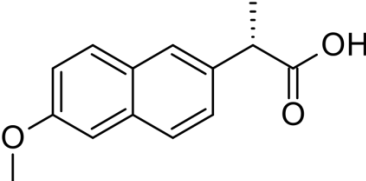
NAP which is non-steroidal anti-inflammatory drug (NSAIDs) is commonly used as analgesic, anti-inflammatory, and antipyretic agent in both human and veterinary

application. The physical and chemical characteristics are shown in Table 2.3. Large amount of it is consumed in many countries; whereas, it is not fully degraded after using and released to the environment. As a result of the detection at high concentration of NAP was found in many countries; for instant, Canadian wastewater treatment up to 33.9 $\mu\text{g/L}$ (Metcalf, Koenig et al. 2003), Canadian local septic tank up to 300 ng/L , and Spanish Turia River up to 7.2 $\mu\text{g/L}$ (Carrara, Ptacek et al. 2008, Carmona, Andreu et al. 2014).

According to the occurrences of naproxen, its ecotoxicity has been concerned. Many researchers reported that the acute effect of duck weed, rotifers, and fish were 24.2 mg/L , 62.48 mg/L , and up to 900 mg/L respectively. Average of chronic toxicity values on algae, rotifers, and crustaceans were 31.82, 0.56, and 0.33 mg/L (Isidori, Lavorgna et al. 2005). Moreover, acceptable daily intake value (ADI) of it is 46 $\mu\text{g/kg}\cdot\text{day}$ and toxicity endpoint is reproductive and developmental in rat (de Jesus Gaffney, Almeida et al. 2015).

Additionally, a study of photodegradation was shown that photoproducts of NAP found to be more toxic than parent compound and their behavior had lower hydrophilic character (Isidori, Lavorgna et al. 2005). NAP can affect the enzymes of zebra fish which involved in the maintenance of redox balance in intestine in a medium manner demonstrating a significantly adverse effect during chronic exposure (Stancova, Zikova et al. 2015).

Table 2.3 Overview of physical and chemical characteristics of NAP

Parameters	Naproxen (NAP)
CAS-number	22204-53-1 ^a
Therapeutic class	Non-steroidal anti-inflammatory drug (NSAIDs)
Structure	
Molecular weight	230.26 ^a
Solubility (mg/L)	15.9 ^b
pK _a	4.15 ^c
Log K _{ow}	3.18-3.24 ^c

^a(Lindqvist, Tuhkanen et al. 2005), ^b(Yu, Peldszus et al. 2008), and ^c(Tixier, Singer et al. 2003)

Table 2.4 The detection of NAP

Country	Source	Concentration (ppt)
Canada	Sewage treatment plant	2,700 – 33,900 ^{a, b}
Spain	Drinking water	11 ^c
Spain	Wastewater treatment	2,399 ^c
Spain	Surface water	7,200 ^d

^a(Verenitch, Lowe et al. 2006), ^b(Metcalfe, Koenig et al. 2003), ^c(Carmona, Andreu et al. 2014), and ^d(Carrara, Ptacek et al. 2008)

2.4 REMOVAL PROCESS

Some of the removal processes such as coagulation-flocculation, biodegradation, photo degradation, ozonation, advanced oxidation processes (AOPs), and adsorption have been used in previous studies.

2.4.1 Biodegradation

Biodegradation is the disintegration of materials by bacteria, fungi, or other biological means which is high attended process. It has been reported by many researchers as followed. The degradation of CFA was reported in aerobic sequencing batch reactors (SBRs) with mixed microbial cultures, and the maximum degradation reached 51% (Salgado, Oehmen et al. 2012). The degradation of NAP by the natural microbial community of the River Tiber had significantly efficiency up to 47% after treatment for 3 hours (Grenni, Patrolecco et al. 2013). A bacteria stain which is *Stenotrophomonas maltophilia* KB2 was reported that it can degrade NAP around 28% especially up to 78% and 40% under co-metabolic condition with glucose or phenol as a carbon sources (Wojcieszynska, Domaradzka et al. 2014). The white-rot fungus *Trametes vesicolor* was shown that it can almost completely degrade NAP in very high efficiency up to 95% with purified laccase plus mediator 1-hydroxybenzotriazol (Marco-Urrea, Perez-Trujillo et al. 2010).

2.4.2 Photodegradation

Photodegradation is the alteration of materials by light. Typically, the term refers to the combined action of sunlight and air usually oxidation and hydrolysis. However, it can destroy paintings and other artifacts. Ultraviolet (UV) degradation at monochromatic wavelength of 185 nm using Milli-Q water and sewage treatment plant

(STP) effluent was reported the removal of CFA. When using real STP effluent CFA degradation was reached 97.4% (without filtration) and 99.3% (with filtration) after 1-hour irradiation (Li, Lu et al. 2009). In addition, under ultraviolet (UV) degradation at monochromatic wavelength of 254 nm was observed in the degradation of NAP, with UV intensity lamps of 0.384 mW cm^2 . The removal efficiency was around 30% and 90% in 10 and 73 min respectively (Kim, Yamashita et al. 2009, Kim, Yamashita et al. 2009). The degradation of sodium NAP was reported using the MgAl calcined hydrotalcites. The results showed that they have a great photoactivity in the degradation up to 90% (Jácome-Acatitla, Tzompantzi et al. 2014).

2.4.3 Ozonation

Ozonation is a chemical water treatment technique based on the infusion of ozone into water. Ozone is a gas composed of three oxygen atoms (O_3), which is one of the most powerful oxidants. Ozonation with catalytic titanium dioxide was reported the complete removal of CFA at pH 5 less than 10 minutes and at pH 3 less than 60 minutes; nonetheless, without catalytic showed a conversion of 85% at pH 3 in 1 hour with an integral ozone exposure of 1500 mMh (Rosal, Gonzalo et al. 2009) and high activity and stability for CFA ozonation with catalytic ozonation using hydrotalcite derive was observed. The results of $\text{Mg}_3\text{Fe}_{0.5}\text{Al}_1$ and $\text{Cu}_{0.75}\text{Mg}_{0.5}\text{Al}_2\text{O}_4$ can reach mineralization degrees up to 58% and 55%, respectively, for 2 hours, and 71% and 79%, respectively, for 6 hours (Sable, Medina et al. 2014). Likewise, NAP was also reported in ozonation process with and without catalytic titanium dioxide. With catalytic showed 62% reduction at pH 5 and without catalytic reported 50% removal at neutral pH (Rosal, Rodríguez et al. 2008).

2.4.4 Advance oxidation processes (AOPs)

AOPs are the set of chemical treatment procedures designed to remove organic (and sometimes inorganic) materials in water and wastewater by oxidation through reactions with hydroxyl radicals ($\cdot\text{OH}$). They have been investigated for the removal efficiency. Oxidation was shown high efficiency above 80% for CFA by biological advanced oxidation of the white-rot fungus *Trametes vesicolor* (Marco-Urrea, Radjenovic et al. 2010). Over 99% degradation of CFA in a real wastewater treatment plant (WWTP) was reported using $\text{UV}_{254}/\text{H}_2\text{O}_2$ under 30°C but negative effect was appeared by dissolved organic matters (Li, Lu et al. 2010) and the removal of CFA using ozonation and $\text{H}_2\text{O}_2/\text{UV}$ showed complete degradation after 20 minutes with ozonation 34% (Andreozzi, Caprio et al. 2003). Beside, TiO_2 photocatalytic degradation was reported in laboratory-scale photoreactor. The result showed complete degradation of NAP in single solution after 15 minutes (Kanakaraju, Motti et al. 2015). UV solar photodegradation was investigated the degradation of NAP. The report showed that NAP was degraded 83% after 3 hours with 11% chemical oxygen demand (COD), and 98% with 25% COD (Jallouli, Elghniji et al. 2016). Additionally, Oxidation of NAP was investigated using $\alpha\text{-MnO}_2$ with no more than 20% (Zhang, Yang et al. 2012).

However, some intermediate or final compounds are more toxic than the parent compound; for instant, 4-chlorophenol, 2-hydroxyisobutyric acid, hydroquinone, and 4-chlorocatechol are the products from CFA as shown in Figure 2.2. On the other hand, 7,8-dihydroxynaproxen, hydroxyquinol 1,2-dioxygenase, and catechol 2,3-dioxygenase are the products from NAP (Figure 2.3), and some pathways of degradation are still not clear (Rosal, Gonzalo et al. 2009, Wojcieszynska, Domaradzka et al. 2014). Thus, the most appropriate process is adsorption owing to easy setup, low operation cost, and no undesired products.

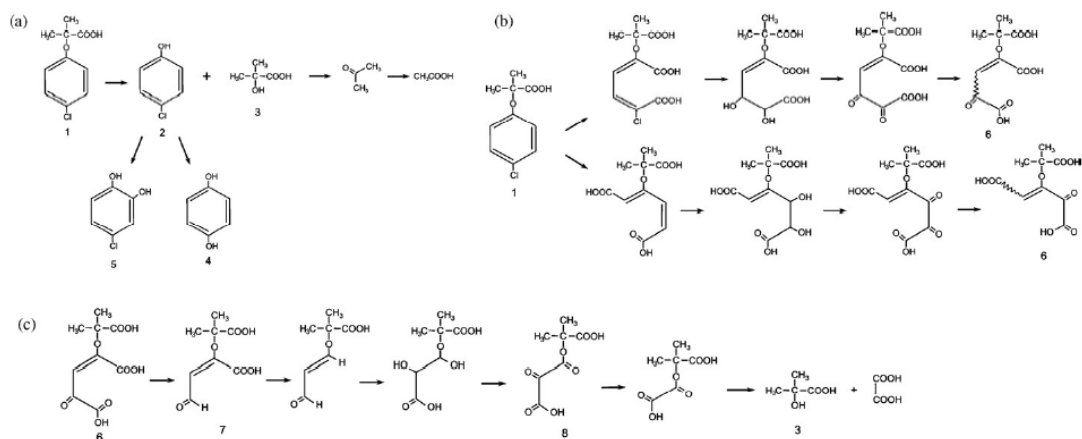


Figure 2.2 Degradation pathway and some intermediate compound of CFA

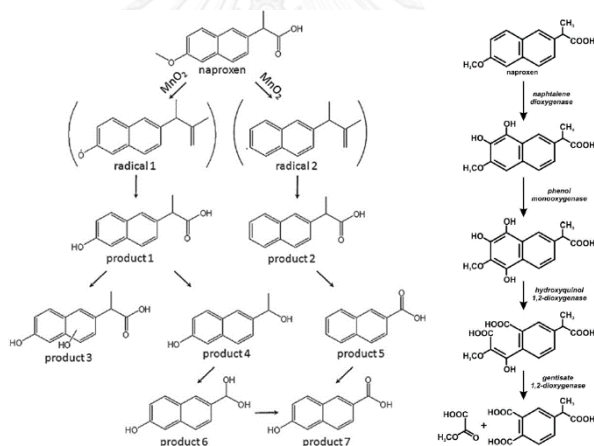


Figure 2.3 Degradation pathway and some intermediate compound of NAP

2.4.5 Adsorption

Adsorption is adhesion of atom, ions, or molecules to a surface. A film of the adsorbates, i.e., accumulation of atoms or molecules, is created on the surface of the adsorbent. Occurrence of removal will be generated when the adsorbates adsorb on the adsorbents. Adsorption can be classified into two types. Physical adsorption is the

attractions between adsorbates and adsorbents as Van der Waals' force, and chemical adsorption is the attractions are almost the same strength as chemical bonds.

There are three steps of adsorption mechanism as Figure 2.4. The first step is film diffusion process involving with adsorbates movement from the boundary layer to the external surface of adsorbents. The second step is intraparticle diffusion process which is the transportation of adsorbates into the interior of the adsorbent particles. The last step is adsorption process that is energetic interaction between adsorbates and the site of adsorbents. Particularly, adsorption process is the fastest step; therefore, the rate limiting step might be film diffusion or intraparticle diffusion.

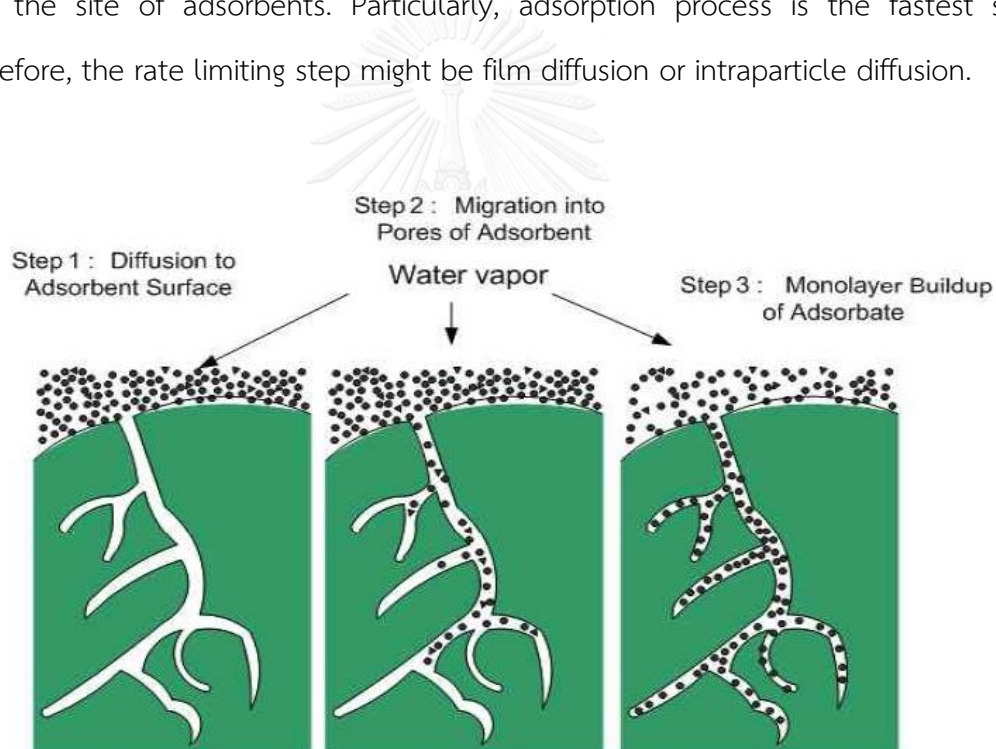


Figure 2.4 Three step of adsorption mechanism (Myoung-Jun and Gyu-Hoon 2012)

2.4.5.1 Adsorption capacity

The adsorption capacity of adsorbent can be calculated from the equation (2.1) as shown;

$$q_e = \frac{(C_o - C_e)}{M} \times V \quad (2.1)$$

Where C_0 and C_e are an initial and equilibrium concentration of the adsorbates (mg/L) respectively, M is the mass of adsorbent (g), V is the volume of solution in (L), and q stands for the adsorption capacity (mg/g).

2.4.5.2 Adsorption kinetic

Adsorption kinetic is an identification of the adsorption rate and it is used to predict and design adsorption model. In addition, it is described the uptake rate of adsorbates and the regulation of the residual time of all adsorption process.

2.4.5.2.1 Pseudo-first-order model

Pseudo-first-order model is normally used to one reactant in aqueous solution and the model can be determined from the equation 2.2 as shown;

$$\ln(q_e - q_t) = \ln q_e - k_1 t \quad (2.2)$$

Where q_e and q_t are the amount of adsorbate adsorbed at equilibrium and time (mg/g). t is time (min). k_1 is the pseudo-first-order rate constant (mg/g). The values of k_1 and q_e are determined from slope and intercept of graph plotting between $1/q$ and $1/t$.

2.4.5.2.2 Pseudo-second order model

Pseudo-second order model is mostly used as a model of chemisorption and it can be calculated from the equation 2.3 as followed;

$$\frac{t}{q_t} = \frac{1}{k_2 q_e^2} + \frac{t}{q_e} \quad (2.3)$$

Where k_2 is the pseudo-second order rate constant (g/mg*h).

2.4.5.2.3 Ritchie-second order model

Ritchie-second order model is usually used as a model for the adsorption of gaseous system which can be given as the equation 2.4;

$$\frac{1}{q_t} = \frac{1}{k_r q_e t} + \frac{1}{q_e'} \quad (2.4)$$

Where k_r is the Ritchie-second-order rate constant (1/min) derived from the plots of $1/q_t$ and $1/t$.

2.4.5.3 Adsorption isotherm

Adsorption isotherm is a description of the relationship between the amounts of adsorbate on the adsorbent as a function of concentration at constant temperature. The quantity adsorbed is mostly conducted from the comparison of adsorbent's mass in different materials. There are three mathematic models of isotherm;

2.4.5.3.1 Linear adsorption model

Linear adsorption model or Henry adsorption isotherm is the simplest adsorption isotherm. It is normally used to describe the initial part of isotherms and determined by the equation 2.5 as shown;

$$q_e = K_p C_e \quad (2.5)$$

Where K_p is the linear constant (L/g).

2.4.5.3.2 Langmuir adsorption model

Langmuir adsorption model explains adsorption by assumption of an adsorbate behaving as an ideal gas at isothermal condition and it can be calculated by the equation 2.6;

$$\frac{1}{q_e} = \frac{1}{q_m} + \frac{1}{K_L q_m C_e} \quad (2.6)$$

Where K_L is the Langmuir constant ($L \cdot mg^{-1}$), and q_m is the maximum of the adsorption capacity (mg/g).

2.4.5.3.3 Freundlich adsorption model

Freundlich adsorption model is an empirical equation representing the isothermal variation of adsorption. It relates with the concentration of a solute on the surface of adsorbent to the concentration of the solute in the contacted liquid as equation 2.7;

$$\ln q_e = \ln K_F + \frac{1}{n} \ln C_e$$

Where K_F is the Ferundlich constant, and n is adsorption intensity (dimensionless).

2.4.5.5 Materials of adsorbents

2.4.5.5.1 Mesoporous silica adsorbent

The development of porous materials with high specific surface area is presently an area of substantial research, especially with considering to significant applications in many fields such as adsorption, chromatography, catalysis, sensor technology, even gas storage. Mesoporous silica as Figure 2.5 was found in 1992 by Mobil scientists (Tanev, Chibwe et al. 1994). Use of amphiphilic triblock copolymer to direct the organization of polymerizing silica species has resulted in the preparation of well-ordered hexagonal mesoporous silica structure with uniform pore sizes up to approximately 300 angstroms, it is named Santa Brabara Acid-15 (SBA-15) (Zhao, 1998). Owing to high specific surface area, large pore volume, and stable pore structure, it has been used in separation, catalysis, and adsorption.

SBA-15 is one of the mesoporous silica which is widely used today. It provides a stable mesoporous support structure, with hexagonally packed cylindrical channels, thick pore walls, and good solubility in aqueous solutions. In additions, it has been reported to the adsorption efficiency of metal, organic and inorganic compounds. (Bui and Choi 2009, Bui, Pham et al. 2013).



Figure 2.5 Mesoporous silica (Hoffmann, Cornelius et al. 2006)

2.4.5.5.2 Surface modification of mesoporous silica

Mesoporous silica can be modified by organic functional groups at the silanol group of silica wall to apply in biotechnology, nanotechnology, and adsorption. There are two methods for functionalization which are post-synthesis method, and direct co-condensation method.

2.4.5.5.2.1 Post- synthesis method

Post-synthesis method or post-grafting method has two steps of synthesis. The first step is synthesis of mesoporous materials. The second step is modification by grafting the functional group on the surface under reflux condition. Silanol groups of mesoporous material act as an active site, and form a covalent coupled layer on the surface. This method provides good protection of structure after modification; however, the limitation of functional groups is due to the density of silanol groups on the surface (Stein, Melde et al. 2000) as Figure 2.6.

2.4.5.5.2 Direct co-condensation method

Direct co-condensation method has one step of synthesis. The functional groups are added during the synthesis of mesoporous material giving better control. This method gives higher surface coverage of functional group and better stability of organic group. Nevertheless, it loses the original structure and provides defective control of functional group on the surface (Hoffmann, Cornelius et al. 2006) as Figure 2.6.

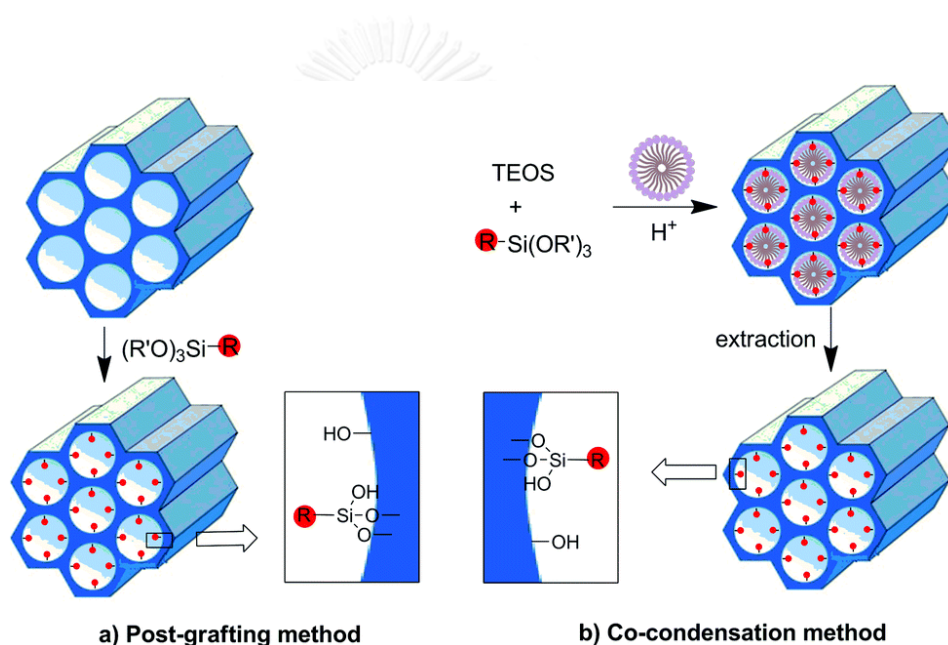


Figure 2.6 Post-grafting method and co-condensation method (Cheng, Zhao et al. 2015)

2.4.5.5.3 Graphene oxide (GO)

Graphene, i.e., the carbon-based materials, were discovered in 2004. Due to large amount of specific area, extraordinary electrical property, and its exceptional properties such as fast carrier mobility, excellent optical transparency, high fracture strength, and high thermal conductivity, it has been widely applied as electrode

materials, and adsorbents in both solid-phase microextraction and magnetic solid-phase extraction (Li, Wang et al. 2015).

In addition, graphene oxide is the oxidation form of graphene which has high water solubility and large quantities of oxygen containing surface functionalities, e.g. hydroxyl, carboxylic, and epoxide group as Figure 2.7. Because of these properties, GO is an interesting material in adsorption-based technology. Previous studies showed that GO could be used as adsorption material for removal of heavy metal ions, organic dyes, and antibiotic from water (Chowdhury and Balasubramanian 2014).

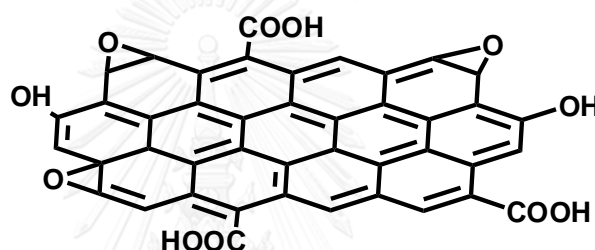


Figure 2.7 Structure of graphene oxide (GO)

2.4.5.5.4 Surface modification of GO

In order to improve charge, surface functional group on GO, and ability in adsorption capacity and water separation of GO, the modification of function group was applied by covalently bonding as Figure 2.8 (Yang, Li et al. 2015).



Figure 2.8 Structure of surface modified GO (Yang, Li et al. 2015)

2.4.5.5.5 Graphene oxide modified SBA-15

Because of strong interplanar interaction of graphene oxide, occurrence of irreversible aggregation might present. This occurrence could reduce adsorption capacity of adsorbent. Thus, modification of graphene oxide might be needed to prevent its aggregation, and increase recovery from water.

According to literatures, GO was reported with very high adsorption efficiency. The maximum adsorption capacity was found to be 994 mg/g for CFA (Zhang, Liu et al. 2014) but it can aggregate and hardly collects from water. Moreover, SBA-15 was reported to be good adsorbent with stable mesoporous structure and good potential in collecting from water but the adsorption capacity is not high comparing with GO. Besides, modification of functional group on SBA-15 surface can increase the adsorption efficiency and increase the possibility to be further modified by GO.

In order to increase adsorption capacity of SBA-15 and to improve ability to collect from water of GO, the combination between GO and SBA-15 by using covalent bond was performed in this study (Li, Wang et al. 2015). Aforementioned, adsorption capacity of SBA-15 may be increase by GO. On the other hand, possibility in the real practice of GO may be improved by SBA-15 as Figure 2.9.

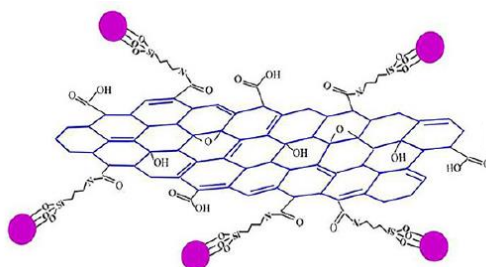


Figure 2.9 Structure of graphene oxide modified SBA-15 (Li, Wang et al. 2015)

2.4.5.5.6 Surface functionalized graphene oxide modified SBA-15

In order to increase specific surface area, modification of functional group was applied by ring opening on GO surface. Thus, there are two steps of graphene oxide modification. The first step was combining with mesoporous materials (SBA-15), and the second step was surface modification with functional group. In this study, amine functional group was selected to modified GO surface that grafted on amine functionalized SBA-15.

2.5 LITERATURE REVIEWS

Previously, many studies investigated the removal of PPCPs by using adsorption process in the different of adsorbent materials as shown;

(Bui and Choi 2009) investigated the removal of carbamazepine, diclofenac, ibuprofen, ketoprofen, and CFA using mesoporous silica-based materials, SBA-15. The results showed high adsorption efficiency for carbamazepine, diclofenac, ibuprofen, and ketoprofen except CFA because of hydrophilic interaction. Potentially, SBA-15 could be regenerated by combustion without loss, owing to stability of mesoporous silica structure up to 850°C.

(Ruangtrakul 2010) showed the removal of naproxen by adsorption of superparamagnetic hexagonal mesoporous silicates (HMS-SPs). The highest adsorption capacity was presented by modification of hydrophobic functional group, e.g. phenyl group, mercapto group, on HMS-SP. The potential interactions might be hydrophobicity, and electrostatic interaction. Potentially, in phenyl functional group might have electrostatic repulsion of π - π interaction between aromatic ring in adsorbate and adsorbent.

(Cabrera-Lafaurie, Roman et al. 2012) reported that the metal modified on inorganic-organic pillared clays (IOCs) could remove PPCPs such as clofibric acid, salicylic acid, carbamazepine, and caffeine from water with high adsorption capacity. The results of mechanism might involve with hydrophobic partitioning, electrostatic interaction, and complexation with the transition metals.

(Hasan, Jeon et al. 2012) studied the adsorptive removal of clofibric acid and naproxen using metal-organic frameworks (MOFs). The adsorption mechanism might be explained with an electrostatic interaction between PPCPs and the adsorbent. Due to high porosity and large pore size, MOFs could be suggested to be potential adsorbents for removing PPCPs in contaminated water.

(Kaosaiphun 2013) showed that the superparamagnetic hexagonal mesoporous silicate (HMS-SP) can remove clofibric acid. High adsorption capacity was reported in amine functionalized on the superparamagnetic hexagonal mesoporous silicate (3N-HMS-SP) and the adsorption capacity might relate to nitrogen atom because of electronegativity. Moreover, it might associate with hydrophilic and electrostatic interaction between amine functional group and clofibric acid.

(Permrunguang 2013) studied the removal of clofibric acid on mesoporous silicate (SBA-15). The highest adsorption capacity was reported in the amine functionalized on SBA-15. It might be hydrophilicity and electrostatic interaction combining with hydrogen bonding. The results also showed that surface area might not be the main reason for clofibric acid adsorption, but the main point might be the functional group grafted on the surface.

(Hasan, Choi et al. 2013) investigated clofibric acid and naproxen with the virgin and modified MIL-101s which is one of the typical metal-organic frameworks (MOFs) with acidic and basic groups. The results showed that the higher rate adsorption was

found in the base functionalized on the adsorbent. Moreover, the base functionalized on the adsorbent could be reused several times by simple washing with ethanol

(Reynel-Avila, Mendoza-Castillo et al. 2015) studied the adsorption of naproxen on bone char under batch condition. The results of adsorption might involve with combination of physical and chemical mechanisms in both electrostatic and non-electrostatic interactions depend on pH solution. Despite of the low degree in adsorbent utilization (below 4%), the application of packed-bed column was not effective for the treatment.

(Zhang, Liu et al. 2014) reported that graphene oxide nanosheet could remove clofibric acid from aqueous solution with very high adsorption capacity as a result of electrostatic repulsion and π - π interaction. Additionally, the adsorption efficiency was increased with decreasing pH and adding humic acid because humic acid could act as a bridge between clofibric acid and graphene oxide to improve the sorption at low pH values.

(Suriyanon, Permrunguang et al. 2015) investigated the adsorption mechanism of PPCPs using functionalized silica-based porous materials. The report showed that clofibric acid gives high adsorption capacity in hydrophilic adsorbents and the adsorption efficiency increased when pH decreased owing to hydrophilicity, electronegativity, and electrostatic interaction. However, naproxen provides high adsorption capacity in hydrophobic adsorbents and the adsorption efficiency increased with increasing pH because of hydrophobicity, electronegativity, and electrostatic interaction.

(Asgharinezhad and Ebrahimzadeh 2016) showed that Poly(2-aminobenzothiazole) coating on GO/ Fe₃O₄ could promote the extraction efficiency by increasing the active surface sites on the sorbent through hydrogen bonding formation,

and hydrophobic interactions with naproxen, diclofenac, and ibuprofen, with high adsorption efficiency. Moreover, it could protect Fe₃O₄ NPs as a shell.



CHAPTER III
MATERIALS AND METHODOLOGY

3.1 MATERIALS

3.1.1 Chemical reagents

3-aminopropyltriethoxysilane	99%	ALDRICH
Acetone	98%	RCI LABSCAN
Acetonitrile	99.9%	RCI LABSCAN
Clofibric acid	97%	ALDRICH
Diethylenetriamine	99%	Sigma Aldrich
Dimethylformamide	99.8%	RCI LABSCAN
Dipotassium hydrogenphosphate	99%	CARLO ERBA
Ethanol	95%	RCI LABSCAN
Graphite powder		ALDRICH
Hydrochloric acid	37%	QRëC
Hydrogen peroxide	30%	MERCK
Methanol	99.9%	RCI LABSCAN
N,N'-dicyclohexylcarbodiimide	99%	ALDRICH
Naproxen	98%	ALDRICH

Pluronic P123		ALDRICH
Potassium dihydrogenphosphate	99.5%	QRëC
Potassium permanganate		MERCK
Sodium hydroxide	99%	MERCK
Sulfuric acid	98%	QRëC
Tetraethoxysilane	98%	ALDRICH
Toluene	99.5%	RCI LABSCAN



3.2 METHODOLOGY

3.2.1 Experimental framework

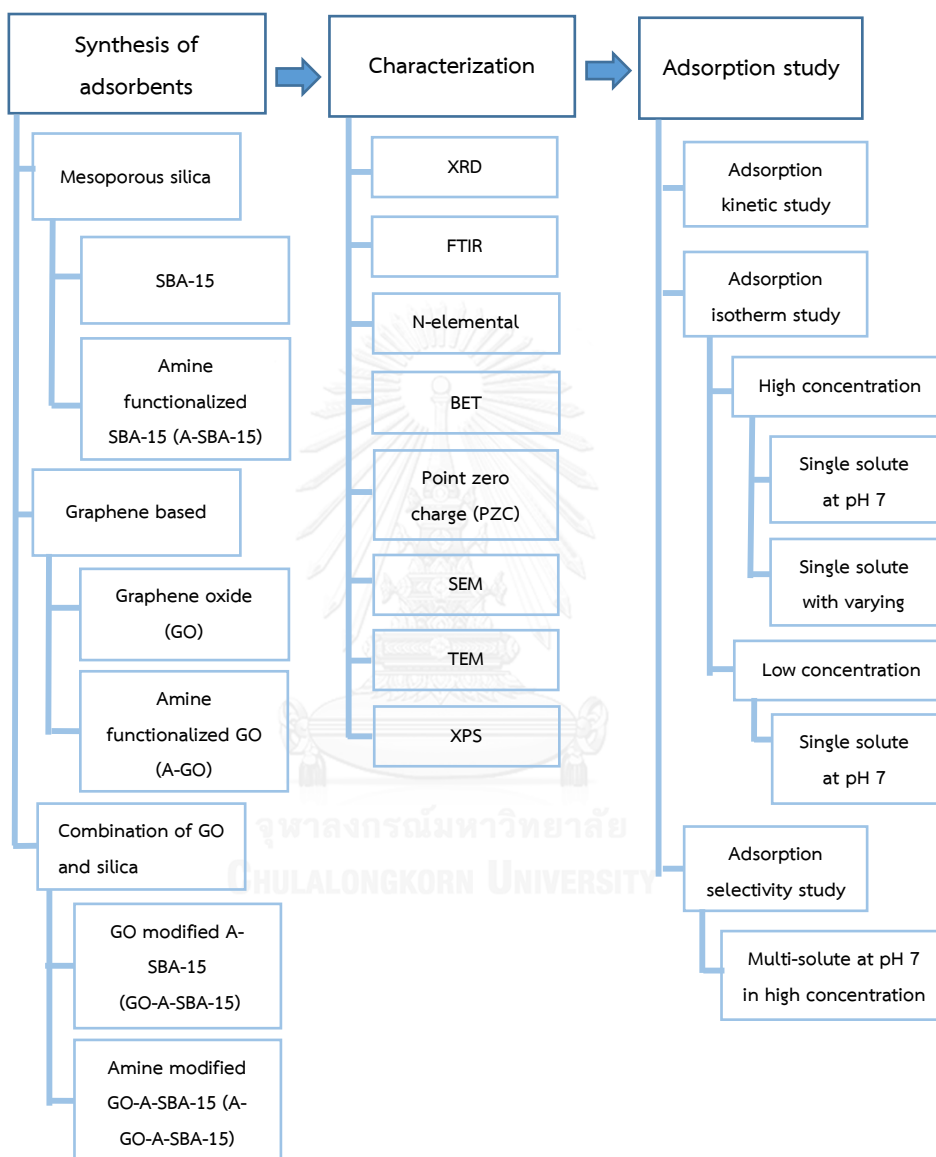


Figure 3.1 Experimental framework in this study

3.2.2 Preparation of CFA, and NAP stock solutions

Clofibric acid (CFA), and naproxen (NAP) standard stock solutions were prepared by dissolving in methanol in concentration of 20,000 mg/L, and were stored in the amber bottles at 4°C.

3.2.3 Preparation of adsorbent

3.2.3.1 Synthesis Santa Brabara Acid-15 (SBA-15) (Hoffmann, Cornelius et al. 2006)

SBA-15 was synthesized under acid condition, pluronic P123 was used as a structure directing agent, and tetraethoxysilane (TEOS) was used as silica source (Zhao, Feng et al. 1998). 4 g. of pluronic acid were dissolved in the mixture between 21 mL of 37% hydrochloric acid and 117 mL of deionized water in a 250 mL bottle under stirring at 40°C. When the homogeneous solution was appeared, 9.2 mL of TEOS were dropped wisely under stirring at 40°C. After that, the resulting gel was aged under stirring at 40°C for 24 hours and transferred to Teflon bottle then was aged at 105°C for 24 hours. The product was filtrated and washed with deionized water. Next, the white solid precipitation was dried at room temperature overnight. Lastly, the material was calcined to remove the organic template at 550°C for 5 hours as Figure 3.2.

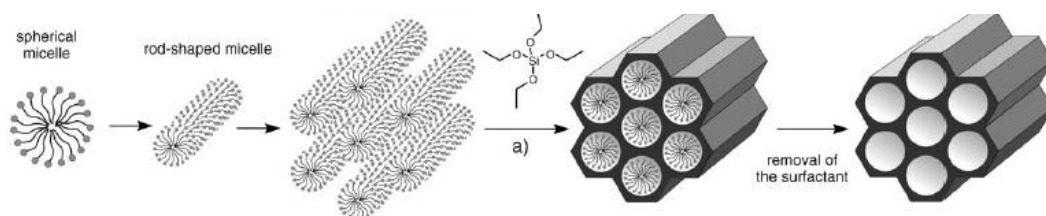


Figure 3.2 Synthesis of SBA-15 (Hoffmann, Cornelius et al. 2006)

3.2.3.2 Synthesis amino functionalized of SBA-15 (A-SBA-15)

SBA-15 was modified using 3-aminopropyltriethoxysilane (APTES) by post-grafting method. First of all, 0.5 g. of calcined SBA-15 was pretreated at 105°C for 24 hours. Next, 30 mL of toluene, and 5 mL of APTES were added into the pretreated SBA-15 under stirring. Then the reaction was kept under stirring at room temperature for 24 hours. After that, the product was filtrated and washed with toluene. Finally, the white solid was dried at 85°C for three hours and this modified product was named as A-SBA-15 following Figure 3.3.

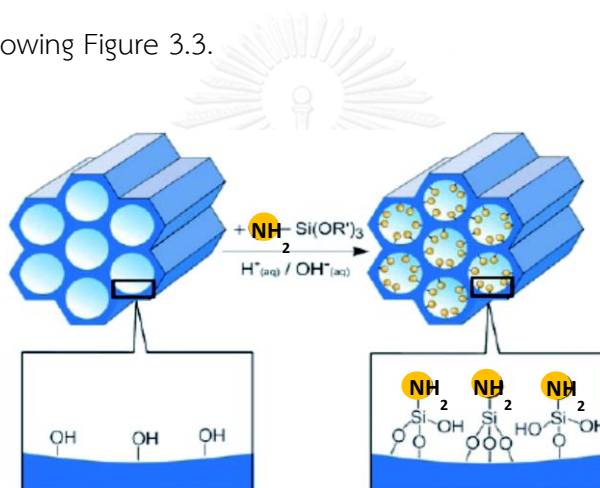


Figure 3.3 Synthesis of amine functionalized SBA-15 (A-SBA-15) (Kanamori and Nakanishi 2011)

3.2.3.3 Synthesis graphene oxide (GO)

Graphene oxide was synthesized from graphite powder by a modified Hummers method (Hummers and Offeman 1958). Firstly, 120 mL of concentrated sulfuric acid was cooled at 0°C in 2L bottle. Secondly, 2 g. of graphite powder was added under stirring. Thirdly, 15 g. of potassium permanganate was added gradually under stirring, and the temperature of this mixture was kept to be below 20°C. The bottle was transferred to water bath at 35°C and stirred for 2 hours. Next, 230 mL of deionized

water were dropped wisely (Note that this step the temperature was kept under 20°C) and then the mixture was stirred at room temperature for 2 hours. After that, 700 mL of deionized water were added under stirring and stirred for 5 minutes at room temperature. Then 20 mL of 30% hydrogen peroxide were added under stirring, brilliant yellow was obtained. The product was centrifuged at 4000 rpm for 5 minutes, washed three times with 5% of cool hydrochloric acid, and washed again three times with deionized water. Finally, the product was dried at 60°C overnight (Xu, Bai et al. 2008) as Figure 3.4.

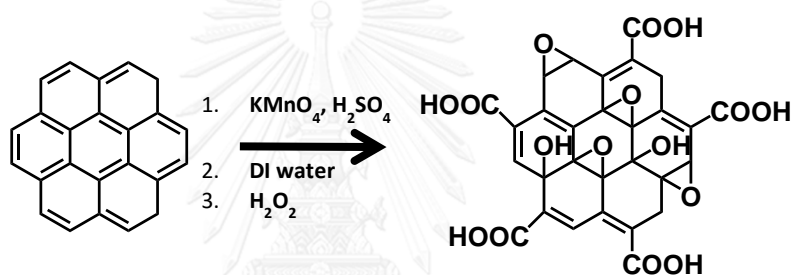


Figure 3.4 Synthesis of graphene oxide (GO)

3.2.3.4 Synthesis amine functionalized graphene oxide (A-GO)

GO was functionalized using diethylenetriamine through ring-opening reactions of epoxy group on the surface of graphene oxide. Firstly, 0.1 g of GO, and 1 g of diethylenetriamine were added into 100 mL of 95% ethanol. Then it was sonicated for 40 minutes. Next, the mixture was stirred at room temperature for 24 hours. Then the product was filtrated and it washed several times with ethanol then methanol and following by acetone. Finally, the product was dried at room temperature and named A-GO-A-SBA-15 (Yang, Li et al. 2015) as Figure 3.5.

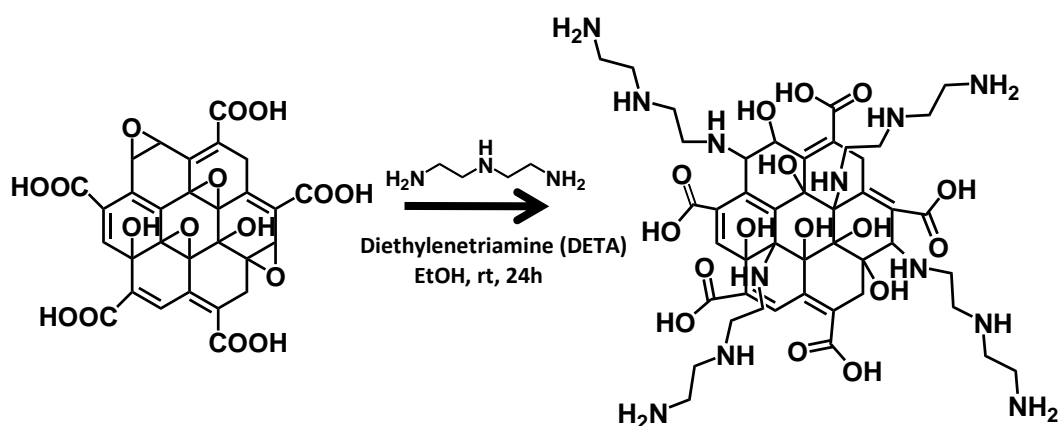


Figure 3.5 Synthesis of amine functionalized graphene oxide (A-GO)

3.2.3.5 Synthesis GO modified A-SBA-15 (GO-A-SBA-15)

Synthesized GO was modified with A-SBA-15 by the chemical linkage between amine functional group and carboxyl group of graphene oxide. First, 0.04 g of graphene oxide was added into 100 mL of dimethylformamide. The mixture was sonicated for 30 minutes and yellow-brown homogenous solution was obtained. Then 0.2 g of A-SBA-15, and 0.04 g of N,N'-dicyclohexylcarbodiimide (DCC) were added and continuously sonicated until the solution was homogenous. After that, the solution was stored in water bath at 60°C for 24 hours. The product was filtrated, washed with dimethylformamide, and washed again with ethanol. Last, the gray solid precipitation was dried at 50°C for 24 hours. The product was named GO-A-SBA-15 as Figure 3.6 (Li, Wang et al. 2015).

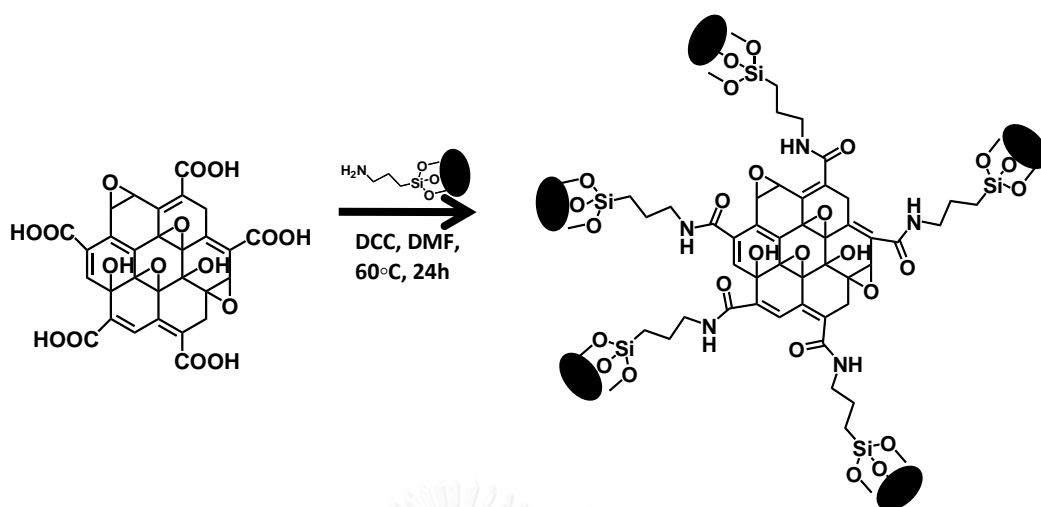


Figure 3.6 Synthesis of graphene oxide modified A-SBA-15 (GO-A-SBA-15)

3.2.3.6 Synthesis amine functionalized of GO-A-SBA-15 (A-GO-A-SBA-15)

GO-A-SBA-15 was functionalized using diethylenetriamine through ring-opening reactions of epoxy group on the surface of graphene oxide. The reaction was applied from literature (Yang, Li et al. 2015). Firstly, 0.1 g of GO-A-SBA-15, and 1 g of diethylenetriamine were added into 100 mL of 95% ethanol. Next, the mixture was stirred at room temperature for 24 hours. Then the product was filtrated and it washed several times with ethanol then methanol and following by acetone. Finally, the product was died at room temperature and named A-GO-A-SBA-15 as Figure 3.7.

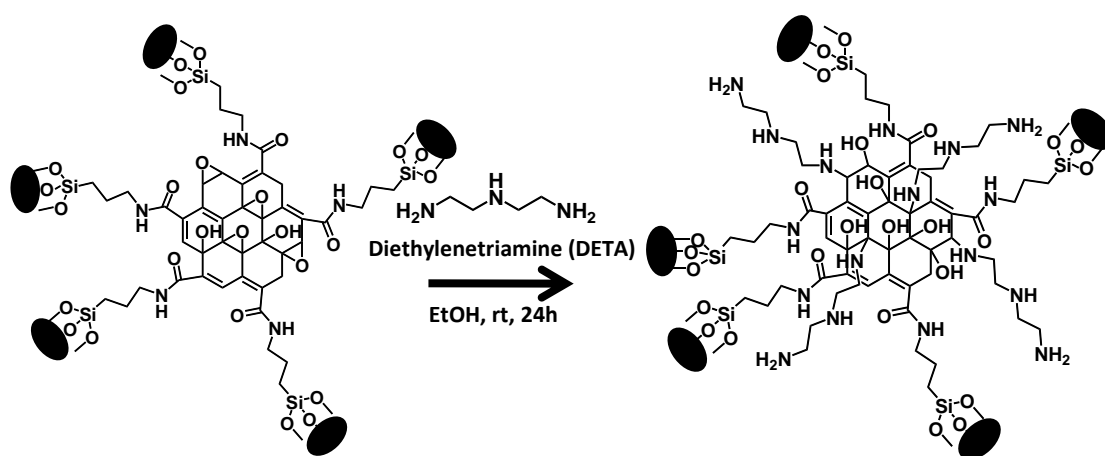


Figure 3.7 Synthesis of amine functionalized GO-A-SBA-15 (A-GO-A-SBA-15)

3.2.4 Characterization of adsorbent

The physical structure of the synthesized adsorbent was characterized by the techniques as shown;

Parameter	Measurement
Structure	X-ray Diffraction (XRD)
Surface area and pore size	Nitrogen adsorption-desorption isotherm
Surface functional group	Fourier Transform Infrared Spectrometer (FT-IR)
Elemental composite on surface	X-ray photoelectron spectroscopy (XPS)
Point of zero charges (PZC)	Batch equilibrium method
Amount of Nitrogen	Elemental analyzer
Material morphology	Scanning electron microscopy (SEM)
Material morphology	Transmission electron microscopy (TEM)

3.2.4.1 Structure

XRD pattern and crystal structure were measured by low and high angle X-ray diffraction (XRD) using fixed monochromator with Cu, 40 kV, 20 mA, and scanning rate 1,000 deg min⁻¹ between 0.7° – 5° (2 Θ) for low angle and 5° - 40° (2 Θ) for high angle at Department of Chemistry, Faculty of Science, Chulalongkorn University.

3.2.4.2 Surface area and pore size

Surface area and pore size were calculated from nitrogen adsorption-desorption isotherms at 77 k by an Autosorb-1 Quantachrome automatic volumetric sorption analyzer. Moreover, specific surface area (S_{BET}) was conducted using Brunner-Elmer-Teller (BET) method. Pore size distribution was performed using Barrett-Joyner-Halenda (BJH) method at Science and Technology Service Center, Faculty of Science, Chiang Mai University.

3.2.4.3 Surface functional group

Surface functional groups were characterized by Fourier Transform Infrared spectrometer (FTIR) between transmittance spectra 400-4000 cm⁻¹ at Scientific and Technological Research Equipment Centre, Chulalongkorn University.

3.2.4.4 Elemental composite on surface

Elemental composite on surface was measured by X-ray photoelectron spectroscopy (XPS) at Analytical and Testing Service Center, Petroleum and Petrochemical College, Chulalongkorn University and the results were analyzed using fitting program.

3.2.4.5 Point of zero charge (PZC)

Point of zero charge (PZC) was conducted by batch equilibrium method. 0.25 g/L of synthesized adsorbent were shaken with 10 mL under 200 rpm at room temperature in for 24 hours. The pH was varied from 3 – 12 using nitric acid or sodium hydroxide solution. The initial pH and final pH were measured and plotted the relationship. Finally, point of zero charge was investigated from the common plateau of the graph (Babić, Milonjić et al. 1999).

3.2.4.6 Amount of nitrogen

Amount of nitrogen was measured using elemental analyzer (CHNS/O) at Scientific and Technological Research Equipment Centre, Chulalongkorn University.

3.2.4.7 Material morphology

Material morphology was investigated using Scanning electron microscopy (SEM) to focus on surface and composition of adsorbents and Transmission electron microscopy (TEM) to focus on detail in internal composition at Scientific and Technological Research Equipment Centre, Chulalongkorn University.

3.2.5 Adsorption experiments

The adsorption of CFA and NAP were conducted under batch experiment. Stock solutions were prepared in phosphate buffer for keeping pH even ionic strength.

Adding 10 mL of adsorbate solutions and 0.25 - 0.5 g/L of adsorbent (using 0.25 g/L in GO series and 0.5 g/L in silicate series) in 125 mL Erlenmeyer flask with glass stopper was shaken under 200 rpm at room temperature. After that, the solid was removed by filtration through 0.45 mm pore size of nylon syringe filter. Then the

remaining was analyzed by reverse phase high performance liquid chromatography (HPLC) with a DAD detector (254 nm in high concentration and 230 nm at low concentration). The C18 column (4 x 250 mm, 5 μ m.) was used in this study. For CFA, the condition was conducted with isocratic of 40% water and 60% acetonitrile at 25°C. The flow rate was set at 1 mL/min. Another NAP, the condition was conducted with isocratic of 40% dihydrogenphosphate potassium salt and 60% acetonitrile at 25°C. The flow rate was set at 0.8 mL/min.

3.2.5.1 Adsorption kinetic study

Adsorption kinetic study was performed by varying the contact time under batch condition. The initial concentration of CFA was set at 10 mg/L in 10 mM phosphate buffer at pH 7; however, the initial concentration of NAP was set at 3 mg/L except in GO and PAC the initial concentration of NAP was set at 10 ppm in the same condition. Ratio of adsorbent and solution was fixed at 0.25 - 0.5 g/L. The slurry was stirred in a beaker at room temperature. Then the mixture was separated by filtration through a nylon syringe filter with pore size 0.45 μ m. The remaining concentration was measured by HPLC with DAD detector.

3.2.5.2 Adsorption isotherm study in high concentration at pH 7 (Single solute)

Adsorption isotherm study was conducted by varying the initial concentration from 2 to 15 mg/L in 0.25 - 0.5 g/L of adsorbent (using 0.25 g/L in GO series and 0.5 g/L in silica series). The ionic strength of solution was fixed at 10 mM adjusting with phosphate buffer to pH 7. The reaction was shaken at 200 rpm at room temperature until reached the equilibrium following by adsorption kinetic study. Then the mixture

was separated by filtration using a nylon syringe filter with pore size 0.45 μm . The remaining concentration was analyzed by HPLC with DAD detector.

3.2.5.3 Adsorption isotherm study in high concentration at vary pH (Single solute)

Adsorption isotherm study was conducted by varying the initial concentration from 2 to 15 mg/L in 0.25 - 0.5 g/L of adsorbent (using 0.25 g/L in GO series and 0.5 g/L in silica series). The ionic strength of solution was fixed at 10 mM adjusting with phosphate buffer. Moreover, pH was varied as 5, 7 and 9 by HCl and NaOH. The reaction was shaken at 200 rpm at room temperature until achieved the equilibrium time as the information from adsorption kinetic study. After that the mixture was separated by filtration using a nylon syringe filter with pore size 0.45 μm . The remaining concentration was analyzed by HPLC with DAD detector.

3.2.5.4 Adsorption isotherm in low concentration level at pH 7 (Single solute)

Adsorption isotherm study in low concentration level (ppb) was studied by varying the initial concentration in range of 0-200 $\mu\text{g/L}$ at 0.25 - 0.5 g/L of adsorbent (using 0.25 g/L in GO series and 0.5 g/L in silica series). The phosphate buffer was used to control pH 7 and ionic strength of solution will be fixed at 10 mM. The reaction was shaken at 200 rpm at room temperature until reached the equilibrium following by adsorption kinetic study. Then the mixture was separated by filtration using a nylon syringe filter with pore size 0.45 μm . The remaining concentration was analyzed by HPLC with DAD detector.

3.2.5.5 Adsorption selectivity in high concentration at pH 7 (Multi-solute)

Adsorption isotherm study in multi-solute was performed by varying the initial concentration in mixed solution of CFA and NAP from 2 to 15 mg/L in 0.25 - 0.5 g/L of adsorbent (using 0.25 g/L in GO series and 0.5 g/L in silica series). The phosphate buffer was used to control pH 7 and ionic strength of solution was fixed at 10 mM. The reaction was shaken at 200 rpm at room temperature until reached the equilibrium following by adsorption kinetic study. Then the mixture was separated by filtration using a nylon syringe filter with pore size 0.45 μ m. The remaining concentration was analyzed by HPLC with DAD detector.



CHAPTER IV

RESULTS AND DISCUSSION

4.1 CHARACTERIZATION OF SYNTHESIZED ADSORBENTS

All synthesized adsorbents were characterized physio-chemical properties; for instant, X-ray diffraction (XRD), Nitrogen adsorption-desorption isotherm, Fourier Transform Infrared Spectrometer (FTIR), X-ray photoelectron spectroscopy (XPS), Point of zero charges (PZC), CHNS Elemental analyzer, Thermogravimetric analysis (TGA), Scanning electron microscopy (SEM), and Transmission electron microscopy (TEM). These parameters were used to analyzed and described the structure of synthesized adsorbents and adsorption mechanism of each adsorbent.

4.1.1 X-ray diffraction (XRD)

X-ray diffraction was used to analyzed XRD pattern and crystal structure of A-SBA-15, GO, and GO-A-SBA-15 as shown in Figure 4.1. The synthesized A-SBA-15 showed the peaks at $2\theta = 0.5-2.5^\circ$ indexing to the (100), (110), and (200) diffraction peaks involve with the P6 symmetry pattern which reflects to the well-ordered two-dimensional (2D) hexagonal symmetry structure for highly order SBA-15. After GO grafting, the diffraction pattern is shown at $2\theta/^\circ = 0.92$ meaning that the mesoporous structure was preserved as Fig 4.1a. Moreover, GO exhibited a single sharp peak at $2\theta/^\circ = 8.88$ which is characteristic of the interplanar d_{200} spacing, after modification the disappearance of peak was investigated and new board peak at $2\theta/^\circ = 21.516$ was observed as Figure 4.1b indexing the changing of oxygen-containing functional group on GO through the chemical reaction with A-SBA-15. These changes can be indicated the successfully synthesized GO-A-SBA-15 (Li, Wang et al. 2015, Yang, Li et al. 2015)

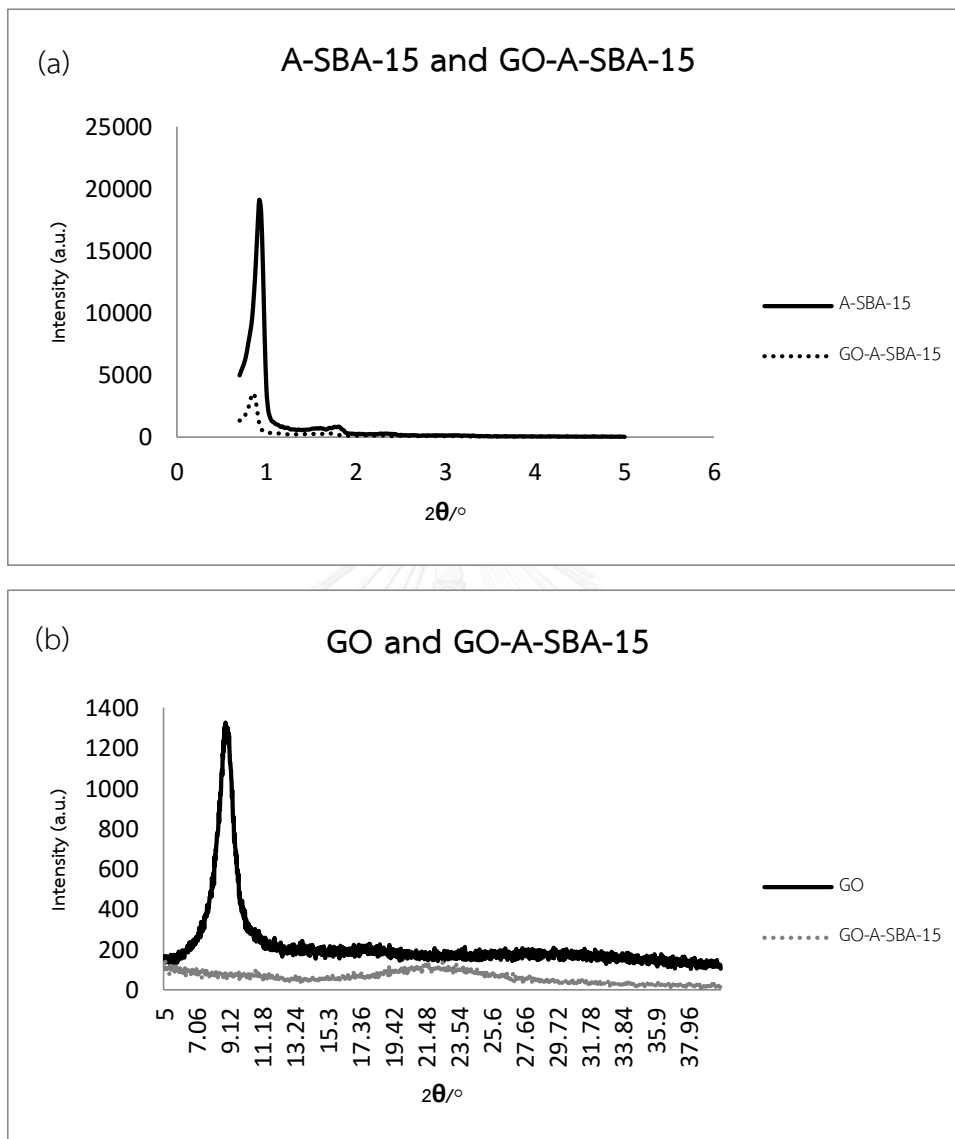
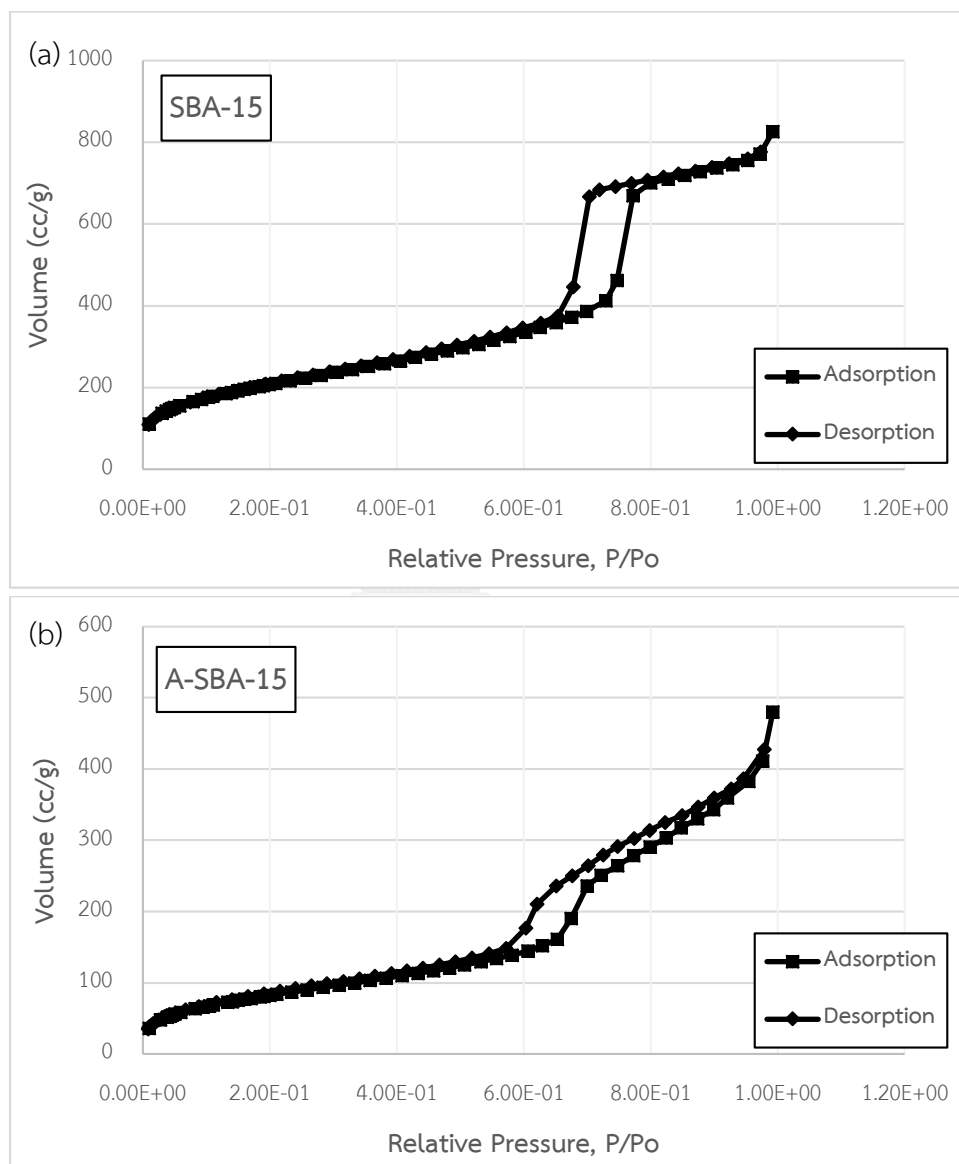


Figure 4.1 (a) XRD pattern of GO and GO-A-SBA-15 at high angle ($5-40^\circ$), and (b) XRD pattern of A-SBA-15 and GO-A-SBA-15 at low angle ($0.7-5^\circ$)

4.1.2 N_2 adsorption-desorption isotherms

N_2 adsorption-desorption isotherms were used to analyze surface area, pore size, and pore volume of SBA-15, A-SBA-15, GO, GO-A-SBA-15, and A-GO-A-SBA-15 (Fig

4.2). Synthesized adsorbents except GO showed the classified in type IV isotherm indicating to the mesoporous structure (2-50 nm) with the hysteresis loop generated by capillary condensation of N_2 in mesoporous structure as show in Figure 4.3.



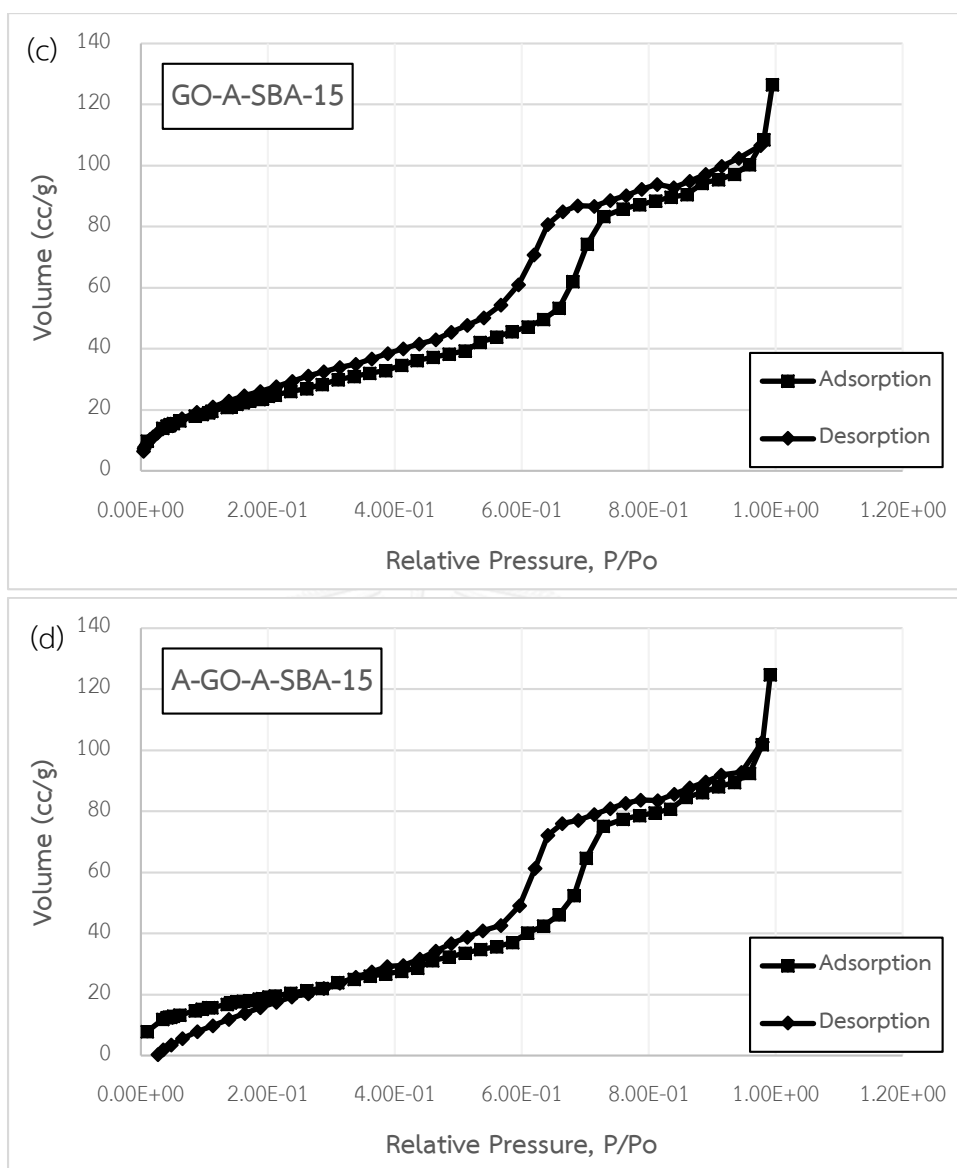


Figure 4.2 N₂ adsorption-desorption isotherms of (a) A-SBA-15, (b) A-SBA-15, (c) GO-A-SBA-15, and (d) A-GO-A-SBA-15

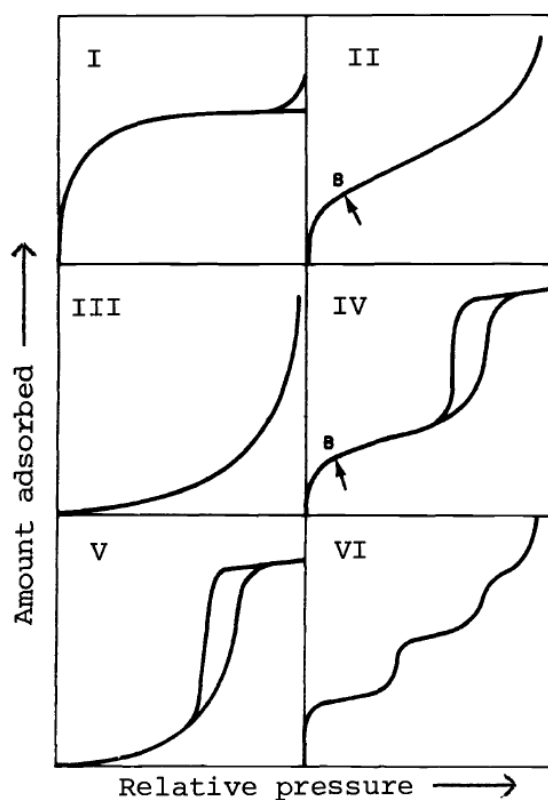


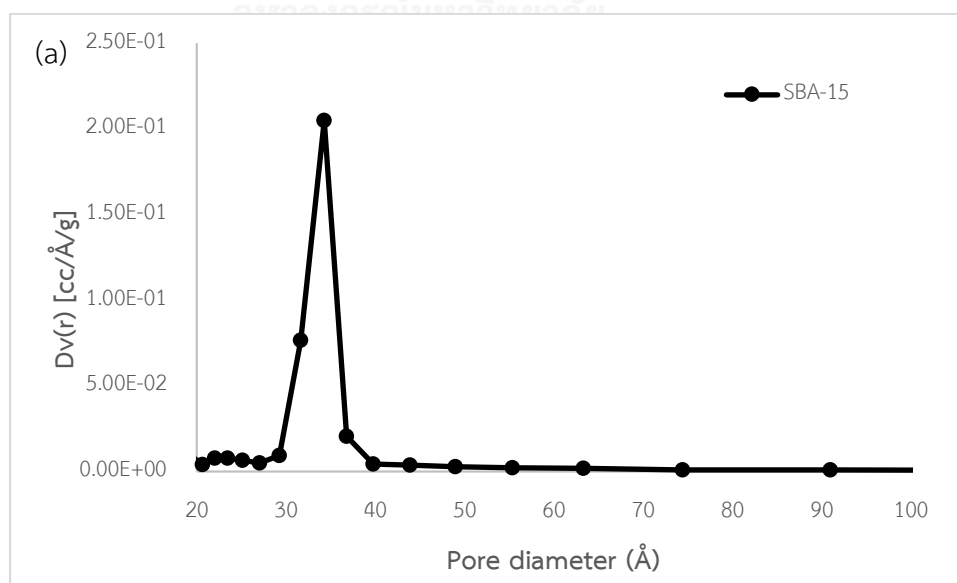
Figure 4.3 Type of physisorption isotherms (Sing 1982)

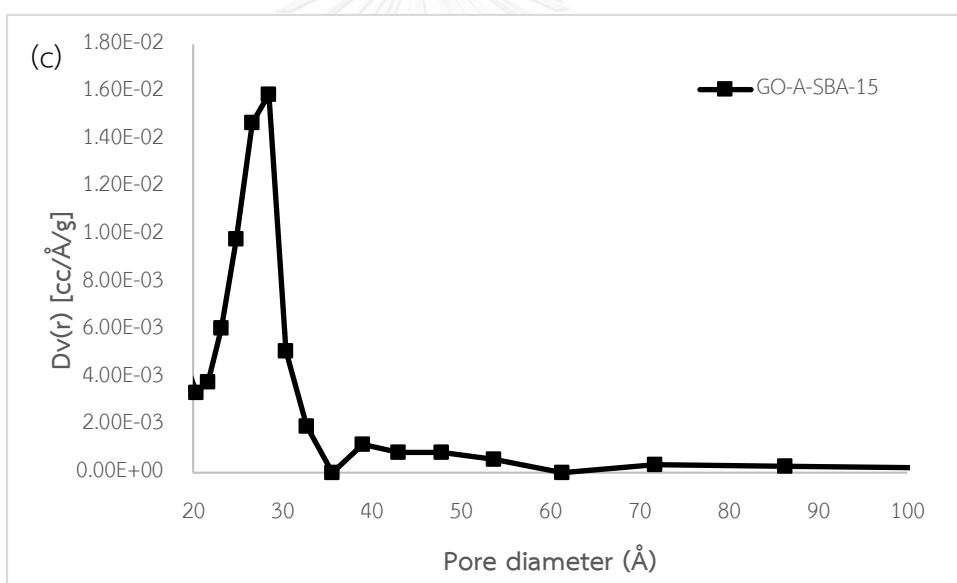
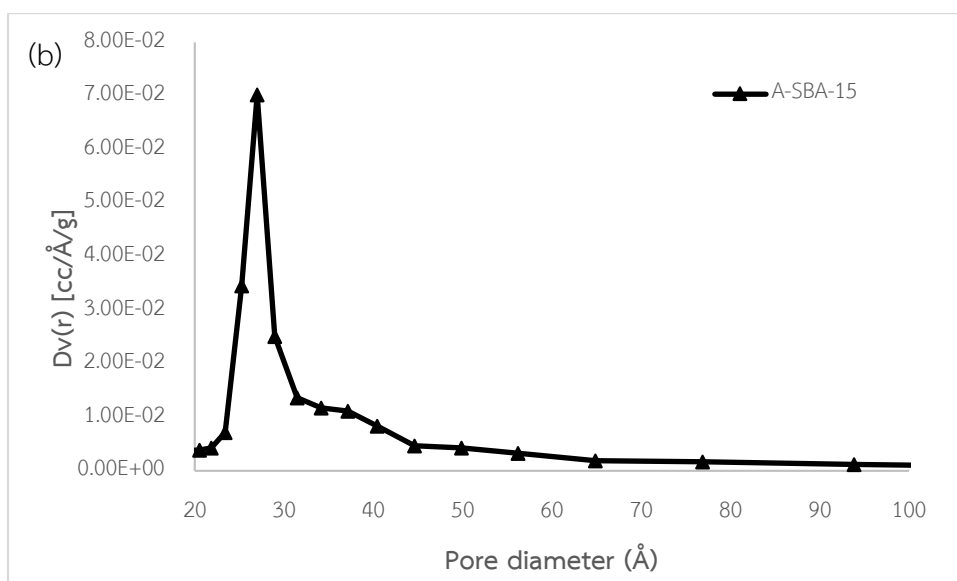
Specific surface area was calculated using Brunauer-Emmett-Teller (BET), pore size and pore volume was calculated using Barrett-Joyner-Halenda equation (BJH) which were summarized in Table 4.1. The obtained BET surface area and pore volume had the same trend. The result of BET surface area showed that SBA-15 has larger surface area than A-SBA-15, GO-A-SBA-15, and A-GO-A-SBA-15. It might be caused by the damage of silicate structure after modification with amine group on pristine SBA-15 and some structure was covered by GO in GO-A-SBA-15. Similarly, pore volume was decrease after functionalized amine group and modified with GO following the order; SBA-15 > A-SBA-15 > GO-A-SBA-15 > A-GO-A-SBA-15. Whereas, pore size distribution of A-GO-A-SBA-15 was more than A-SBA-15, GO-A-SBA-15, and SBA-15 as shown in Figure 4.4. SBA-15 reported the smallest pore size. Owing to amine functionalized SBA-15, it

might ruin the structure of SBA-15 and modification of GO might affect pore size distribution. According to the pore size of all synthesized adsorbents, CFA could access to the internal surface area, since molecular size of CFA (0.94 nm (9.4 Å)) are smaller than the pore size. However, NAP (64 nm (640 Å)) could be adsorbed only on external surface of the adsorbents (de Villiers, Aramwit et al. 2008, Nie, Deng et al. 2014).

Table 4.1 Pore diameter, pore volume, and BET surface area of SBA-15, A-SBA-15, GO-SBA-15, and A-GO-A-SBA-15.

Adsorbent	BET surface area (m ² /g)	Pore volume, V _p (cc/g)	Pore diameter (Å)
SBA-15	734.77	1.2780	34.79
A-SBA-15	310.79	0.7421	47.76
GO-A-SBA-15	96.15	0.1957	40.70
A-GO-A-SBA-15	72.84	0.1931	53.01





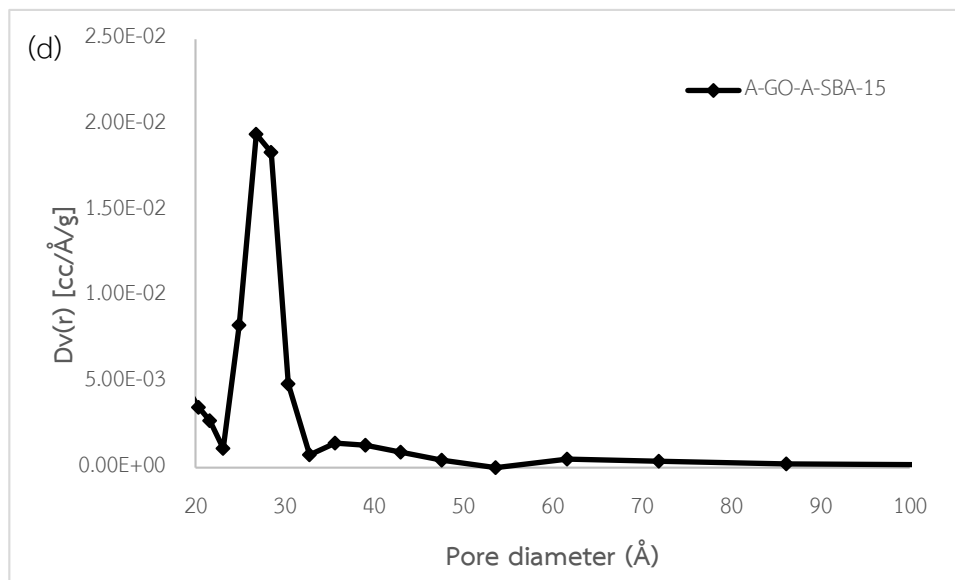


Figure 4.4 Pore size distribution (BJH) of synthesized adsorbents (a) SBA-15, (b) A-SBA-15, (c) GO-A-SBA-15, and (d) A-GO-A-SBA-15

4.1.3 Fourier Transform Infrared Spectrometer (FTIR)

Fourier Transform Infrared Spectrometer was used to analyze surface functional groups of all synthesized adsorbents i.e. SBA-15, A-SBA-15, GO, A-GO, GO-A-SBA-15, and A-GO-A-SBA-15 as shown in Figure 4.5. According to GO, the characteristic peak was represented at $3,267.84\text{ cm}^{-1}$ O-H stretching of alcohol and carboxylic group, $1,729.23\text{ cm}^{-1}$ C=O stretching, $1,615.38\text{ cm}^{-1}$ C=C stretching, and $1,224.62\text{ cm}^{-1}$ C-O-C stretching (epoxy group) of GO. After functionalized amine functional group, N-H stretching was shown at $2,927.85$ and $2,866.83\text{ cm}^{-1}$ and C-O-C stretching of epoxy group at $1,224.62\text{ cm}^{-1}$ was disappeared. For mesoporous silica (SBA-15), the characteristic peak of Si-O-Si stretching was shown at $1,081.74\text{ cm}^{-1}$. After amine group grafting, $2,927.85$ and $2,866.83\text{ cm}^{-1}$ N-H stretching of amine functional group were reported. Moreover, the combination of GO and A-SBA-15 (GO-A-SBA-15) showed both of characteristic peaks

of GO at 3,267.84, 1,661.54, 1,541.54, and 1,224.62 cm^{-1} which were O-H stretching, C=O stretching, C=C stretching, and C-O-C stretching, respectively, and A-SBA-15 at 2,927.85, 2,866.83, and 1,081.74 cm^{-1} which were N-H stretching and Si-O-Si stretching. Similarly with A-GO-A-SBA-15, the characteristic peaks of GO and A-SBA-15 were exhibited at 267.84, 1,661.54, 1,541.54 and 1,224.62 cm^{-1} which were O-H stretching, C=O stretching, C=C stretching, and C-O-C stretching, respectively. Therefore, FTIR spectra could be confirmed that all synthesized adsorbents were successful except A-GO-A-SBA-15 (Solomons and Fryhle 2011, Permrunguang 2013, Li, Wang et al. 2015, Yang, Li et al. 2015)



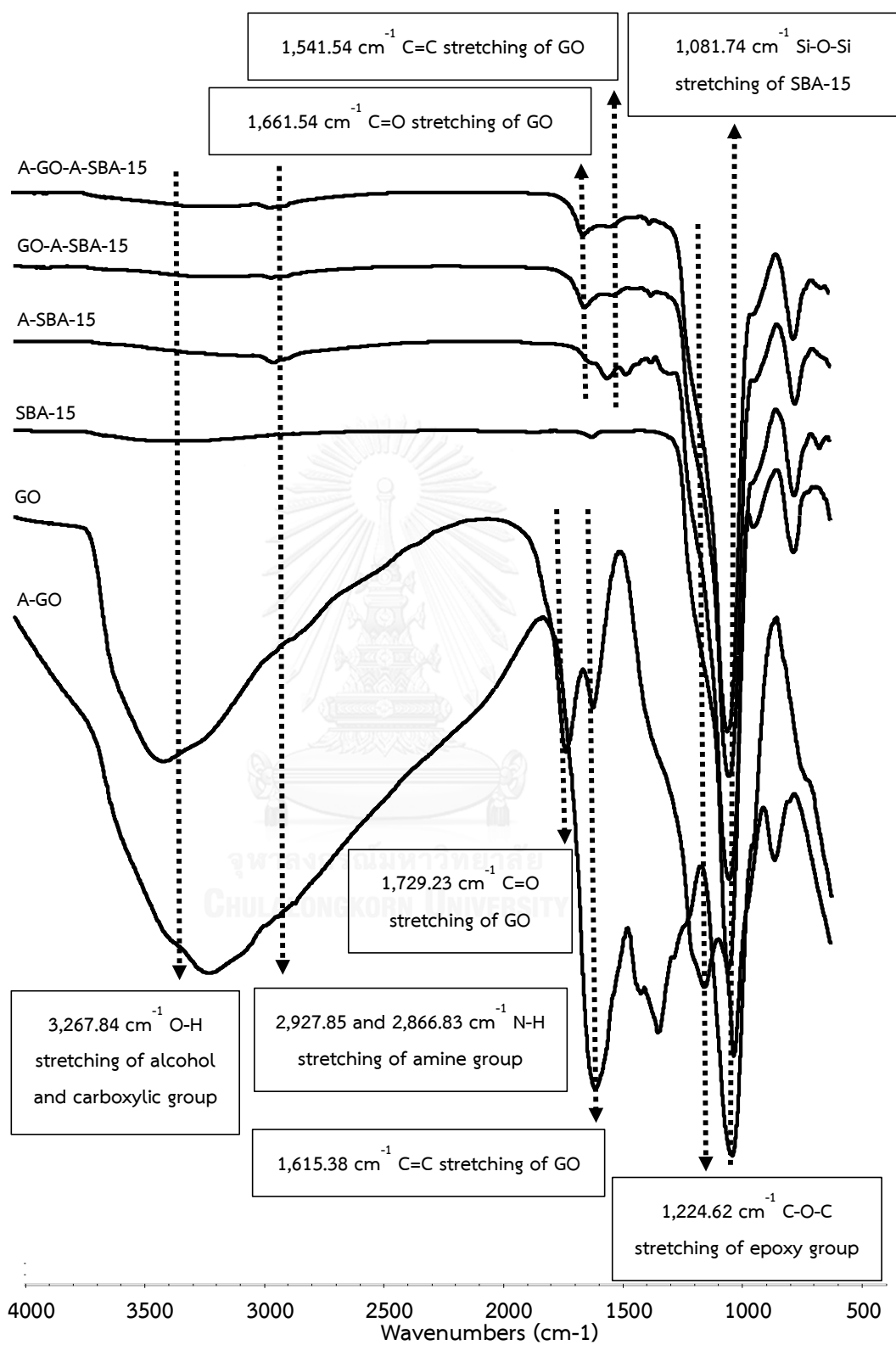


Figure 4.5 FTIR spectra of all synthesized adsorbents

4.1.4 Point of zero charges (PZC)

Batch equilibrium method was used to determine point of zero charge (PZC). PZC of all synthesized adsorbents was reported in Table 4.2 which was different in each adsorbent due to surface modification. PZC of SBA-15, A-SBA-15, GO, A-GO, GO-A-SBA-15, and A-GO-A-SBA-15 were 5.26, 9.60, 3.19, 7.63, 9.24, and 9.35, respectively. Thus, amine functional group could increase PZC and it might be concluded that PZC could confirm that all synthesized adsorbents (Permrunguang 2013).

Table 4.2 PZC of all synthesized adsorbents

Adsorbent	Surface functional group	Surface characteristic	PZC
SBA-15	Silanol	Hydrophilic	5.26
A-SBA-15	Amine and silanol	Hydrophilic	9.60
GO	Carboxylic, epoxy, and hydroxyl	Hydrophobic	3.19
A-GO	Amine, carboxylic, epoxy, and hydroxyl	Hydrophilic	7.63
GO-A-SBA-15	Carboxylic, epoxy, hydroxyl, amine, and silanol	Hydrophobic	9.24
A-GO-A-SBA-15	Amine, carboxylic, epoxy, hydroxyl, and silanol	Hydrophilic	9.35

4.1.5 CHNS elemental analyzer

CHNS elemental analyzer was used to determine the quantitation of nitrogen, carbon, hydrogen, sulfur content of synthesized adsorbents as Table 4.3 which could confirm the successful synthesis. In case of A-SBA-15, and A-GO, the appearance of N was shown comparing with pristine material and A-GO-A-SBA-15 reported the increasing of %N comparing with GO-A-SBA-15. Therefore, CHNS elemental analyzer could be confirm that all synthesized adsorbents were successful.

In addition, the percentage of GO was measured by using furnace at 800°C for 12 hours as Figure 4.6, GO-A-SBA-15 had 12.44% of GO and 87.56% of A-SBA-15, and A-GO-A-SBA-15 had 13.36% of A-GO and 86.64% of A-SBA-15.

Table 4.3 Elemental content of all synthesized adsorbents

Adsorbent	%N	%C	%H	%S
SBA-15	0.00	0.02	0.72	0.00
A-SBA-15	3.53	10.06	0.46	0.00
GO	0.00	38.53	2.85	4.06
A-GO	7.71	48.73	3.61	1.63
GO-A-SBA-15	3.13	15.30	2.20	0.59
A-GO-A-SBA-15	3.44	15.50	2.21	0.29

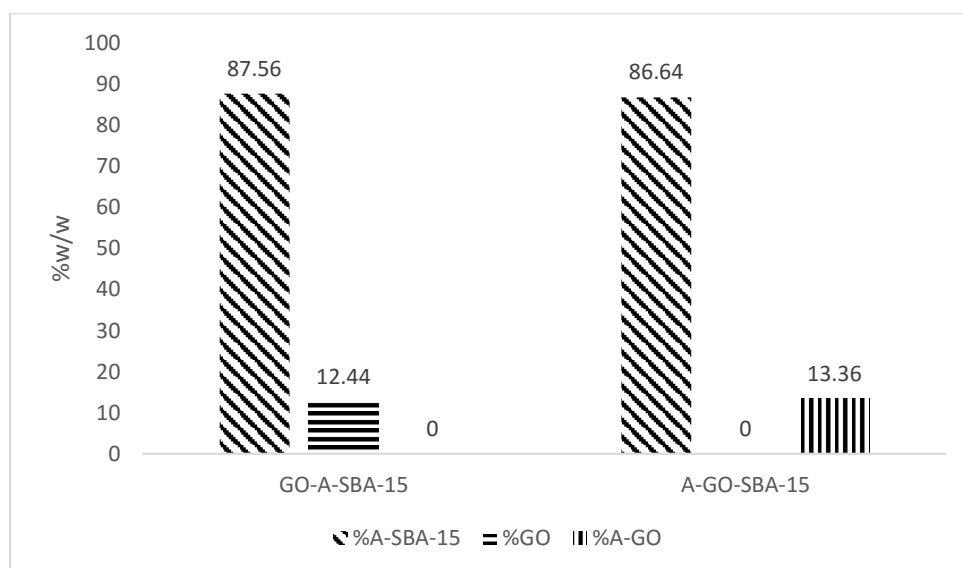


Figure 4.6 Percentage of GO and A-GO in GO-A-SBA-15 and A-GO-A-SBA-15

4.1.6 Scanning electron microscopy (SEM)

The morphologies of all synthesized adsorbents were observed using Scanning electron microscopy (SEM) as shown in Figure 4.7. The adsorbents were prepared by sonicating in water. Then they were dropped on glass slide and dried at room temperature. The shape of SBA-15 was investigated to be rod shape as Fig 4.7a. After grafting amine functional group, the structure of A-SBA-15 was damaged by hydrolysis interaction of hydrophilic functional group on the amine functionalized process as shown in Fig 4.7b. Besides, the surface of GO sheets was exhibited quite smooth and transparent surface; however, aggregation of GO sheets could be observed in Fig 4.7c. After modification by amine functional group, GO sheets were detected with a rough and folded surface (as shown in Fig 4.7d) due to intra-interaction of grafted amine functional groups on the GO surface. Moreover, the complexity of GO-A-SBA-15 was presented in Fig 4.7e, indicating that the rod shape of A-SBA-15 was attached to smooth GO sheets. The SEM image of A-GO-A-SBA-15 also showed that GO sheets could cover the rod shape of A-SBA-15 as Fig 4.7f. However, the sheet of GO attached to A-SBA-15 did not show the

folding. It could be discussed that GO was fixed on A-SBA-15 material that made GO sheet cannot move freely. Thus, intra-interaction among functional groups on GO (or A-GO) such as amine functional group and hydroxyl group might rarely occur on GO-A-SBA-15 and A-GO-A-SBA-15 (Yang, Li et al. 2015).

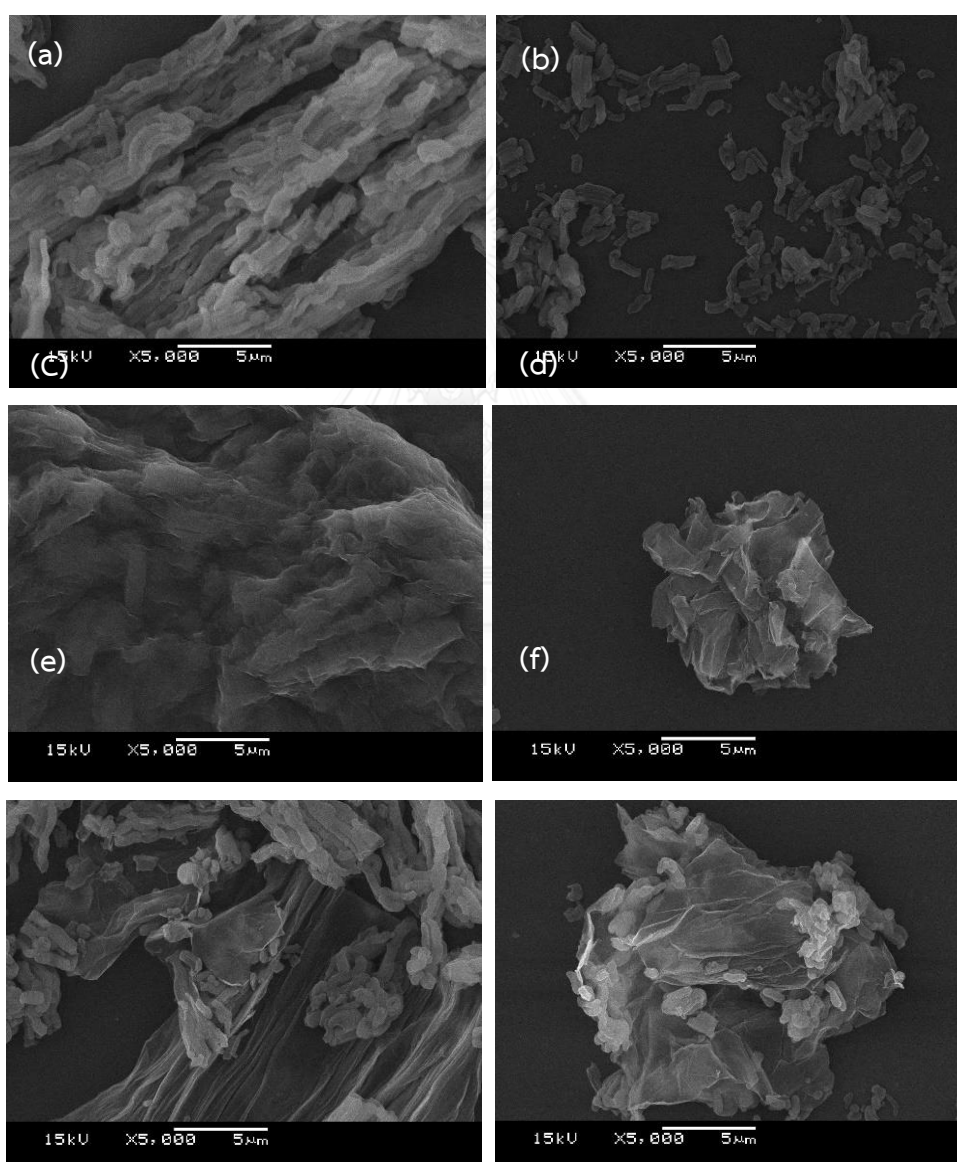


Figure 4.7 Images $\times 5,000$ of SEM (a) SBA-15, (b) A-SBA-15, (c) GO, (d) A-GO, (e) GO-A-SBA-15, and (f) A-GO-A-SBA-15

4.1.7 Transmission electron microscopy (TEM)

The internal morphologies of synthesized adsorbents were also observed using transmission electron microscopy (TEM) as shown in Figure 4.8. Synthesized adsorbents were dropped on copper grid and dried at room temperature. Synthesized SBA-15 presented the U-shaped which was indeed almost straight, indexing the high ordering of hexagonal mesoporous silica as Fig 4.8a (Janssen, Van Der Voort et al. 2002). For A-SBA-15, the TEM image also showed well ordering of hexagonal mesoporous silica as Fig 4.8b. Additionally, the TEM image of GO reported the smooth sheet and also the aggregation of GO (as Fig 4.8c). As showed in Fig 4.8d, after functionalized amine functional group, A-GO was presented rough curled surface comparing with GO. It might be caused by the H-bonding and hydrophilic interaction making A-GO sheet to be crumpling sheet (Yang, Li et al. 2015). TEM image of GO-A-SBA-15 (Fig 4.8e) illustrated the mixture of well ordering mesoporous silica of A-SBA-15 and smooth sheet of GO. It can be seen clearly that A-SBA-15 was attached on GO sheet via interaction at grafted amine groups on A-SBA-15. Moreover, A-GO-A-SBA-15 TEM's image (Fig 4.8f) showed the structure of A-SBA-15 encapsulated in curled surface of A-GO sheet.

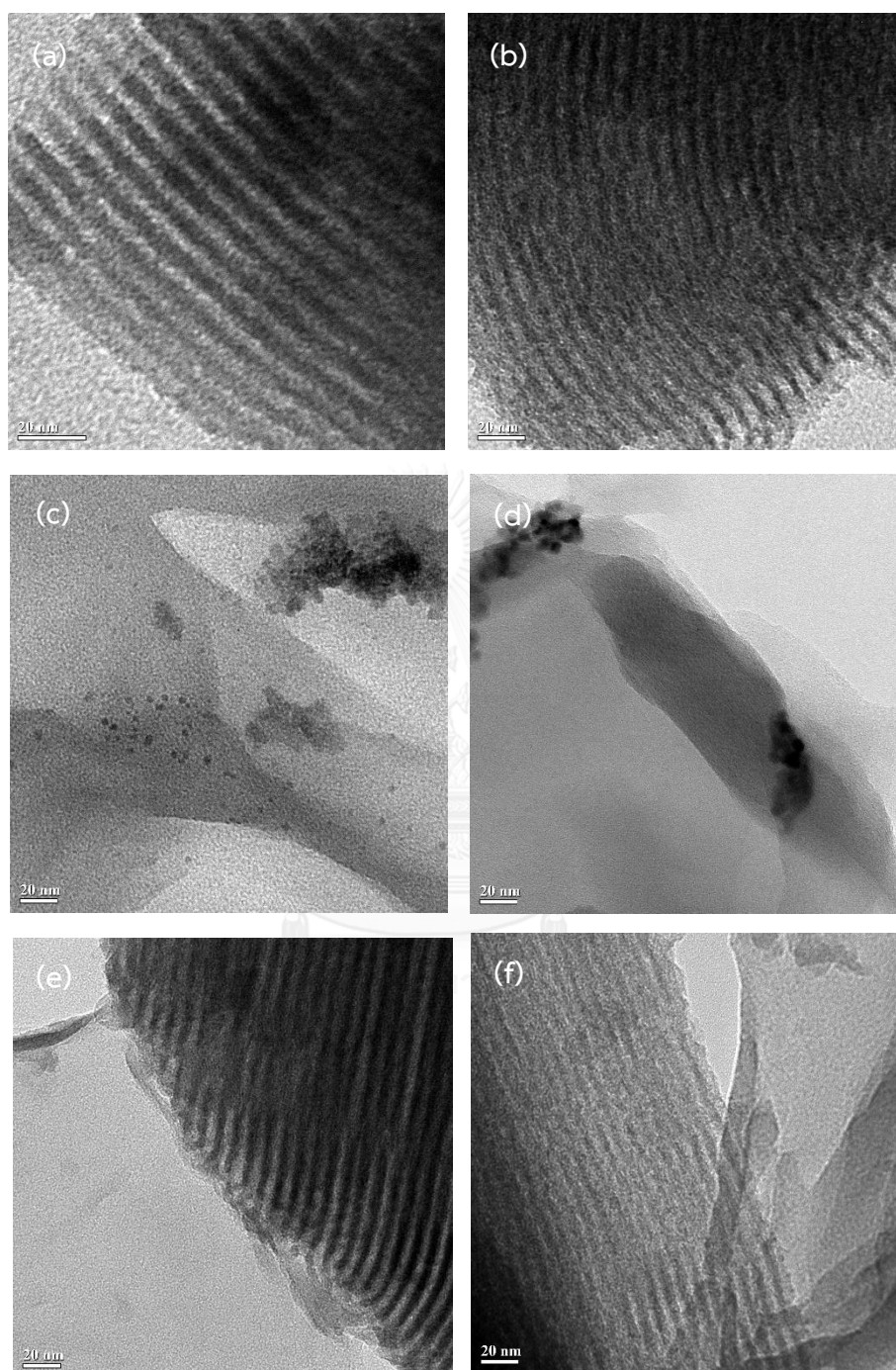


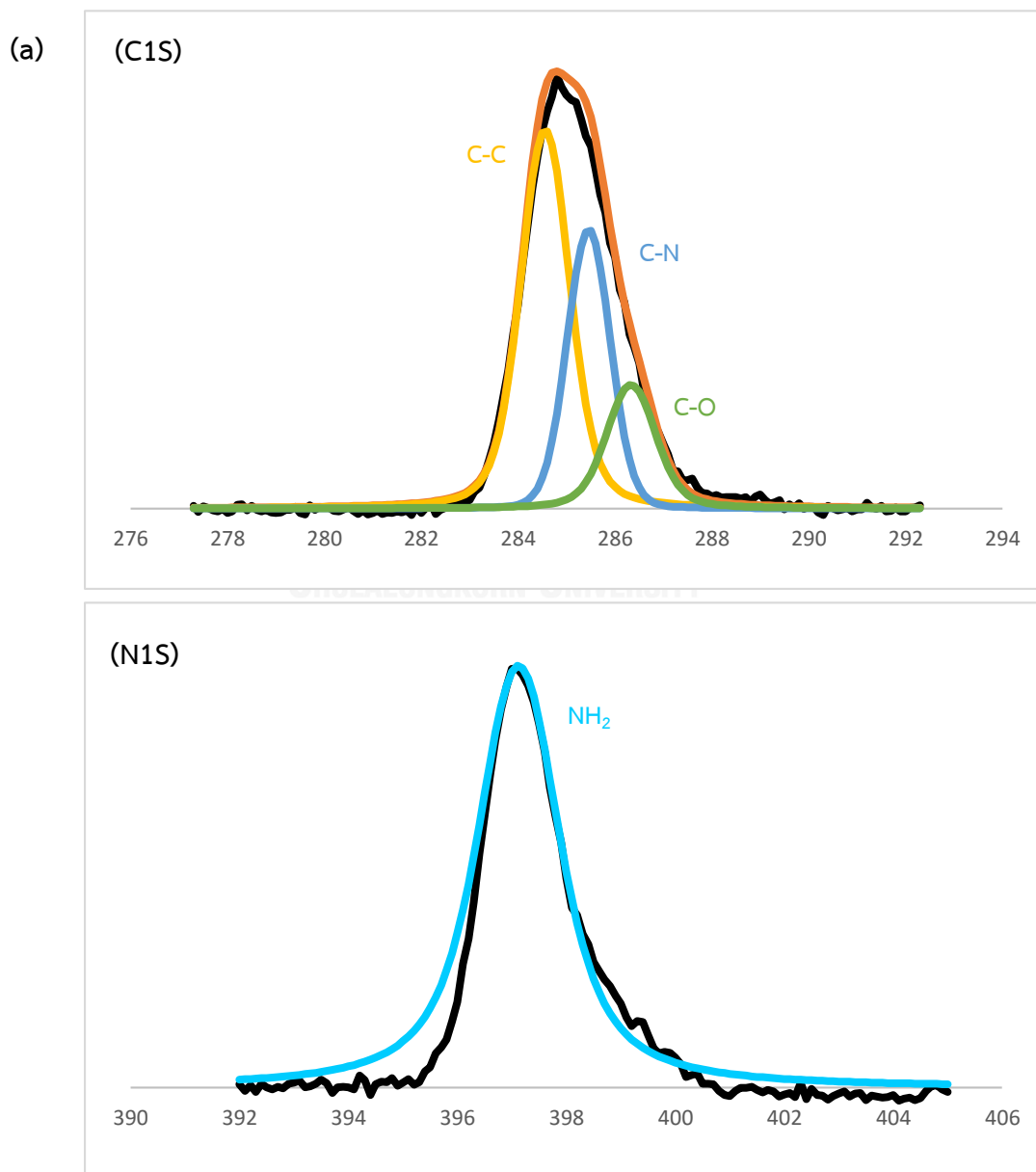
Figure 4.8 TEM images of a) SBA-15, b) A-SBA-15, c) GO, d) A-GO, e) GO-A-SBA-15, and f) A-GO-A-SBA-15

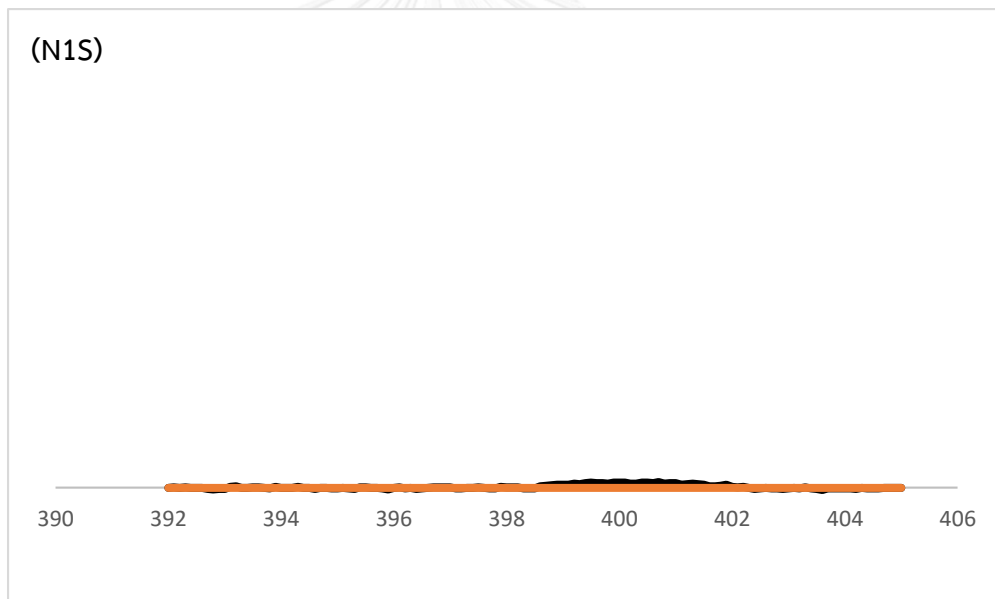
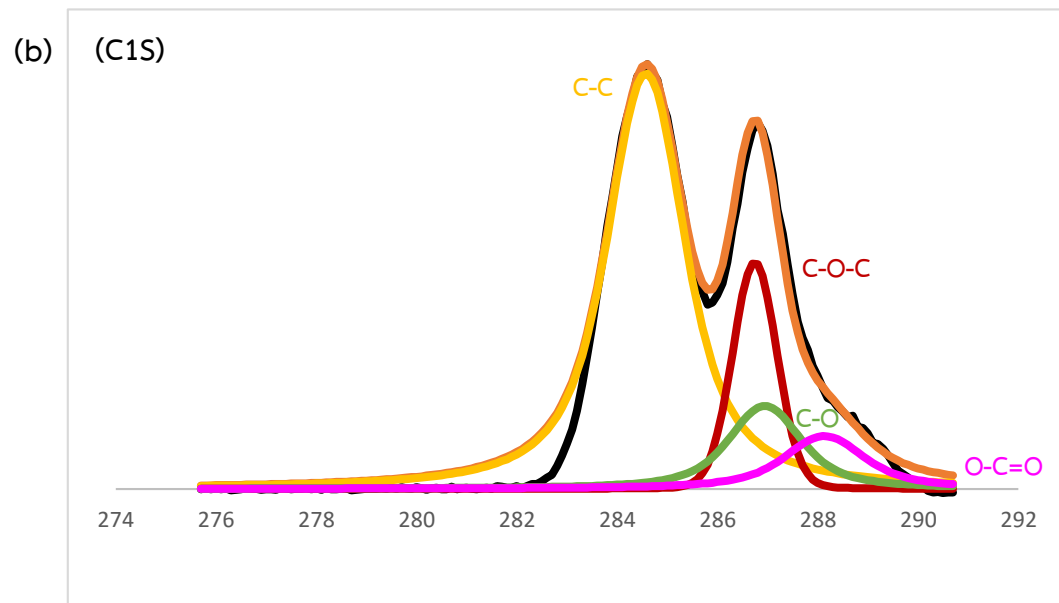
4.1.8 X-ray photoelectron spectroscopy (XPS)

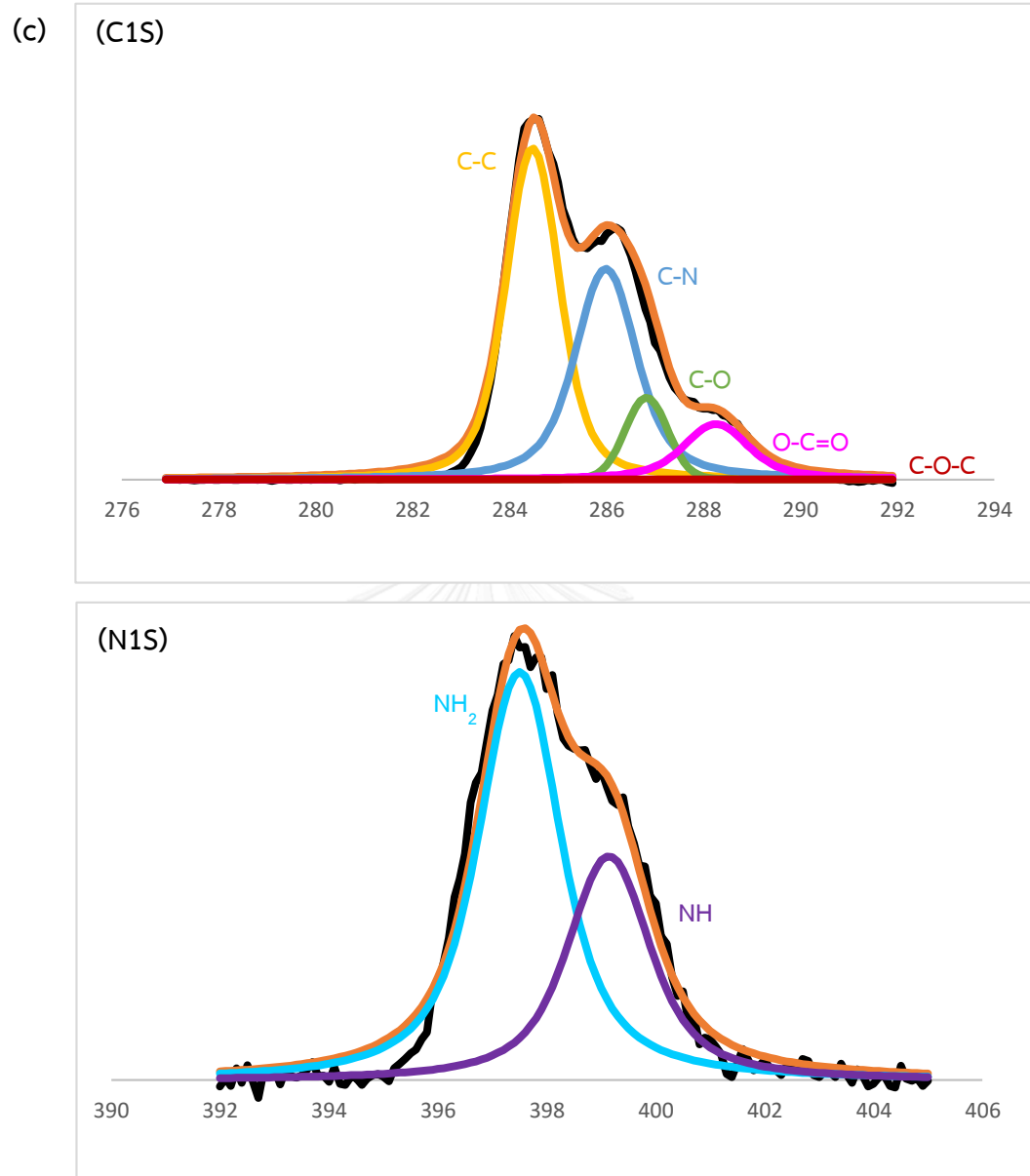
Elemental composites on surface of A-SBA-15, GO, A-GO, GO-A-SBA-15, and A-GO-A-SBA-15 were measured by X-ray photoelectron spectroscopy (XPS) as shown in Figure 4.9. A-SBA-15 represented the bond of C-C, C-N, and C-O at 284.6, 285.4, and 286.3 eV, respectively, in C1S and the bond of NH₂ at 397.2 eV in N1S. It might be confirmed that amine function group was successfully attached on SBA-15 by the covalent bond of C-N and the presence of NH₂ as shown in Figure 4.9a. For GO, the results showed the bond of C-C, C-O-C of epoxy group, C-O, and O-C=O at 284.6, 286.8, 287.0, and 288.3 eV, respectively, in C1S which could be exhibited the characteristic functional group on GO surface (as Figure 4.9b). In case of A-GO, the results demonstrated the bond of C-C, C-N, C-O, and O-C=O at 284.6, 286.1, 286.8, and 288.3 eV, respectively, for C1S and the showing of NH and NH₂ at 397.7 and 399.2 eV, respectively, in N1S (as Figure 4.9c). The presence of C-N, NH, and NH₂ bonding and the disappearance of C-O-C epoxy group on surface of GO could be discussed that amine functional group could interact on the surface of GO.

In addition, GO-A-SBA-15 was reported the bond of C-C, C-N, C-O-C of epoxy group, C-O, and O-C=O at 284.6, 285.6, 286.4, 286.9, and 288.4 eV, respectively, in C1S and the bond of NH and NH₂ at 397.9 and 399.5 eV, respectively, in N1S. The completeness of GO-A-SBA-15 synthesize can be concluded via the outstanding bond of GO as C-O-C of epoxy group and O-C=O of carboxylic group on the surface of GO and the different bond of A-SBA-15 as C-N and NH₂ of amine group on surface of A-SBA-15. Indeed, N-H bond was presented by the interaction of amine functional group or NH₂ bond of A-SBA-15 on GO surface and charged form to N-H bond (as Figure 4.9d) which could be confirmed the successful synthesis.

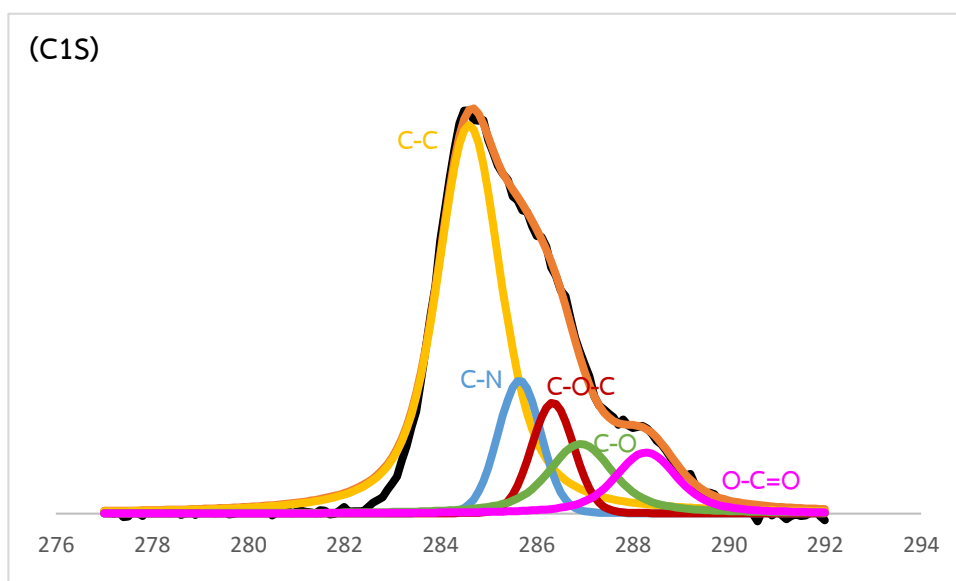
However, A-GO-A-SBA-15 (as Figure 4.9e) showed the bond of C-C, C-N, C-O-C of epoxy group, C-O, and O-C=O at 284.6, 285.6, 286.5, 287.2 and 288.3 eV, respectively, in C1S, as well as NH and NH₂ (in N1S) at 397.9 and 399.4 eV, respectively. This could not be discussed the successful modification of amine functional group on GO-A-SBA-15 (Huang, Tien et al. 2011, Lai, Chen et al. 2011, Pulido, Concepcion et al. 2012, Yang, Li et al. 2015).



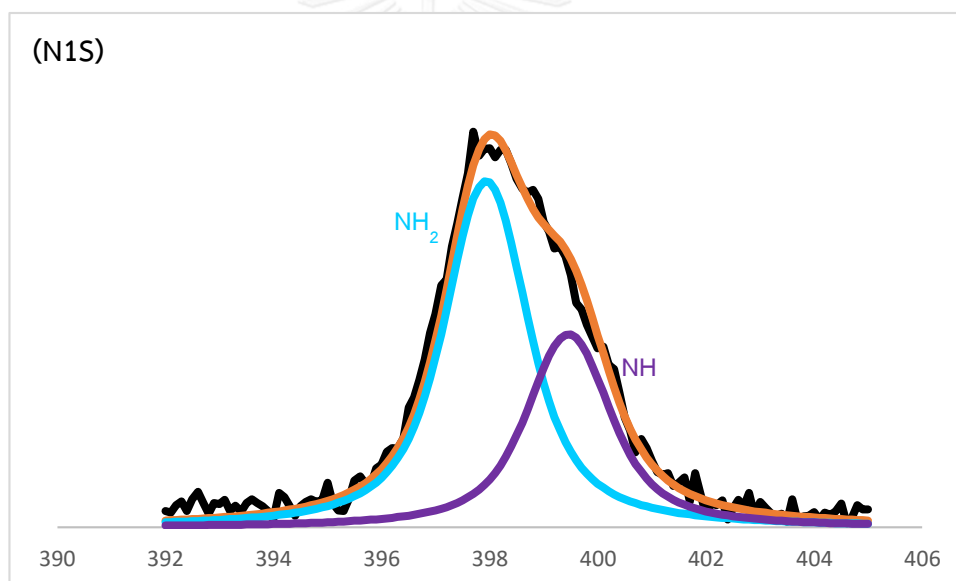




(d) (C1S)



(N1S)



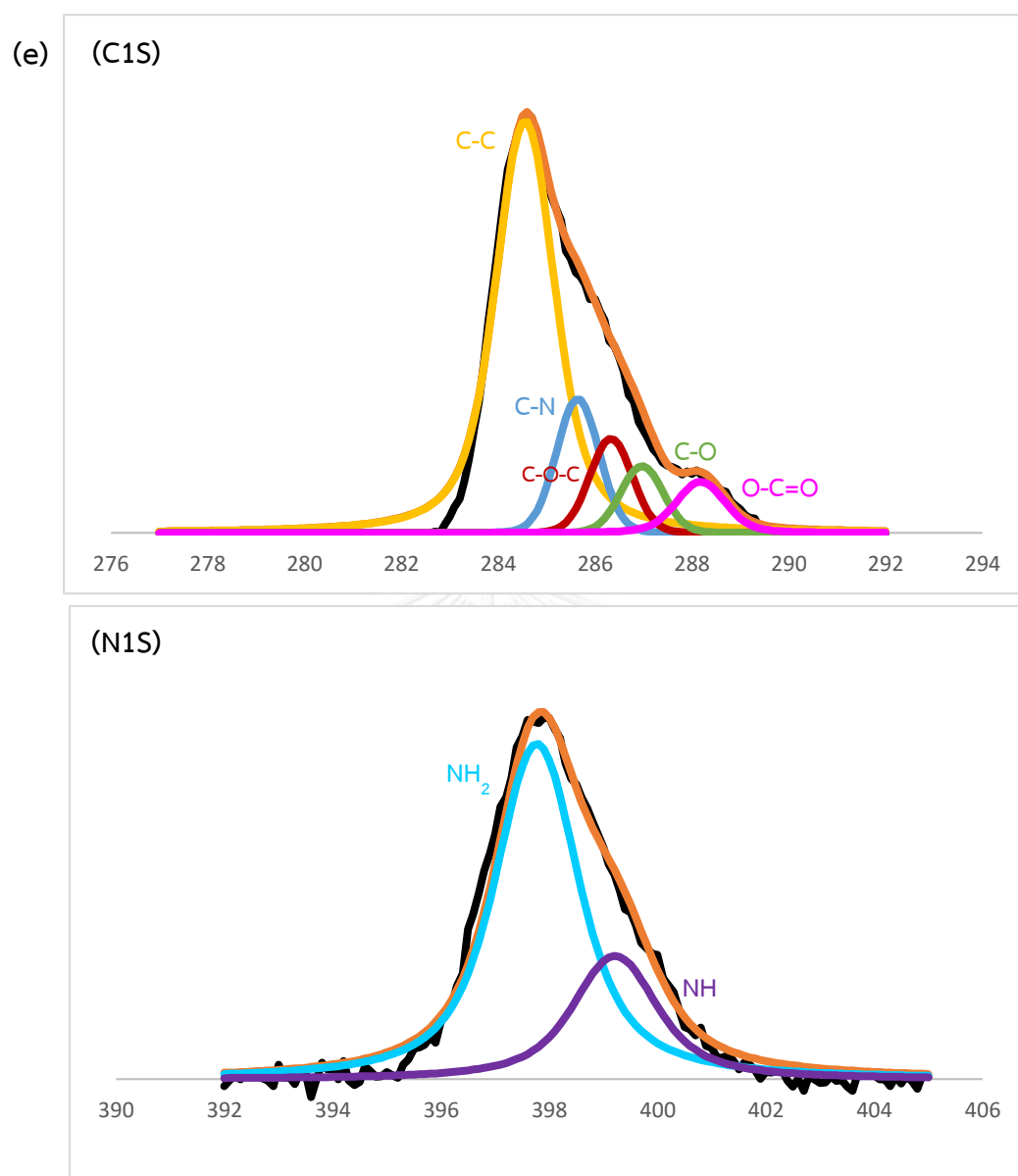


Figure 4.9 XPS spectra of a) A-SBA-15, b) GO, c) A-GO, d) GO-A-SBA-15, and e) A-GO-A-SBA-15

Table 4. 4 Physiochemical characteristic of all synthesized adsorbents

Adsorbents	Surface functional groups	Surface characteristic	BET surface area (m ² /g)	Pore volume (cc/g)	Pore diameter (Å)	PZC	%N	%C
SBA-15	Silanol	Hydrophilic	734.77	1.2780	34.79	5.26	0.00	0.02
A-SBA-15	Amine and silanol	Hydrophilic	310.79	0.7421	47.76	9.60	3.53	10.06
GO	Carboxylic, epoxy, and hydroxyl	Hydrophobic	-	-	-	3.19	0.00	38.53
A-GO	Amine, carboxylic, epoxy, and hydroxyl	Hydrophilic	-	-	-	7.63	7.71	48.73
GO-A-SBA-15	Carboxylic, epoxy, hydroxyl, amine, and silanol	Hydrophobic	96.15	0.1957	40.70	9.24	3.13	15.30
A-GO-A-SBA-15	Amine, carboxylic, epoxy, hydroxyl, and silanol	Hydrophilic	72.84	0.1931	53.01	9.35	3.44	15.50

4.2 ADSORPTION EXPERIMENT

In this study, the adsorptive information was investigated by batch experiment. This adsorption experiment consisted of adsorption kinetic, intraparticle diffusion, and adsorption isotherm which were significant in unit operating process.

4.2.1 Adsorption kinetic experiment

The adsorption kinetic was applied to study rate of adsorption process, rate limiting step, and equilibrium time under batch experiment. In addition, kinetic modeling was used to estimate adsorption characteristic and adsorption mechanism. In this study, the pseudo-first order, the pseudo-second order, and the Ritchie-second order model were investigated.

The pseudo-first order model is given in the linear form as equation 4.1

$$\ln(q_e - q_t) = \ln q_e - k_1 t \quad (4.1)$$

Where q_e and q_t are the amount of adsorbate adsorbed at equilibrium and time (mg/g). t is time (min). k_1 is the pseudo-first-order rate constant (mg/g). The values of k_1 and q_e are determined from slope and intercept of graph plotting between $1/q$ and $1/t$.

Pseudo-second order model can be calculated from the equation 4.2 as followed;

$$\frac{t}{q_t} = \frac{1}{k_2 q_e^2} + \frac{t}{q_e} \quad (4.2)$$

Where k_2 is the pseudo-second order rate constant (g/mg²h).

Ritchie-second order model can be defined as the equation 4.3;

$$\frac{1}{q_t} = \frac{1}{k_r q_e t} + \frac{1}{q'_e} \quad (4.3)$$

Where k_r is the Ritchie-second-order rate constant (1/min) derived from the plots of $1/q_t$ and $1/t$.

4.2.1.1 Adsorption kinetic of CFA at high concentration in pH 7

The adsorption kinetics were performed under batch experiment in controlling of phosphate buffer 0.01 M, pH 7 at 25°C. Moreover, the results of kinetic data were plotted using the pseudo-second order model and the Ritchie-second order model because the pseudo-first order model could not be plotted in some kinetic adsorption due to the indeterminable value and not good correlation coefficient value of R^2 .

4.2.1.1.1 Effect of surface functional group on silica materials

The results of kinetic experiment are shown in Figure 4.10a and Figure 4.10b. On mesoporous silica material (SBA-15 and A-SBA-15), the adsorption capacity of CFA was dramatically increased at an initial stage and reached equilibrium within 1 and 10 minutes, respectively. Thus, the results could be concluded that the equilibrium time became longer after modify cation by amine functional group. It might be caused by the effect of complexity on surface functional group such as steric effect. Moreover, the kinetic curve of SBA-15 and A-SBA-15 showed the best fit with pseudo-second order model as shown in Table 4.5.

4.2.1.1.2 Effect of surface functional group on graphene oxide materials

As Figure 4.10c and Figure 4.10d, the kinetics of GO and A-GO exhibited sharply increase of CFA adsorption at initial stage and reached the equilibrium within 10 and 30 minutes, respectively. It might be caused by the structure of GO surface which had a lot of available active sites on GO nanosheet; therefore, molecules of CFA could

easily be adsorbed on GO sheet. However, for A-GO, it might be the same reason that was discussed in case of amine functionalized SBA-15. Amine functional group on A-GO surface could affect the adsorption rate of CFA due to steric effect. Thus the equilibrium time of A-GO was longer than pristine GO. Moreover, both adsorbents showed the best fit with the pseudo-second order model (as Table 4.5). Comparing with previous study, (Zhang, Liu et al. 2014) also reported that GO reached equilibrium within a few minutes and showed the best correlation coefficient value of R^2 for the pseudo-second order model.

4.2.1.1.3 Effect of GO on silica materials

Adsorption kinetics of GO-A-SBA-15 and A-GO-A-SBA-15 showed greatly increase of capacity at the beginning and achieved the equilibrium within 10 and 15 minutes, respectively (as Figure 4.10e and Figure 4.10f). Comparing with SBA-15 and A-SBA-15, the slightly difference could be observed. Attachment of GO on A-SBA-15 might cause longer time to achieve the equilibrium. Additionally, both adsorbents reported the best correlation coefficient value of R^2 on the pseudo-second order model as Table 4.5.

4.2.1.1.4 Adsorption kinetic of PAC

Adsorption kinetic of PAC showed dramatically increase of capacity at an initial stage and reached the equilibrium within a few minutes (as Figure 4.10g). It might be caused by large specific surface area of PAC and various available functional groups. Thus, the adsorption of CFA on PAC can reach the equilibrium very fast. Moreover, the result could be fit with the pseudo-second order model as shown in Table 4.5.

In summary, CFA adsorption kinetic of SBA-15, A-SBA-15, GO, A-GO, GO-A-SBA-15, A-GO-A-SBA-15, and PAC showed the same equilibrium time that was a few minutes. At the beginning of all kinetic experiments, the concentration of CFA was dramatically decreased (CFA adsorption capacity was increased). Whereas, all adsorbents had different surface such as smooth sheet of GO, porous silica of SBA-15, complex surface functional group of PAC, these factors did not affect the adsorption kinetic of CFA. Moreover, adsorption kinetic of all synthesized adsorbents showed the best correlation coefficient value of R^2 on the pseudo-second order model. The initial rate adsorption of all adsorbents was investigated from the calculation of the pseudo-second order model as ordering; PAC > GO > GO-A-SBA-15 > A-GO-A-SBA-15 > A-GO > SBA-15 > A-SBA-15 (as Table 4.5). It can be seen that the initial rate adsorptions of amine surface functional group adsorbents were less than pristine adsorbents. It could be summarized that complexity of surface structure might decrease the initial rate of adsorption due to steric effect of surface functional groups (except PAC).

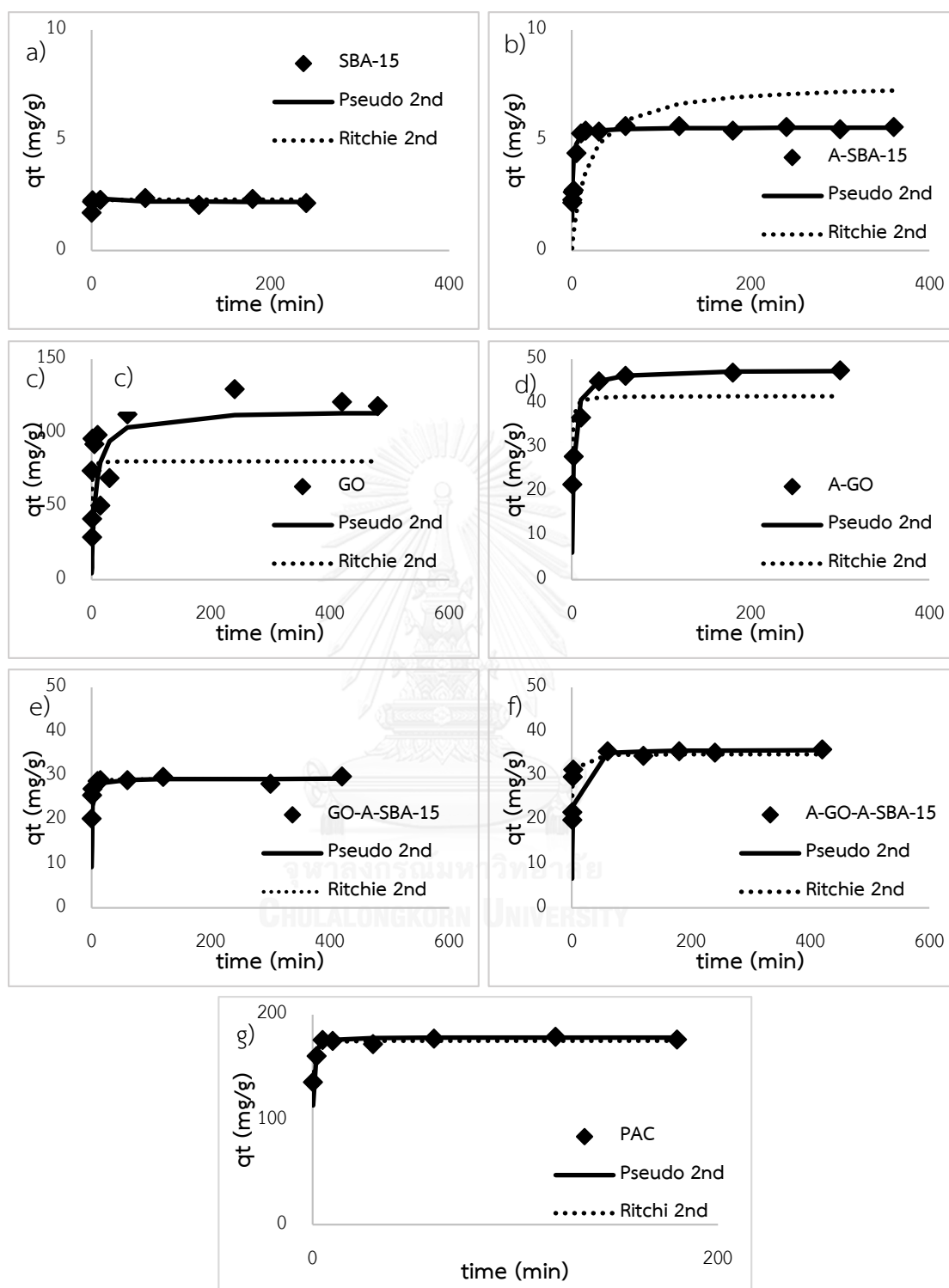


Figure 4.10 The kinetic curves of CFA on a) SBA-15, b) A-SBA-15, c) GO, d) A-GO, e) GO-A-SBA-15, f) A-GO-A-SBA-15, and g) PAC

Table 4.5 The adsorption kinetic parameters of CFA on SBA-15, A-SBA-15, GO, A-GO, GO-A-SBA-15, A-GO-A-SBA-15 and PAC after fitting with the pseudo-second order model and the Ritchie-second order model

Adsorbents	$q_{e,exp}$ (mg/g)	Pseudo-second-order				Ritchie-second-order		
		$q_{e,cal}$ (mg/g)	k_2 (g/mg.min)	h	R^2	$q_{e,cal}$ (mg/g)	k_r (L/min)	R^2
SBA-15	2.1657	2.2065	0.2277	10.8460	0.9972	2.2789	15.6157	0.6423
A-SBA-15	5.6090	5.5866	0.1157	3.6101	0.9998	7.6104	2.2700	0.9958
GO	120.4819	121.9512	0.0101	147.0588	0.9987	89.2857	3.5000	0.2248
A-GO	47.4911	47.6191	0.0062	14.0845	0.9999	41.6667	4.1379	0.7991
GO-A-SBA-15	29.8559	29.3255	0.0316	27.1739	0.9989	29.,2398	9.5000	0.9529
A-GO-A-SBA-15	35.9663	35.8423	0.0127	16.3399	0.9998	34.8432	4.7833	0.9337
PAC	178.4298	178.5714	0.0196	625.0000	0.9999	131.5789	-25.3333	0.8912

4.2.1.2 Adsorption kinetic of NAP on synthesized adsorbents at high concentration in pH 7

The adsorption kinetics were performed under batch experiment in controlling of phosphate buffer 0.01 M, pH 7 at 25°C. Additionally, the results of kinetic data were plotted by using the pseudo-second order model and the Ritchie-second order model. However, the pseudo-first order model could not be plotted in some kinetic adsorption due to the indeterminable value and not good correlation coefficient value of R^2 .

4.2.1.2.1 Effect of surface functional group on silica materials

Adsorption kinetic of NAP on SBA-15 and A-SBA-15 are shown in Figure 4.11a and Figure 4.11b, respectively. Adsorption capacity of NAP on both materials was not occurred.

4.2.1.2.2 Effect of surface functional group on graphene oxide materials

According to Figure 4.11c and Figure 4.11d, the kinetics of GO and A-GO showed dramatically increase of NAP adsorption capacity at initial stage and reached the equilibrium within 1 and 2 hours, respectively. It might be caused by the structure of GO which had an abundant of available active sites on the surface of GO nanosheet. For A-GO, amine functional group on A-GO surface might be an obstacle for NAP adsorption via hydrophilicity. Thus the equilibrium time of A-GO was longer than pristine GO. Besides, adsorption kinetic of GO and A-GO were fitted well with the pseudo-second order model as Table 4.6.

4.2.1.2.3 Effect of GO on silica materials

After modified GO on SBA-15, the kinetics of GO-A-SBA-15 and A-GO-A-SBA-15 showed the strongly increase of NAP capacity at the beginning and achieved the equilibrium within 2 and 4 hours, respectively (as Figure 4.11e and Figure 4.11f). Comparing with GO and A-GO, no significant difference could be investigated. It could be emphasized that the adsorption capacity might be occurred only on GO and A-GO surface, since silicate material (SBA-15 and A-SBA-15) cannot adsorbed NAP. However, the presence of silicate material and amine functional group in GO-A-SBA-15 and A-GO-A-SBA-15 might inhibit the adsorption of NAP on GO. Thus, the adsorption kinetics on GO-A-SBA-15 had longer equilibrium time than GO and A-GO. As same as all

synthesized materials the adsorption kinetics of GO-A-SBA-15 and A-GO-A-SBA-15 showed the best correlation coefficient value of R^2 on the pseudo-second order model (as Table 4.6).

4.2.1.2.4 Adsorption kinetic of PAC

Adsorption kinetic of NAP on PAC are reported in Figure 4.11g. Adsorption capacity was increased at the beginning and reached the equilibrium within 9 hours. Adsorption capacity of NAP on PAC was much higher than synthesized adsorbents. It might be caused by the complexity of PAC surface functional groups. However, the adsorption kinetic of NAP on PAC can achieve the equilibrium stage very slow. This might be caused by the surface and porous complexity of PAC. Obtained kinetic results could be fitted well with the pseudo-second order model (as Table 4.6).

In conclusion, the results of kinetic experiment on mesoporous silica material GO, A-GO, GO-A-SBA-15, A-GO-A-SBA-15, and PAC showed the different equilibrium time depend on the surface functional group and specific surface area of adsorbent following; $GO > A-GO > GO-A-SBA-15 > A-GO-A-SBA-15$. Different surface structure (such as smooth sheet of GO, porous silica of SBA-15 and abounding surface functional group of PAC) might affect the adsorption kinetic of NAP. Moreover, the initial rate adsorption of all adsorbents was investigated from the calculation of the pseudo-second order model as ordering; $GO > PAC > A-GO > GO-A-SBA-15 > A-GO-A-SBA-15 > A-GO$ (as Table 4.6). It could be summarized that amine functional groups might decrease the initial rate of adsorption due to hydrophilicity. Thus, the initial rate adsorptions of amine surface functionalized adsorbents were less than pristine adsorbents.

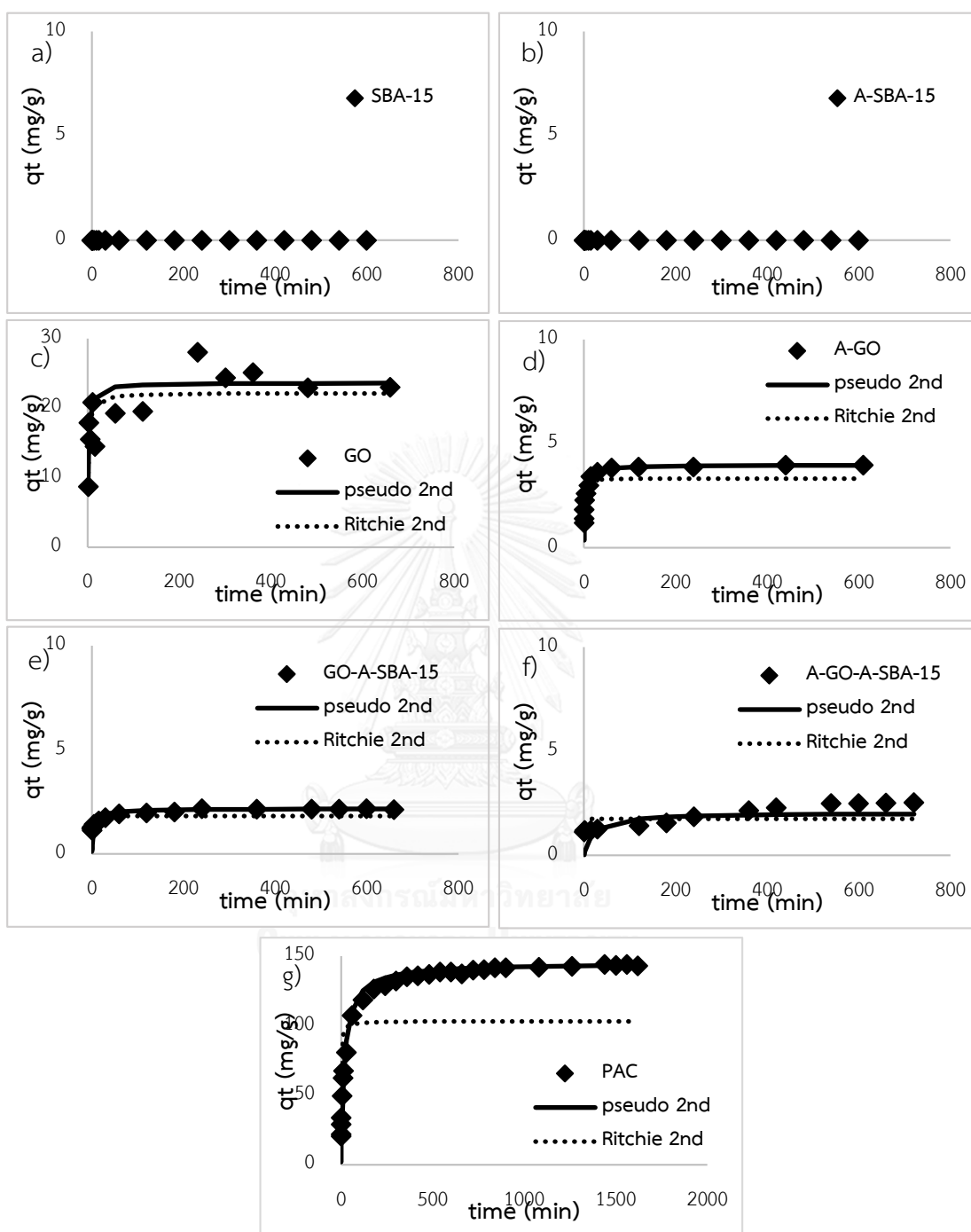


Figure 4.11 The kinetic curves of NAP on a) SBA-15, b) A-SBA-15, c) GO, d) A-GO, e) GO-A-SBA-15, f) A-GO-A-SBA-15, and g) PAC

Table 4.6 The adsorption kinetic parameters of NAP on SBA-15, A-SBA-15, GO, A-GO, GO-A-SBA-15, A-GO-A-SBA-15 and PAC after fitting with the pseudo-second order model and the Ritchie-second order model

Adsorbents	$q_{e,exp}$ (mg/g)	Pseudo-second-order				Ritchie-second-order		
		$q_{e,cal}$ (mg/g)	k_2 (g/mg.min)	h	R^2	$q_{e,cal}$ (mg/g)	k_r (L/min)	R^2
SBA-15	-	-	-	-	-	-	-	-
A-SBA-15	-	-	-	-	-	-	-	-
GO	22.9762	23.6407	0.0132	7.3638	0.9937	22.1730	0.7251	0.7738
A-GO	3.9633	3.9667	0.0535	0.8413	0.9999	3.3289	1.8881	0.8845
GO-A-SBA-15	2.1546	2.1744	0.0568	0.2683	0.9997	1.8278	5.6344	0.4974
A-GO-A-SBA-15	2.5279	2.0458	0.0127	0.0533	0.9627	1.7683	6.3754	0.2521
PAC	143.6627	144.9275	0.0002	3.8256	0.9997	103.0928	0.7760	0.7518

4.2.2 Intraparticle diffusion mechanism

Generally, the mechanism of solid-liquid phase adsorption has three steps (Albadarin, Mangwandi et al. 2012). The first step is film diffusion process which is the transportation of adsorbate from bulk solute through the external surface of adsorbent. The second step is intraparticle diffusion or pore diffusion process which is the movement of adsorbate through the interior of adsorbent particle. The last step is adsorption process which is the adsorption of adsorbate onto the interior active sites of adsorbent. The intraparticle diffusion mechanism of all kinetic data were analyzed using Weber and Morris intraparticle diffusion to study the diffusion mechanism and the rate limiting step of adsorption process. The Weber and Morris intraparticle diffusion model can be shown as Equation 4.4;

$$q_t = k_p t^{\frac{1}{2}} + C \quad (4.4)$$

Where k_p is the intraparticle diffusion rate constant ($\text{mg/g}\cdot\text{min}^{1/2}$) and C is constant related to the thickness of boundary layer (mg/g) which was calculated from the plot of q_t versus $t^{1/2}$.

According to intraparticle diffusion model, the graph is plotted between q_t and $t^{1/2}$ which should be a linear line. Additionally, if the graph passes through the origin, it can be suggested that the intraparticle diffusion step is rate limiting step (Lewinsky 2007). On the other hand, if the graph does not pass through the origin, it means that the external mass transfer has important role in the adsorption process.

4.2.2.1 Intraparticle diffusion of CFA

The intraparticle plots of CFA onto all adsorbents could be divided into three stages (multi-linearity pattern as Figure 4.12). Similar behaviors were reported for all adsorbents which had three step of adsorption. The external diffusion mechanism was occurred at the initial step followed by the intraparticle diffusion mechanism as the second step. The results of both steps showed that the first step of the external diffusion mechanism had more rate constant (k_i) than the second step of the intraparticle diffusion mechanism.

The rate of external diffusion mechanism could be discussed base on the characteristics of the surface of adsorbents. The results were reported as shown in Table 4.7 that the pristine surface functional group had more value than the modified amine functional group on adsorbents which could be ordered as following; GO, GO-A-SBA-15, A-GO-A-SBA-15, A-GO, SBA-15, and A-SBA-15. This can be suggested that amine functional group could decrease the adsorption rate of CFA on the all synthesized adsorbents. It might be caused by steric effect from multi-functional group

on the surface of adsorbent (as Figure 4.13). Moreover, there might be no doubt that the modification of GO could increase the rate of the external diffusion mechanism.

For the second step, pore size of adsorbent might have the important role in this part. The pore size of mesoporous silica materials could be ordered as A-SBA-15 > SBA-15. Thus the rate constant of the intraparticle diffusion of SBA-15 was less than A-SBA-15 as shown in table 4.7. Similarly, GO modified SBA-15 materials showed the same trend as mesoporous silica material. The pore size of GO modified SBA-15 materials could be ordered as A-GO-A-SBA-15 > GO-A-SBA-15. Therefore, the rate constant of the intraparticle diffusion of GO-A-SBA-15 was less than A-GO-A-SBA-15 as shown in table 4.7. For all synthesized adsorbents, GO modified SBA-15 materials exhibited larger value than mesoporous silica materials. Definitely, CFA could be adsorbed easily on all synthesized adsorbents because CFA has very small size (9.4 Å) comparing with the pore sized of SBA-15, A-SBA-15, A-GO, GO-A-SBA-15, and A-GO-A-SBA-15 which were 34.79, 47.76, 40.70, and 53.01 Å, respectively.

Besides, the plots of CFA on SBA-15, A-SBA-15, A-GO, GO-A-SBA-15, and A-GO-A-SBA-15 showed that they did not pass through the origin (as Figure 4.13), thus the intraparticle diffusion was not only the rate-limiting step but the external mass transfer also had the crucial role in the adsorption process. Although, the plot of GO showed passing through the origin, intraparticle diffusion should be neglected. Since, GO do not have porous structure.

For adsorption of CFA on PAC, the rate constant of the external diffusion showed nearly the highest value when comparing with all synthesized adsorbent. Whereas, the intraparticle diffusion mechanism, PAC did not exhibit the lowest value even the pore size was the smallest (13.92 Å) comparing with all synthesized adsorbents. Moreover, a plot of the intraparticle diffusion model did not pass through

the origin, hence external mass transfer might play the significant role in this adsorption process (as Figure 4.12).

In short, the study of adsorption mechanism by using Weber and Morris model showed that the slowest step of all porous adsorbents was the intraparticle diffusion step. And it might be the rate limiting step; however, the plots of all adsorbents (except GO) did not pass through the origin, the external mass transfer might play the important role in the adsorption process.



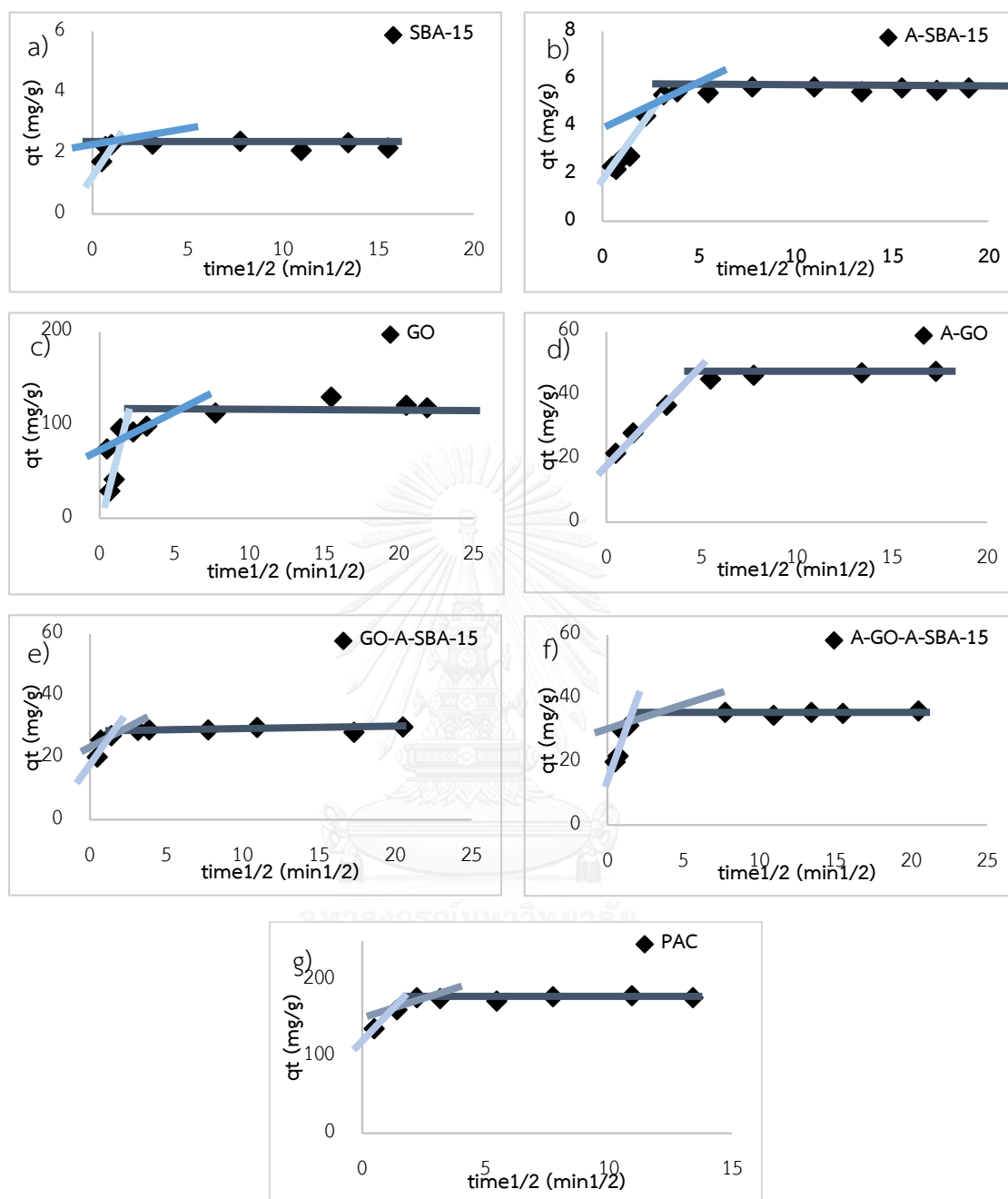


Figure 4.12 Plots of intraparticle diffusion model (Weber and Morris) for the adsorption of CFA on a) SBA-15, b) A-SBA-15, c) GO, d) A-GO, e) GO-A-SBA-15, f) A-GO-A-SBA-15, and g) PAC.

Table 4.7 Intraparticle diffusion parameters of CFA adsorption on SBA-15, A-SBA-15, GO, A-GO, GO-A-SBA-15, A-GO-A-SBA-15, and PAC

Adsorbents	External diffusion step			Intraparticle diffusion step		
	k_s (mg/g.min ^{1/2})	C	R ²	k_p (mg/g.min ^{1/2})	C	R ²
SBA-15	2.4275	0.5072	1	0.0178	2.2562	0.9736
A-SBA-15	1.4571	1.1841	0.9996	0.0643	5.1677	0.9404
GO	27.5850	11.4950	0.9964	-	-	-
A-GO	5.5925	19.3480	0.9926	-	-	-
GO-A-SBA-15	25.9560	7.2484	1	0.1122	28.5130	0.9986
A-GO-A-SBA-15	20.1650	8.9488	0.9368	0.7698	29.6210	0.9492
PAC	27.0740	122.5900	1	0.4710	173.8900	0.9999

4.2.2.2 Intraparticle diffusion of NAP

The intraparticle plots of NAP onto all adsorbents could be divided into three stages multi-linearity pattern as Figure 4.13. The same mechanism was reported for all adsorbents which had three step of adsorption. The external diffusion mechanism was occurred at the initial step then the intraparticle diffusion mechanism was occurred in the second step. The results of both steps reported that the rate constant (k_i) of the external diffusion mechanism was higher than the rate constant (k_i) of the intraparticle diffusion mechanism.

Particularly, the external diffusion rate mechanism could be described by the functional group on the surface of adsorbents. The results were shown in Table 4.8 that amine functional group could be decrease the rate of external diffusion mechanism as followed; GO, A-GO, GO-A-SBA-15, and A-GO-A-SBA-15 meaning that amine functional group might have the negative effect on the rate adsorption of NAP on the all synthesized adsorbents. When comparing with the GO material and GO modified SBA-15 material, the results of rate constant showed that after modified with

SBA-15, the rate of adsorption exhibited the strongly decrease. It could be obviously concluded that the presence of A-SBA-15 might disturb the adsorption of NAP on GO-A-SBA-15.

For the intraparticle diffusion step, pore size of adsorbent might play the crucial role in this part. The pore size of mesoporous silica material could be ordered as A-GO-A-SBA-15 > GO-A-SBA-15. In contrast, the rate constant of the intraparticle diffusion of A-GO-A-SBA-15 was less than GO-A-SBA-15 as shown in Table 4.8. It might be the size of NAP (640 Å) which is bigger than pore size of GO-A-SBA-15 and A-GO-A-SBA-15 (40.70 and 53.01 Å, respectively). Thus the pore size of adsorbent could not play important role in this part because NAP cannot access into the internal surface of adsorbent.

Moreover, the plots of GO, A-GO, GO-A-SBA-15, and A-GO-A-SBA-15 showed that they did not pass through the origin. Hence the intraparticle diffusion might not be only the rate-limiting step but the external mass transfer also had the crucial role in the adsorption process (as Figure 4.13).

For adsorption of NAP on PAC, the rate constant of the external diffusion mechanism and the intraparticle diffusion mechanism showed the highest value when comparing with all synthesized adsorbent. Moreover, a plot of the intraparticle diffusion model passed through the origin so the intraparticle diffusion was the rate limiting step of the adsorption of NAP on PAC (as Figure 4.13). Whereas, the mean pore size of PAC (13.92 Å) was the smaller than the size of NAP (640 Å). Thus, pore size of all adsorbents might not involve with this mechanism. However, according to the pore size distribution of PAC (Prarat 2011) that showed very wide range of pore size up to macro pore, this make the intraparticle diffusion phenomena of NAP on PAC surface still can be detected.

Overall, the investigation of mechanism by Weber and Morris model reported that the slowest step of all adsorbents was the intraparticle diffusion step (except GO and A-GO). However, the plots of all adsorbents except PAC did not pass through the origin, the external mass transfer might have the important role in the adsorption of NAP. In addition, the adsorption of NAP on PAC could be obvious that the intraparticle diffusion was rate limiting step because the plot passed through the origin.

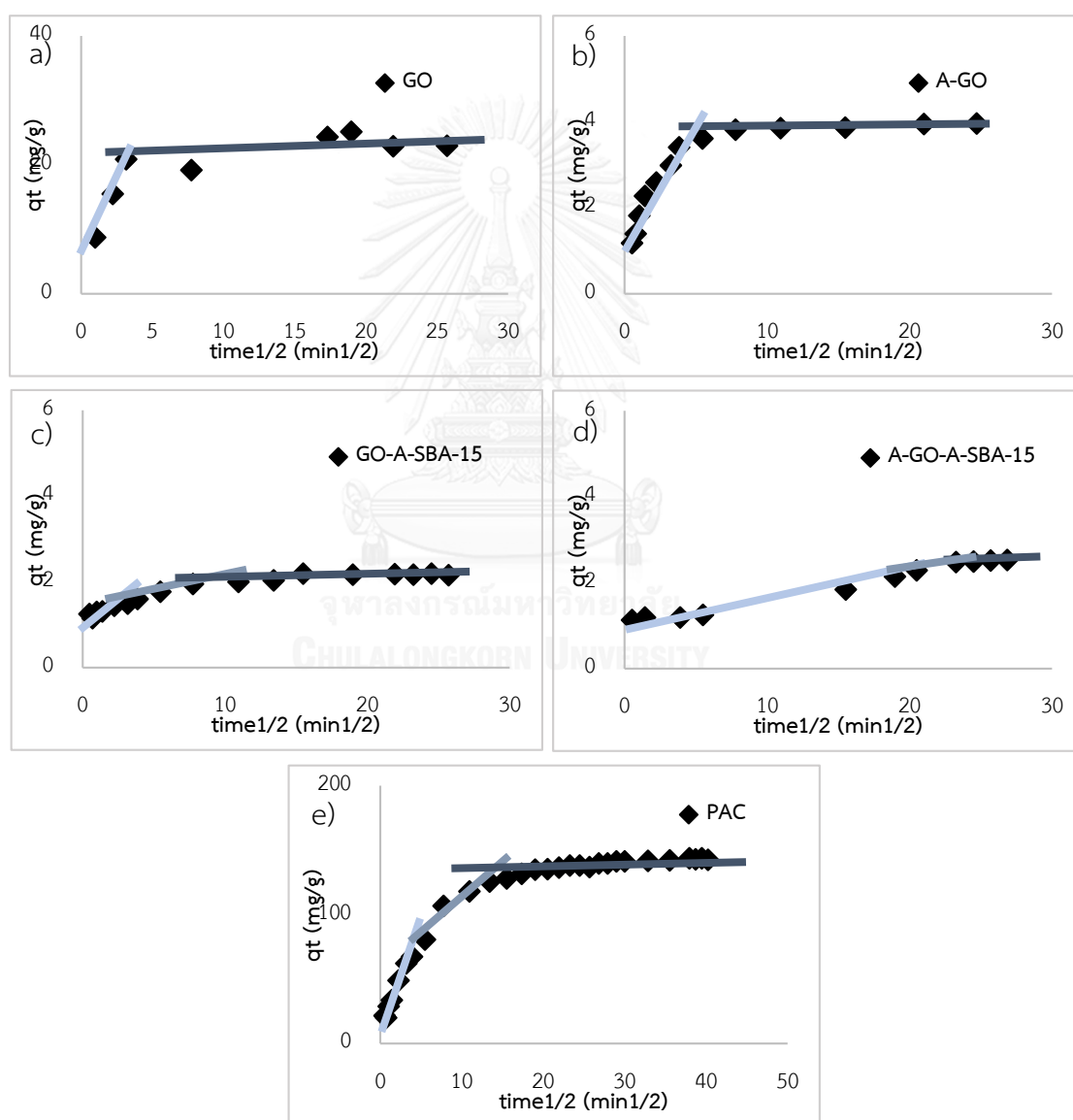


Figure 4.13 Plots of intraparticle diffusion model (Weber and Morris) for the adsorption of NAP on a) GO, b) A-GO, c) GO-A-SBA-15, d) A-GO-A-SBA-15, and e) PAC.

Table 4.8 Intraparticle diffusion parameters of NAP adsorption on SBA-15, A-SBA-15, GO, A-GO, GO-A-SBA-15, A-GO-A-SBA-15, and PAC

Adsorbents	External diffusion step			Intraparticle diffusion step		
	k_s (mg/g.min ^{1/2})	C	R ²	k_p (mg/g.min ^{1/2})	C	R ²
SBA-15	-	-	-	-	-	-
A-SBA-15	-	-	-	-	-	-
GO	5.6076	3.0509	0.9998	-	-	-
A-GO	1.2344	0.5348	0.9891	-	-	-
GO-A-SBA-15	0.2091	1.0306	0.7026	0.0967	1.2057	0.9885
A-GO-A-SBA-15	0.0543	1.0448	0.9711	0.0164	2.0920	0.9658
PAC	16.6820	10.3380	0.9905	9.8079	29.5220	0.9904

4.2.3 Adsorption isotherms

In order to study the relationship between equilibrium concentration of adsorbate and adsorption capacity of adsorbent, adsorption isotherms were investigated after equilibrium time. The adsorption model of both pharmaceuticals on all adsorbents; the linear, Langmuir, and Freundlich mathematical isotherm models, were used to evaluate the adsorption isotherm data. The linear isotherm can be given as Equation 4.5;

$$q_e = K_p C_e \quad (4.5)$$

Where K_p is the linear constant (L/g)

The linear form of the Langmuir isotherm can be described as Equation 4.6;

$$\frac{1}{q_e} = \frac{1}{q_m} + \frac{1}{k_L q_m q_e'} \quad (4.6)$$

Where k_L is the Langmuir constant and q_m is the maximum adsorption capacity (mg/g).

The linear form of the Freundlich isotherm can be described as Equation 4.7;

$$\ln q_e = \ln k_F + \frac{1}{n} \ln C_e \quad (4.7)$$

Where k_F is the Freundlich constant and n is the adsorption intensity (dimensionless).

4.2.3.1 Adsorption isotherms of CFA at high concentration in pH 7 (single solute)

The adsorption isotherms were performed under batch experiment in controlling of phosphate buffer 0.01 M, pH 7 at 25°C. The results were reported in the relationship between equilibrium concentration (C_e) in the unit of mg of adsorbate per L of solute as X axis and adsorption capacity (q_e) in the unit of mg of adsorbate per g of adsorbent as Y axis. Moreover, the results of isotherm data were fitted using linear model, Langmuir model, and Freundlich model.

4.2.3.1.1 Effect of surface functional group on silica material

The results of adsorption capacity on SBA-15 and A-SBA-15 were showed in Figure 4.14. On pristine SBA-15, the adsorption capacity was reported around 2 mg/g at the equilibrium concentration 10 ppm. Interestingly, after modification of amine functional group, the adsorption capacity was increase to 6 mg/g at the same equilibrium concentration (10 ppm). The effect of amount of grafted amine functional groups was already reported by previous researcher. In this study, amine functional group on SBA-15 also increased adsorption capacity of CFA. Moreover, adsorption isotherm in form of capacity per amount of nitrogen was also reported in figure 4.15 It might be caused by hydrophilic interaction, hydrogen bonding as well as elctrostatic

interaction between amine functional group and CFA (Water solubility of CFA is 582.5 mg/L as Table 2.1).

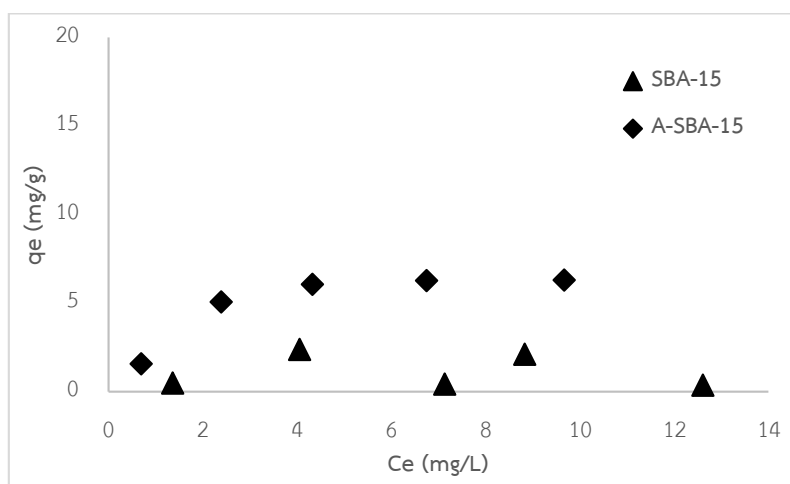


Figure 4.14 Comparison of pristine functional group and amine functional group on mesoporous silica materials in adsorption capacity of CFA

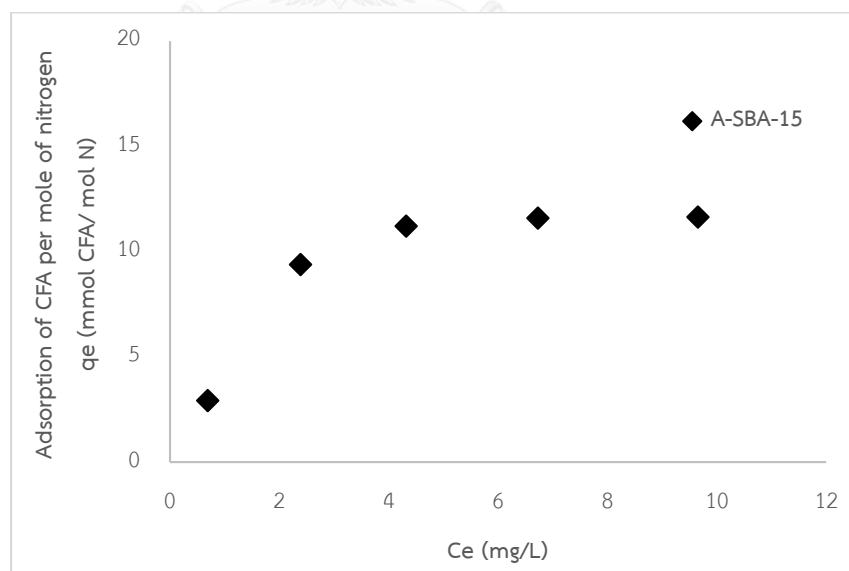


Figure 4.15 Effect of the amount of nitrogen on mesoporous silica materials in adsorption capacity of CFA

In order to deduce the effect of surface area on CFA adsorption capacity, adsorption capacity per unit of square meter (m^2) was plotted to investigate only the effect of surface functional group of mesoporous silica adsorbents on the adsorption capacity of CFA (as Figure 4.16). The results of BET reported the surface area of SBA-15 and A-SBA-15 at 734.77 and 310.79 m^2/g , respectively. It was clear that amine functional groups on A-SBA-15 had more affinity to adsorb CFA than silanol groups on pristine SBA-15. Thus comparing with effective surface functional group (amine group), surface area might have no significant impact on the adsorption of CFA.

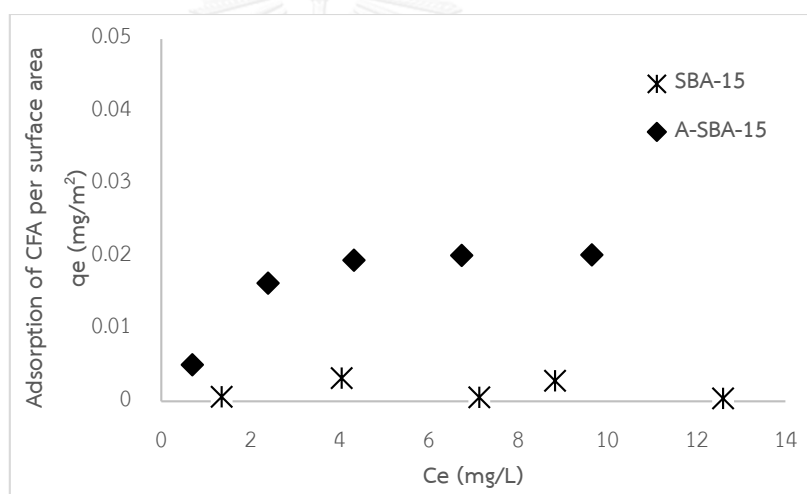


Figure 4.16 Effect of surface area on mesoporous silica materials in adsorption capacity of CFA

In addition, electrostatic attraction is supposed to involve with enhancing the adsorption capacity. According to the results of PZC, SBA-15 was reported the PZC at 5.26 meaning that at pH 7 surface charge of SBA-15 represents negative charge. On the other hand, PZC of A-SBA-15 was 9.60 indexing the positive charge at pH 7. Moreover, pKa of CFA was 2.84 representing negative charge at pH 7 as Table.4.15 and Table 4.16

When fitting with the adsorption isotherm model such as Linear, Langmuir, Freundlich isotherm model. The results of SBA-15 did not showed the good fit with any isotherm model; however, the adsorption isotherm of A-SBA-15 represented the best correlation coefficient value of R^2 on Langmuir isotherm model meaning that the adsorption of CFA was monolayer adsorption on A-SBA-15 as Figure 4.20.

Aforementioned, the increasing of adsorption capacity on A-SBA-15 might be the possibility of hydrophobic interaction and H-bonding between CFA and A-SBA-15. Moreover, the electrostatic attraction might be occurred between the negative charge of CFA and the positive charge of A-SBA-15. And the adsorption of CFA on A-SBA-15 was monolayer adsorption.

4.2.3.1.2 Effect of surface functional group on graphene oxide materials

The results of adsorption isotherms on GO and A-GO were showed in Figure 4.17. On pristine GO, the adsorption capacity was reported around 117 mg/g at the equilibrium concentration around 10 ppm. Although GO presented negative surface charge at pH7 as Table 4.16, GO was exhibited very high adsorption capacity for CFA. It might relate to π - π interaction between aromatic ring being the main factor more than electrostatic repulsion in this process. XPS spectra of GO in the phosphate buffer solution (Figure 4.18a) showed the satellite of π to π^* transition from unsaturated structure and XPS spectra after adsorption of CFA (Figure 4.18b) was also exhibited the satellite. It was supposed to be involved with pi conjugation in adsorption mechanism. However, XPS spectra of GO in DI water (Figure 4.18c) did not represented the satellite due to saturated structure and XPS spectra after adsorption process (Figure 4.18d) was presented the same result. It could not reported any mechanisms. Indeed, it might be expected for π - π interaction (Yang, Rochette et al. 2005, Teng, Ma et al. 2011).

Moreover, other forces such as hydrophilicity, H- bonding, and Van der Waals' force might be involve with the adsorption process of CFA on GO materials (Zhang, Liu et al. 2014). Besides, the data of adsorption isotherms of GO was represented the best fit with Freundlich isotherm model indicating the multilayer adsorption.

Expecially, after modification of two amine functional group, the adsorption capacity was strongly decrease to 50.5 mg/g at the equilibrium concentration around 8 ppm even A-GO presented slightly positive surface charge at pH 7. This might be suggested that interaction of amine groups precursor (Diethylenetriamine) during modification step might cause the decreasing of over all active site on A-GO by double interaction between amine (2 amine groups) and epoxy group of pristine GO. It might be the intra-interaction between amine functional group and the epoxy group on the surface of GO. It was not only causing the lose of specific active site on A-GO surface, but it can increase the folding of A-GO sheet as seen in SEM image (Figure 4.7) but also losed the amine functional group which had the ability in adsorption of CFA. Moreover, the adsorption isotherms of A-GO reported the best fit with Linear isotherm model which normally presented in the initial part of many practical isotherms meaning the valid for low surface coverages, and the adsorption energy being independent of the coverage.

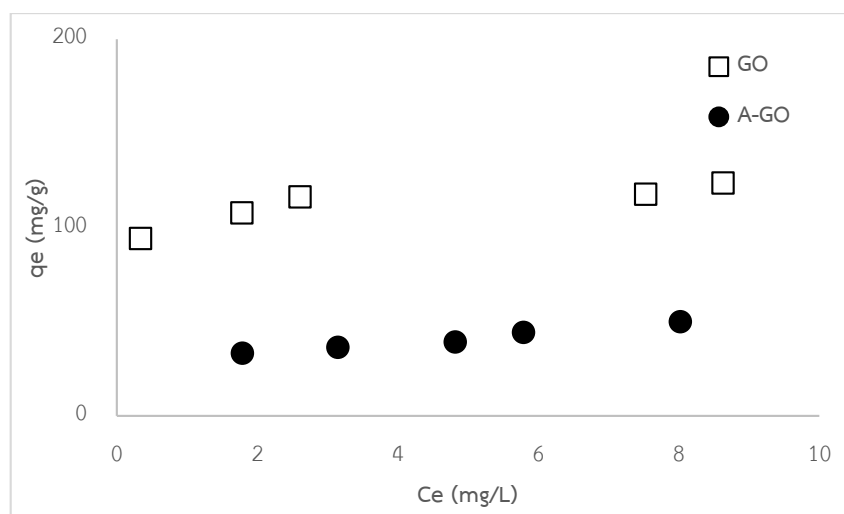
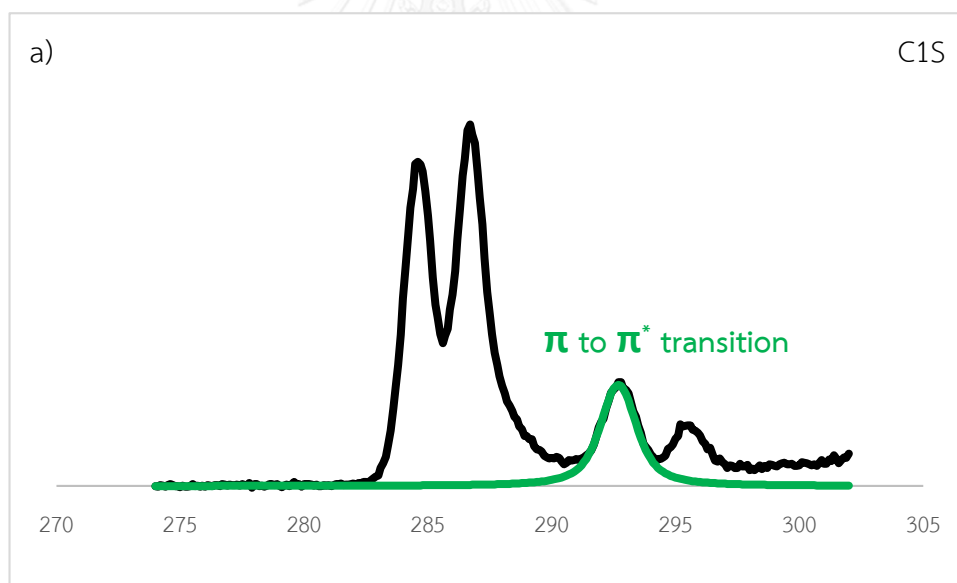
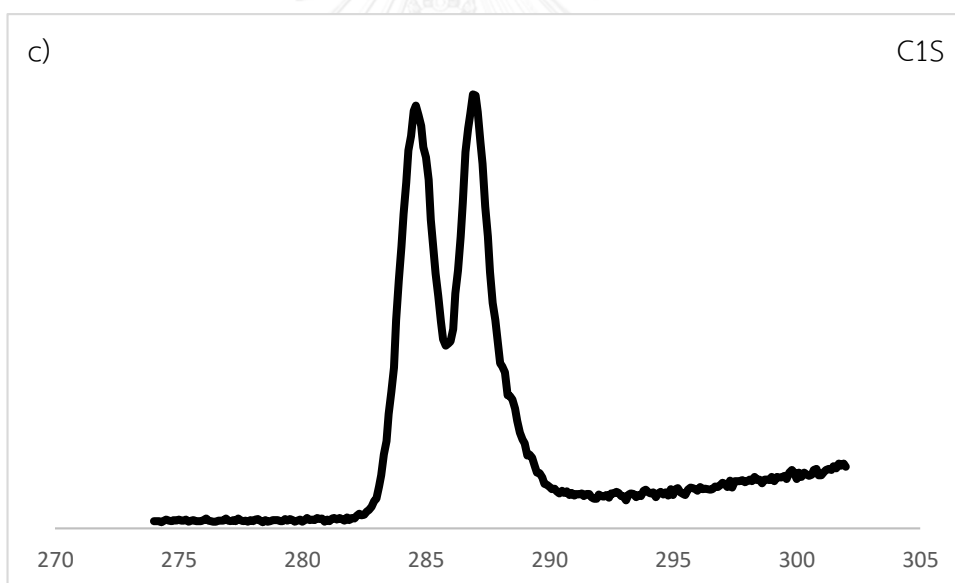
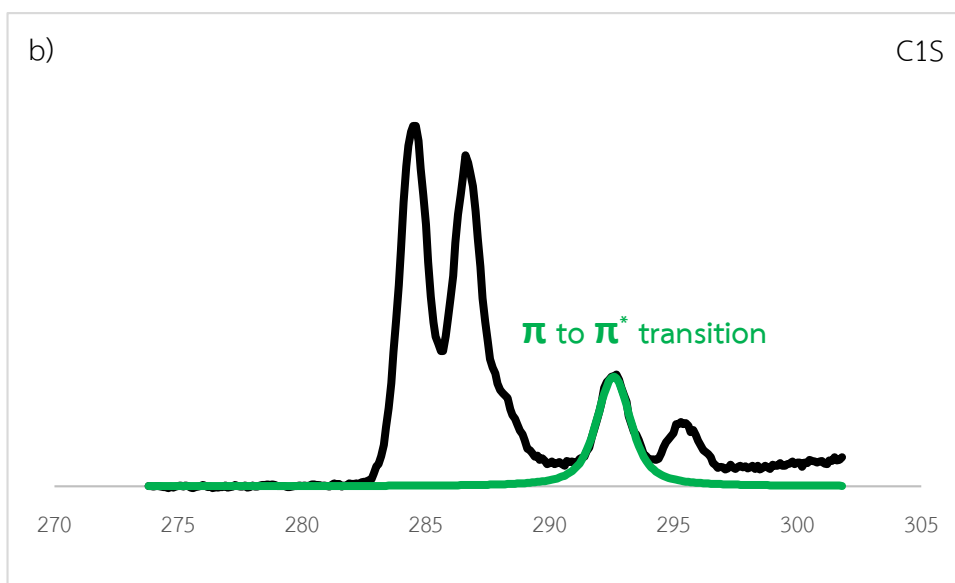


Figure 4.17 Comparison of pristine functional group and amine functional group on GO materials in adsorption capacity of CFA.





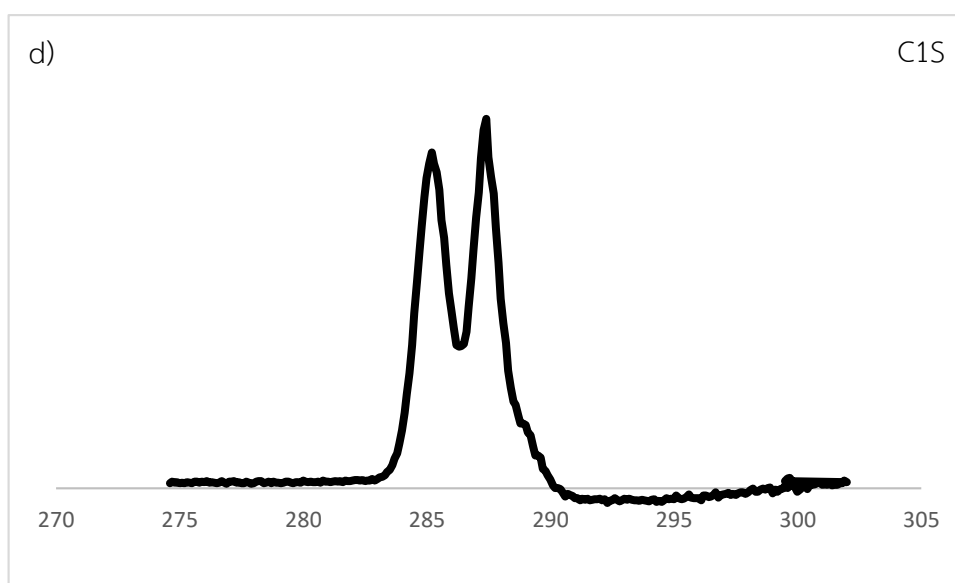


Figure 4.18 XPS spectra of a) GO dispersed in phosphate buffer b) the adsorption for CFA on GO dispersed in phosphate buffer c) GO dispersed in DI d) the adsorption for CFA on GO dispersed in DI

4.2.3.1.3 Effect of GO modified silica materials

Adsorption isotherms on GO-A-SBA-15 and A-GO-A-SBA-15 were shown in Figure 4.19. The adsorption capacity of GO-A-SBA-15 was reported around 29 mg/g at the equilibrium concentration 10 ppm. The main factors might be π - π interaction, hydrophilicity, H-bonding, and electrostatic attraction between negative charge of CFA and positive charge on the surface of GO-A-SBA-15. Moreover, adsorption of CFA on GO-A-SBA-15 was reported the best correlation coefficient value of R^2 on Linear isotherm model which always occurs in the beginning part of many adsorption isotherms.

After modification of amine functional group, the adsorption capacity of A-GO-SBA-15 was slightly increase to 35 mg/g at equilibrium concentration 10 ppm. As a result of adsorption isotherm, Langmuir isotherm model showed the best fit with

adsorption of CFA on A-GO-A-SBA-15 meaning that the adsorption was monolayer. The obtained results showed the opposite trend comparing with the data set of GO and A-GO. The presence of amine group on A-GO attached on A-SBA-15 (A-GO-A-SBA-15) did not reduce the CFA adsorption capacity. It can be suggested that after fixing pristine GO sheet on A-SBA-15, GO could not move freely or hardly move so that the intra-interaction of double amine functional group of Diethylenetriamine on GO surface might rarely occurred in A-GO-A-SBA-15 case.

Thus amine functional group on A-GO-A-SBA-15 could increase adsorption capacity of CFA due to π - π interaction, hydrophilicity, H-bonding, and electrostatic attraction between amine functional group and CFA.

Interestingly, when comparing the adsorption capacity of pure GO and GO-A-SBA-15 which were 117 and 29 mg/g at the equilibrium concentration 10 ppm, respectively. The obtained results showed the significant difference adsorption capacity between both adsorbents. This should be discussed base on the quantity of GO which attached on GO-A-SBA-15 material as shown in Table 4.9. The percentage of GO in pure GO was 100% and the percentage of GO in GO-A-SBA-15 was 12.44%. After calculation of CFA adsorption capacity of GO 12.44% from pure GO and from GO-A-SBA-15, the approximately capacities were showed at 14.5 mg/g and 18.3 mg/g, respectively. The CFA adsorption capacity GO on GO-A-SBA-15 at the same percentage of pure GO was exhibited the higher than pristine GO. One possible discussion might be the agglomeration of pure (or pristine) GO. Therefore, the results of GO and GO-A-SBA-15 were reasonable when discussion in the quantitative analysis of GO.

Nevertheless, the comparison between A-GO and A-GO-A-SBA-15 did not follow the quantitative analysis as the series of A-GO like discussed above. It might relate to the folding phenomena of A-GO, which did not occur when double amine functional group of Diethylenetriamine was attached on GO-A-SBA-15 surface. Hence, if we

compare the effect of A-GO on A-GO-SBA-15 with the same ratio of pristine GO, the approximately same level of CFA adsorption capacity of A-GO ratio (on A-GO-SBA-15) and pure GO ratio can be detected. Moreover, the effect of amine functional group might be increase adsorption capacity of CFA on A-GO-A-SBA-15.

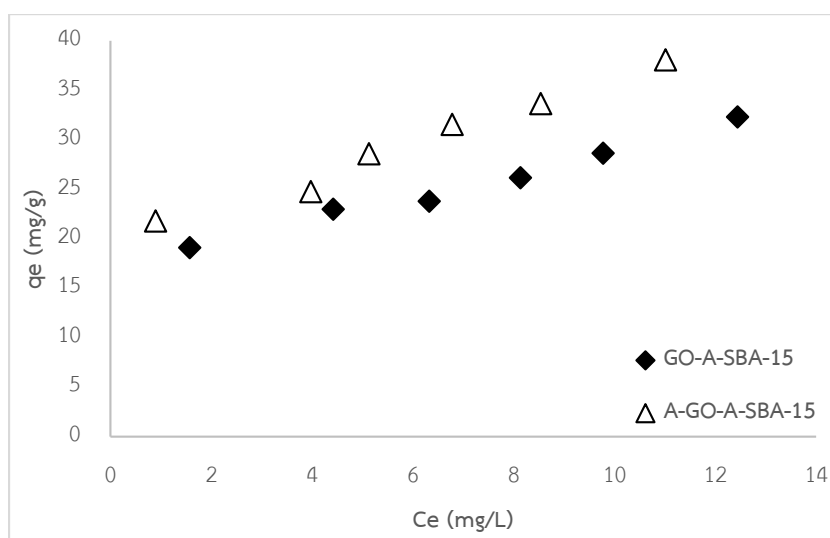


Figure 4.19 Comparison of pristine functional group and amine functional group on GO modified A-SBA-15 materials in adsorption capacity of CFA.

Table 4.9 Percentage of A-SBA-15, GO, and A-GO in synthesized adsorbents for the adsorption capacity of CFA

Adsorbent	Percentage	Adsorption capacity of CFA, q_e (mg/g)
A-SBA-15	A-SBA-15 = 100%	6
	A-SBA-15 = 87.56%	5.3
	A-SBA-15 = 86.64%	5.2
GO	GO = 100%	116.3
	GO = 12.44%	14.5
GO-A-SBA-15	GO-A-SBA-15 = 100%	23.6
	GO = 12.44%	18.3
	A-SBA-15 = 87.56%	5.3
A-GO	A-GO = 100%	33.5
	A-GO = 13.36%	4.5
A-GO-A-SBA-15	A-GO-A-SBA-15 = 100%	24.7
	A-GO = 13.36%	19.5
	A-SBA-15 = 86.64%	5.2

4.2.3.1.4 The adsorption capacity of PAC

Comparing between the synthesized adsorbents and PAC, the adsorption capacity of CFA on PAC was reported the highest adsorption capacity around 125.3 mg/L (as Figure 4.20a) at the equilibrium concentration 10 ppm. As already discussed

in adsorption kinetic, PAC had high specific surface area with various surface functional groups on surface as well as electrostatic attraction between positive charge of PAC and negative charge of CFA. Besides, the data of adsorption isotherms of PAC was reported the best fit with Linear isotherm model indicating the initial part of practical isotherms with low surface coverages, and the adsorption energy being independent of the coverage (as Table 4.10).

Moreover, surface area of PAC was investigated by nitrogen adsorption isotherm. The relationship of surface area of PAC and adsorption capacity of CFA in unit of square meter (m^2) was plotted to study the effect of surface functional groups of PAC adsorbents on the adsorption capacity of CFA. According to BET calculation, the surface area of PAC was showed 1,149.43 m^2/g . The adsorption capacity per surface area was illustrated as in Figure 4.20b. It can be seen clearly that PAC had more active surface functional group for CFA than A-SBA-15 and pristine SBA-15.

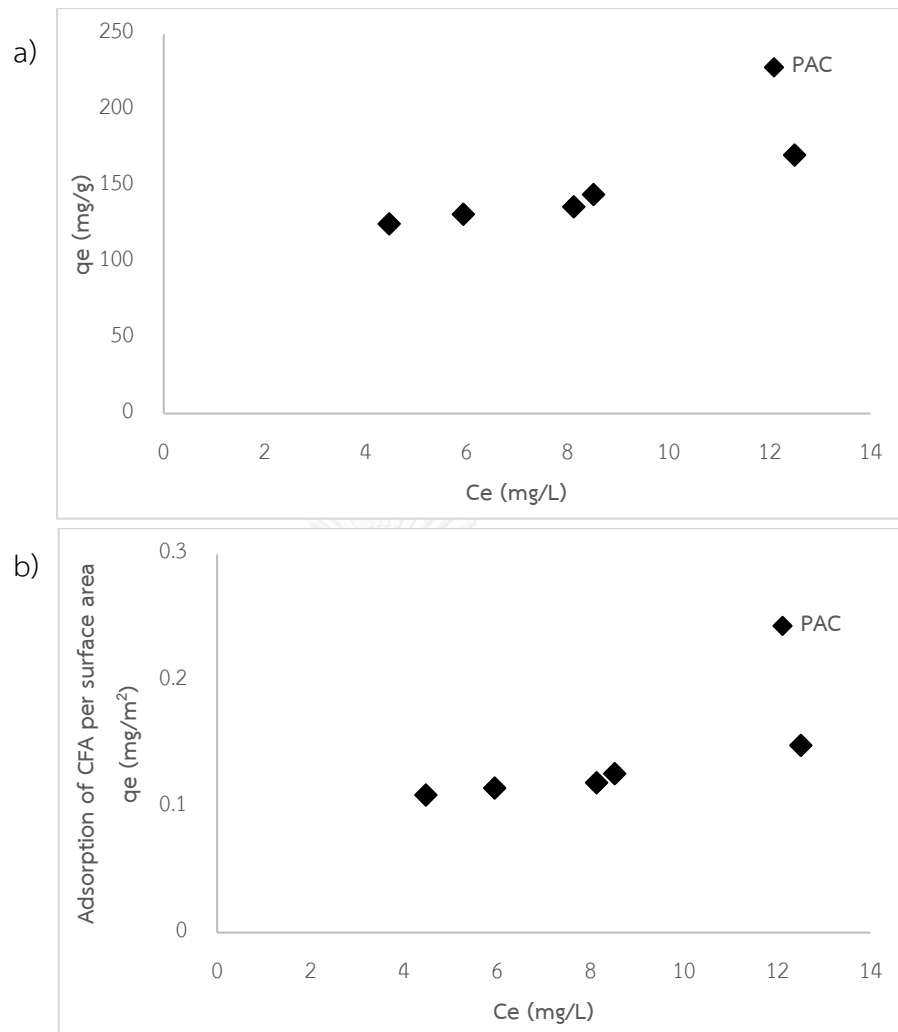


Figure 4.20 Adsorption isotherm of CFA on PAC a) per g of adsorbent and b) per m² of surface area

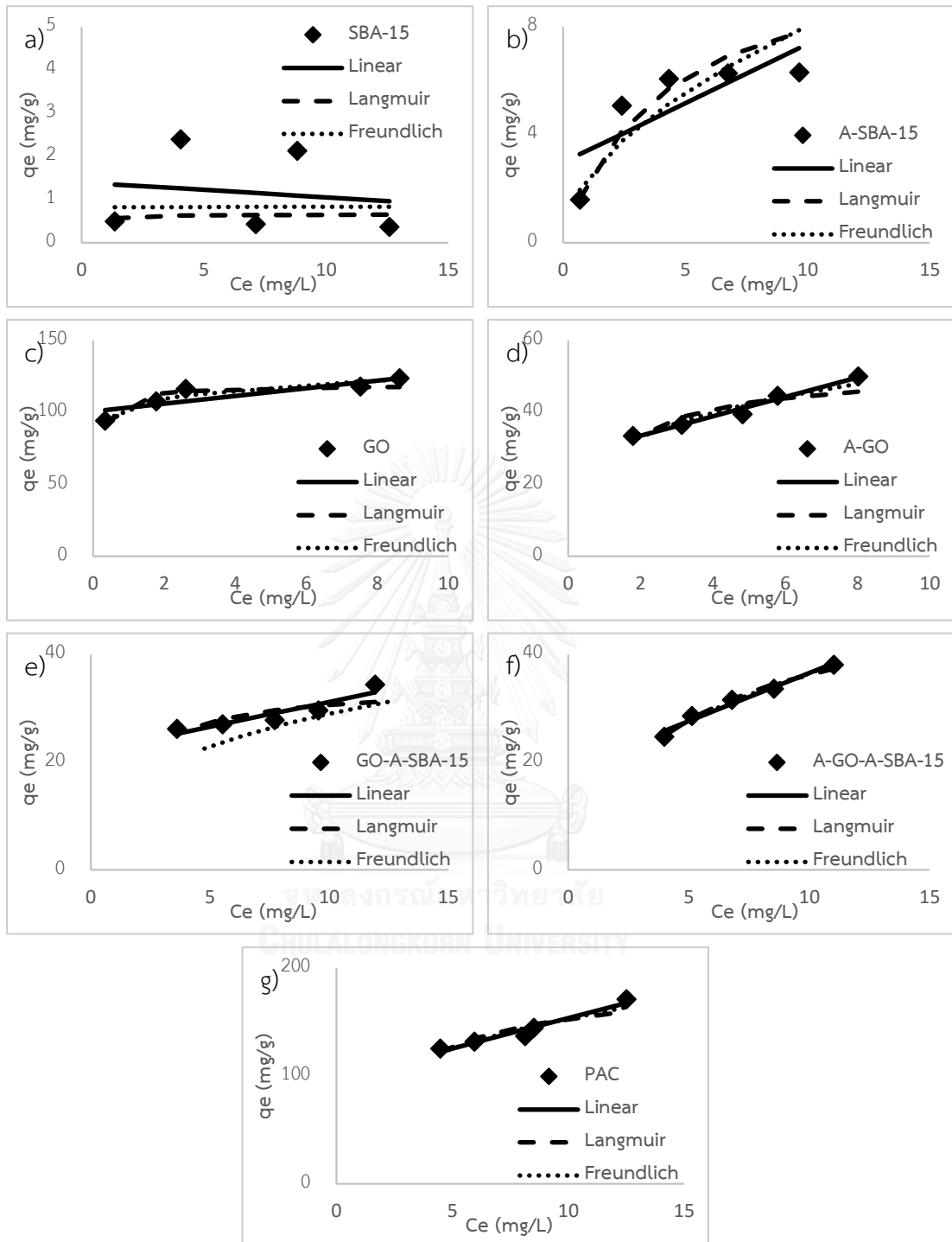


Figure 4.21 The adsorption isotherm of CFA on a) SBA-15, b) A-SBA-15, c) GO, d) A-GO, e) GO-A-SBA-15, f) A-GO-A-SBA-15, and g) PAC

Table 4.10 The adsorption isotherm parameters of CFA on SBA-15, A-SBA-15, GO, A-GO, GO-A-SBA-15, A-GO-A-SBA-15 and PAC at pH 7 after fitting with Linear, Langmuir, and Freundlich isotherm model.

Adsorbent	Linear			Langmuir			Freundlich		
	K_p (L/mg)	c	R^2	K_L (L/mg)	q_m (mg/g)	R^2	n	K_{fr}	R^2
SBA-15	-0.0349	1.3942	0.0226	4.5022	0.6573	0.0071	370.3704	0.8205	0.0000
A-SBA-15	0.4398	2.9658	0.6440	0.2465	11.0742	0.9792	1.8843	2.3651	0.8502
GO	2.6704	100.8700	0.7299	10.5000	119.0476	0.9034	12.7227	103.7205	0.9411
A-GO	2.7006	28.1160	0.9771	0.9415	51.8135	0.8332	3.8081	27.7907	0.9237
GO-A-SBA-15	0.9271	21.9140	0.8618	0.7666	34.6021	0.6587	4.9875	19.5192	0.7649
A-GO-A-SBA-15	1.7846	18.6620	0.9767	0.2291	52.0833	0.9905	10.5153	35.1773	0.8647
PAC	5.6521	96.9880	0.9514	0.3910	192.3077	0.8167	3.4483	78.6887	0.8927

In summary, the adsorption capacity (base on isotherms) of CFA were reported as order PAC > GO >> A-GO > A-GO-A-SBA-15 > GO-A-SBA-15 >>A-SBA-15 > SBA-15. PAC exhibited the best adsorption capacity by a lot of suitable functional group and more specific surface area. Synthesized GO was represented nearly adsorption isotherm of CFA comparing with PAC; however, GO cannot use in the real practice due to limitation of application such as aggregation and hardly separation from water. In this study, the GO modified silica materials were synthesized and reported good adsorption isotherm. It might be π - π interaction, electrostatic attraction, H-bonding, and hydrophilicity.

4.2.3.2 Comparison of adsorption isotherms for CFA on A-GO-A-SBA-15, 3N-SBA-15, 3N-HMS-SP, and NiAlOr-NaBt at high concentration

In order to compare the adsorption isotherm of CFA on synthesized A-GO-A-SBA-15 with other reported adsorbents, the adsorption isotherm data of 3N-SBA-15 (Permrunguang 2013), 3N-HMS-SP (Kaosaiphun 2013), and NiAlOr-NaBt (Cabrera-Lafaurie, Roman et al. 2012) were used to analyzed. The results showed that A-GO-A-SBA-15 was exhibited the highest adsorption isotherm as shown in Figure 4.22.

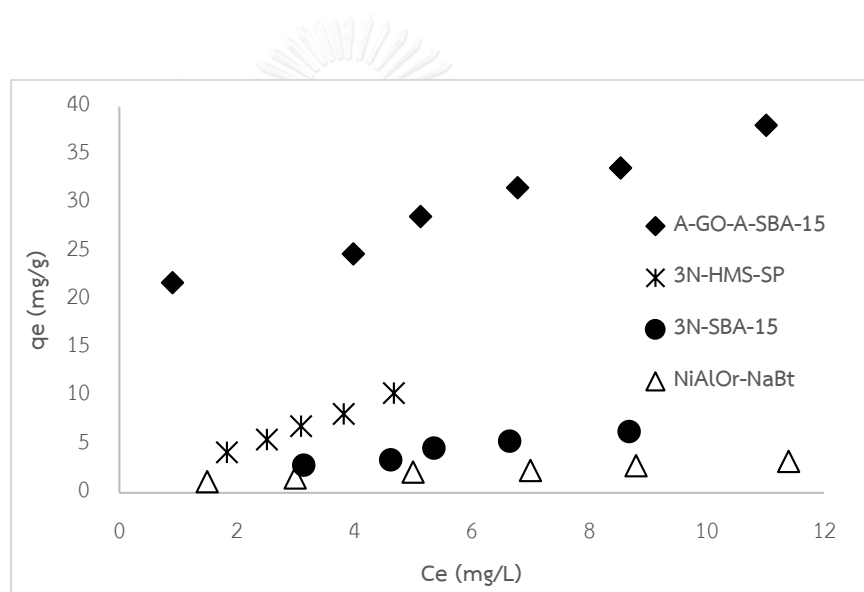


Figure 4.22 The comparison of A-GO-A-SBA-15, 3N-HMS-SP, 3N-SBA-15, and NiAlOr-NaBt adsorption for CFA at high concentration

4.2.3.3 Adsorption isotherms of CFA on A-GO-A-SBA-15 at high concentration in pH 5-9 (single solute)

The adsorption isotherms were performed under batch experiment in controlling of phosphate buffer 0.01 M, pH 5-9 at 25°C on A-GO-A-SBA-15. A-GO-A-SBA-15 was selected because this adsorbent showed the highest adsorption capacity of CFA comparing with all synthesized adsorbents. The effect of pH was compared base

on adsorption isotherms. Moreover, the obtained isotherms were fitted with linear model, Langmuir model, and Freundlich model.

The results of adsorption isotherms on A-GO-A-SBA-15 in pH 5-9 were reported as shown in Figure 4.23. At pH 5, 7 and 9, the adsorption capacities were reported around 44, 34 and 17 mg/g, respectively (at the the equilibrium concentration 9 ppm.).

The PZC of A-GO-A-SBA-15 is supposed to be the important role for CFA adsorption. In this case, CFA presented negative charge in all pH because pKa equals 2.84. Moreover, pH 5, 7, and 9 were less than PZC that made the surface of A-GO-A-SBA-15 presented positive charge. Hence, the electrostatic attractive could be occurred between CFA and A-GO-A-SBA-15. Interestingly, the adsorption capacity of CFA on A-GO-A-SBA-15 in lower pH was more than in higher pH. It could be described that the surface of adsorbent in lower pH can be protonated more than higher pH due to lots of protons in the solution. Thus lower pH can drive the electrostatic interaction to be stronger than higher pH; in other words, the surface of adsorbent in lower pH has more positive charge density than in higher pH.

According to the adsorption isotherm of CFA on A-GO-A-SBA-15 followed as order; pH 5 > pH 7 > pH 9 (Figure 4.23). The highest adsorption isotherm of CFA was presented in pH 5 because of the strongly positive charge on the surface of A-GO-A-SBA-15 then follow by pH 7 and pH 9, respectively. Therefore, it could be concluded that electrostatic interaction is the important role for CFA adsorption on A-GO-A-SBA-15.

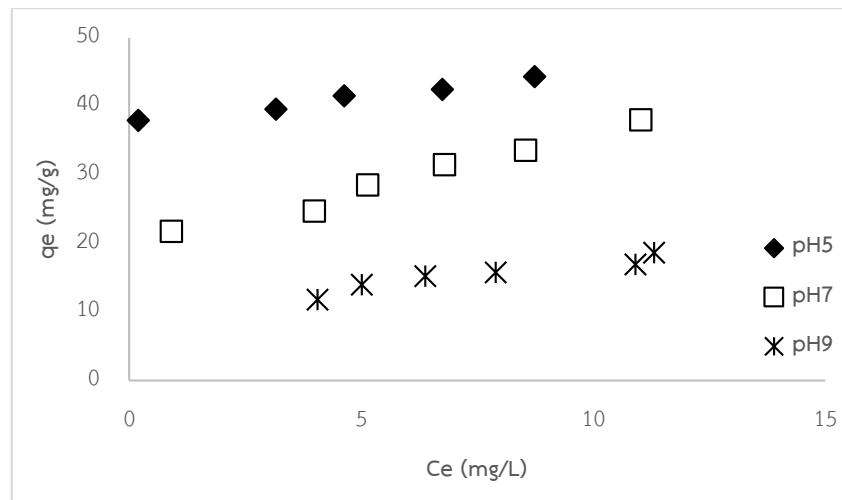


Figure 4.23 Effect of pH on A-GO-A-SBA-15 adsorbent materials in adsorption capacity of CFA

4.2.3.4 Adsorption isotherms of CFA on A-GO-A-SBA-15 at low concentration in pH 7 (single solute)

In case of the application in the real practice, the adsorption isotherm of CFA on A-GO-A-SBA-15 was performed. A-GO-A-SBA-15 was chosen because this adsorbent exhibited the highest adsorption capacity of CFA comparing with all synthesized adsorbents. The result of adsorption capacity and equilibrium concentration were showed in the unit of $\mu\text{g/g}$ and $\mu\text{g/L}$, respectively, as Figure 4.24. Moreover, the adsorption isotherm of CFA at low concentration on A-GO-A-SBA-15 had the best fit with Linear isotherm model as Table 4.11 because adsorption in low concentration basically exhibits the Linear isotherm model because the adsorbate is adsorbed through the fraction of monolayer on adsorbent (Faust and Aly 1987).

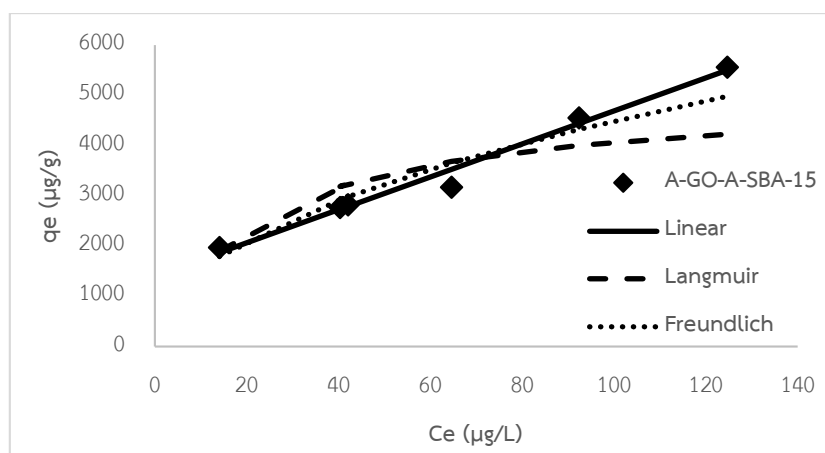


Figure 4.24 Adsorption isotherm of CFA on A-GO-A-SBA-15 at low concentration

Table 4.11 The adsorption isotherm parameters of CFA on A-GO-A-SBA-15 at low concentration after fitting with Linear, Langmuir, and Freundlich isotherm model.

Adsorbent	Linear			Langmuir			Freundlich		
	$K_p(L/\mu g)$	c	R^2	$K_L(L/\mu g)$	$q_m(\mu g/g)$	R^2	n	K_{fr}	R^2
A-GO-A-SBA-15	32.8390	1404	0.9826	0.0435	5000	0.8456	2.1327	517.7021	0.9279

4.2.3.5 Comparison of adsorption isotherms for CFA on A-GO-A-SBA-15, 3N-SBA-15, and 3N-HMS at low concentration

According to comparison of the adsorption isotherms of CFA on synthesized A-GO-A-SBA-15 with other previously reported adsorbents, the adsorption isotherm data of 3N-SBA-15 (Permrunguang 2013), 3N-HMS (Kaosaiphun 2013), were used to study. The results showed the same trend with high concentration isotherms that A-GO-A-SBA-15 exhibited the highest adsorption isotherm as shown in Figure 4.25.

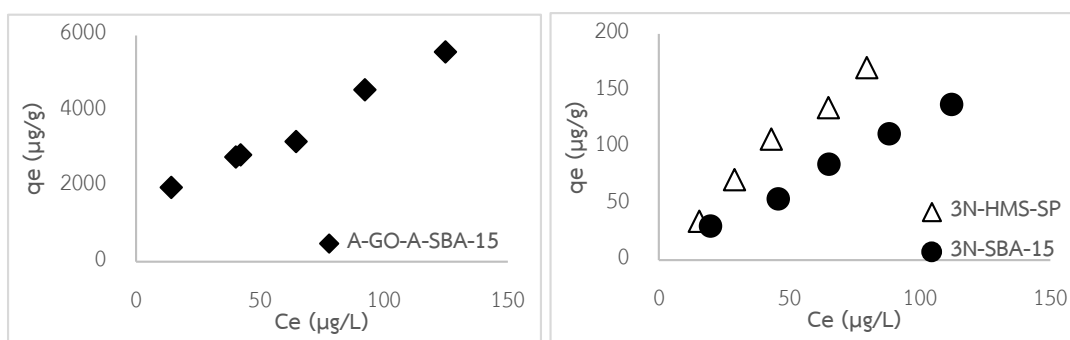


Figure 4.25 The comparison of A-GO-A-SBA-15, 3N-HMS-SP, and 3N-SBA-15 adsorption for CFA at low concentration

4.2.3.6 Adsorption isotherms of NAP at high concentration in pH 7 (single solute)

The adsorption isotherms of NAP were conducted under batch experiment by controlling of phosphate buffer 0.01 M, pH 7 at 25°C. The obtained adsorption isotherms data were fitted with linear model, Langmuir model, and Freundlich model.

4.2.3.6.1 Effect of surface functional group on silica material

The adsorption isotherms on of NAP SBA-15 and A-SBA-15 were shown in Figure 4.26. The results of pristine SBA-15 and A-SBA-15 showed very low adsorption capacity. Although changing the surface charge by modification of amine functional group was applied on A-SBA-15. It could be discussed that electrostatic attraction might not be an important role for NAP adsorption on A-SBA-15. Moreover, possible mechanism might be the repulsive interaction due to hydrophilicity of A-SBA-15 and the hydrophobicity of NAP which showed the contrast of hydrophilic-hydrophobic like phenomena.

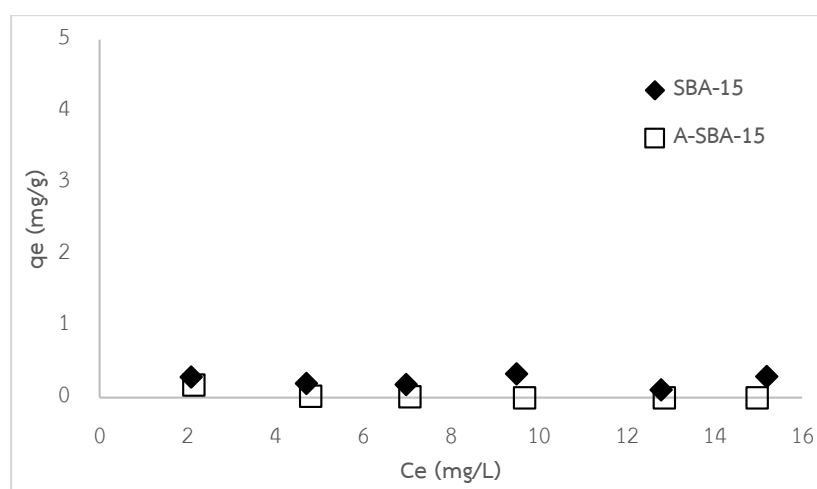


Figure 4.26 Comparison of pristine functional group and amine functional group on mesoporous silica materials in adsorption capacity of NAP.

4.2.3.6.2 Effect of surface functional group on graphene oxide materials

The adsorption isotherms of NAP on GO and A-GO were showed in Figure 4.27. On pristine GO, the adsorption capacity was reported around 14.6 mg/g at the the equilibrium concentration 5 ppm. Although GO presented negative surface charge at pH7 as Table 4.16, the adsorption capacity of NAP can be still detected. It mean that π - π interaction between aromatic ring can be the crucial factor more than eletrostatic replusion from negative charge of NAP and surface of GO and hydrophilic-hydrophobic interaction between NAP and GO in this process. From XPS spectra, GO in the phosphate buffer solution (Figure 4.28a) represented the permission of π to π^* transition from unsaturated bond and XPS spectra after adsorption of NAP (Figure 4.28b) was also exhibited the transition. It was supposed to be involved with π orbital overlap in adsorption mechanism. Nevertheless, XPS spectra of GO in DI water (Figure 4.28c) did not demonstrated the transition of π to π^* due to saturated structure and XPS spectra after adsorption process (Figure 4.28d) was presented the same result. It could not indexed any mechanisms. It might be possibly invloved with π - π interaction

(Yang, Rochette et al. 2005, Teng, Ma et al. 2011). Moreover, Van der Waals force might be involved with the adsorption process of NAP on GO materials. Besides, the data of adsorption isotherms of GO represented the best fit with Langmuir isotherm model indicating the monolayer adsorption.

After modification of two amine functional groups (A-GO), the adsorption capacity did not change significantly, although A-GO presented a slightly positive surface charge at pH 7. Owing to the folding phenomena of A-GO by intra-interaction of amine functional groups on epoxy groups of GO, it might lose the specific surface area of A-GO surface as shown in SEM image (Figure 4.7). Thus, amine functional groups on GO (A-GO) could decrease the adsorption capacity of NAP due to losing the surface area of A-GO sheet. Moreover, the adsorption isotherms of A-GO reported the best fit with Langmuir isotherm model meaning the monolayer adsorption.

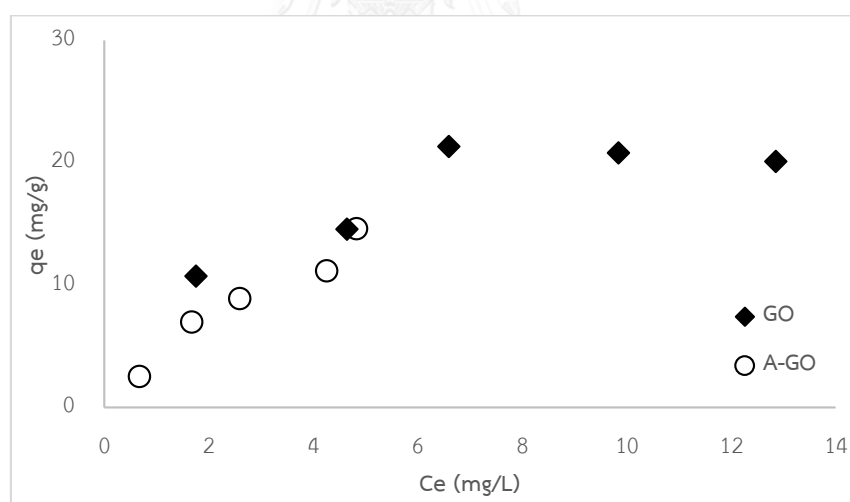
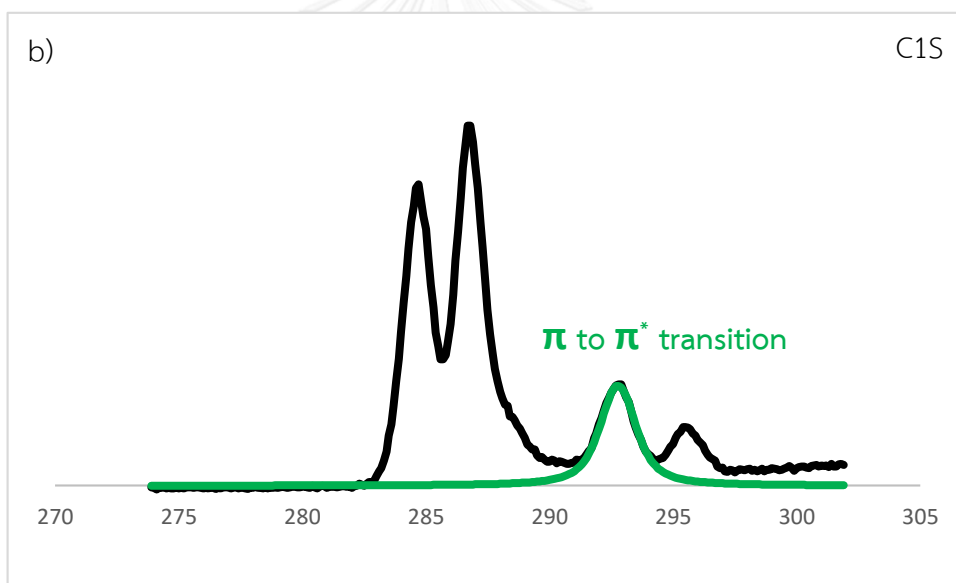
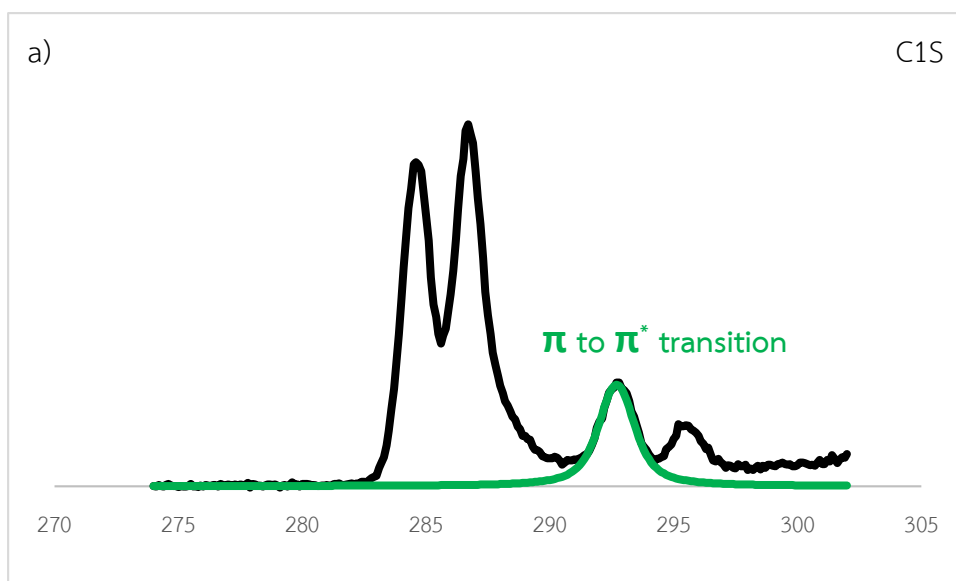


Figure 4.27 Comparison of pristine functional group and amine functional group on GO materials in adsorption capacity of NAP



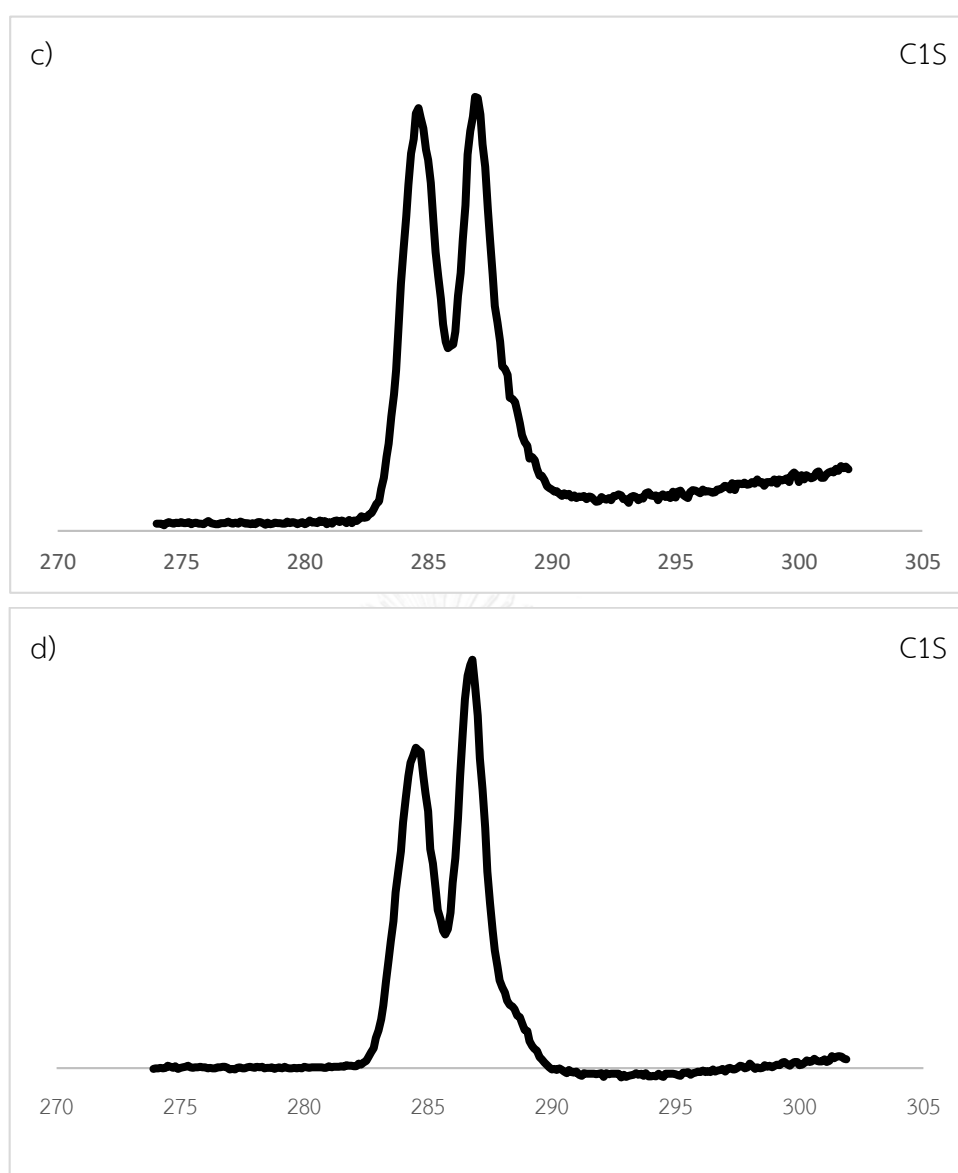


Figure 4.28 XPS spectra of a) GO dispersed in phosphate buffer b) the adsorption for NAP on GO dispersed in phosphate buffer c) GO dispersed in DI d) the adsorption for NAP on GO dispersed in DI

4.2.3.6.3 Effect of GO modified silica materials

Adsorption isotherm of NAP on GO-A-SBA-15 and A-GO-A-SBA-15 were showed in Figure 4.29. For GO-A-SBA-15, the adsorption capacity was reported around 3.7 mg/g at the the equilibrium concentration 10 ppm. Adsorption capacity was increased comparing with pristine A-SBA-15. It might be the influence of GO which had π - π

interaction between aromatic ring of NAP. In addition, adsorption of NAP on GO-A-SBA-15 was showed the best correlation coefficient value of R^2 on Freundlich isotherm model indexing the multilayer adsorption.

After modification by amine functional group on GO-A-SBA-15 (A-GO-SBA-15), the adsorption capacity of NAP was slightly decrease to 2.7 mg/g at the the equilibrium concentration 10 ppm due to the contrast of hydrophilic-hydrophobic like between A-GO-A-SBA-15 and NAP. As a result of adsorption isotherm, Langmuir isotherm model showed the best fit with adsorption of CFA on A-GO-A-SBA-15.

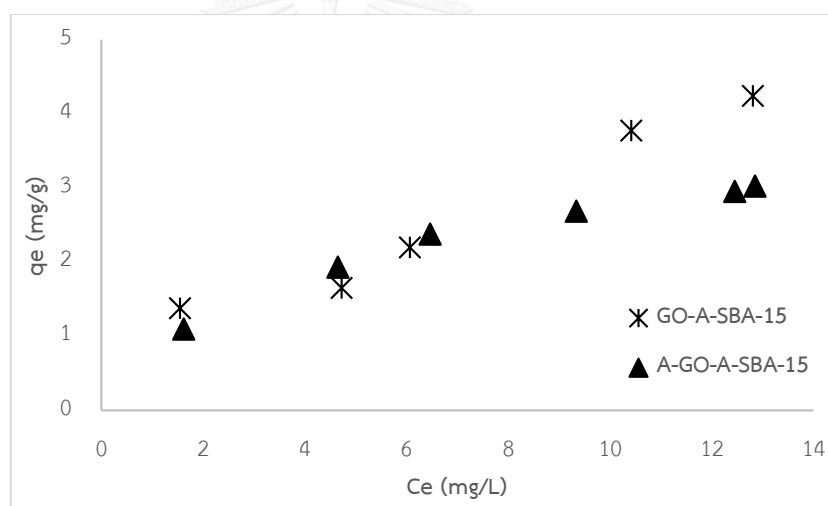


Figure 4.29 Comparison of pristine functional group and amine functional group on GO modified A-SBA-15 materials in adsorption capacity of NAP.

After comparing the adsorption capacity of pure GO and GO-A-SBA-15 which were 14.6 and 1.65 mg/g at the the equilibrium concentration 5 ppm, respectively. The results showed the difference adsorption capacity between both adsorbents. Similarly with the adsorption of CFA, it might be discussed by the quantitative analysis of GO on GO-A-SBA-15 material as Table 4.12. According to the adsorption capacities of SBA-15 and A-SBA-15 can be neglected, hence the adsorption capacity of NAP on GO-A-

SBA-15 should relate to the ratio of GO on GO-A-SBA-15. The obtained characterization results shown the percentage of GO in GO-A-SBA-15 was 12.44%. As shown in table 4.12, the amount of NAP that adsorbed by GO on GO-A-SBA-15 is approximately near the ratio that can be calculated from pure GO (1.65 mg/g vs 1.82 mg/g).

Table 4.12 Percentage of A-SBA-15, GO, and A-GO in synthesized adsorbents for the adsorption capacity of NAP

Adsorbent	Percentage	Adsorption capacity of NAP, q_e (mg/g)
A-SBA-15	A-SBA-15 = 100%	0
	A-SBA-15 = 87.56%	0
	A-SBA-15 = 86.64%	0
GO	GO = 100%	20.8
	GO = 12.44%	2.6
GO-A-SBA-15	GO-A-SBA-15 = 100%	3.7
	GO = 12.44%	3.7
	A-SBA-15 = 87.56%	0
A-GO	A-GO = 100%	11.0
	A-GO = 13.36%	1.5
A-GO-A-SBA-15	A-GO-A-SBA-15 = 100%	2.7
	A-GO = 13.36%	2.7
	A-SBA-15 = 86.64%	0

4.2.3.6.4 The adsorption capacity of PAC

In order to compare NAP adsorption capacity between the synthesized adsorbents and PAC, adsorption isotherm of NAP on PAC are shown in Figure 4.30. The adsorption capacity of NAP on PAC was the highest adsorption capacity around 150 mg/L (as Figure 4.30a) at the equilibrium concentration around 2 ppm. The highest adsorption capacity of PAC might be caused by active complexity of surface functional group on PAC, high specific surface area, as well as electrostatic attraction between positive charge of PAC and negative charge of NAP. Moreover, The adsorption isotherms of PAC showed the best fit with Langmuir isotherm model indicating the monolayer adsorption as Table 4.13.

In addition, adsorption capacity of NAP in unit of square meter (m^2) was plotted to study the effect of active surface functional groups of PAC on adsorption capacity of NAP. From the results of BET, the surface area of PAC was reported 1,149.43 m^2/g which was the highest surface area when comparing with SBA-15 and A-SBA-15. The result of adsorption capacity per surface area was reported as in Figure 4.30b. The results shown that the surface of PAC was very effective for removal of NAP. Adsorption capacity of NAP on PAC was the same level as CFA adsorption on PAC, hence, it might be concluded that surface functional groups on PAC are very active for aromatic structure of both CFA and NAP, although the physical properties of CFA and NAP are different.

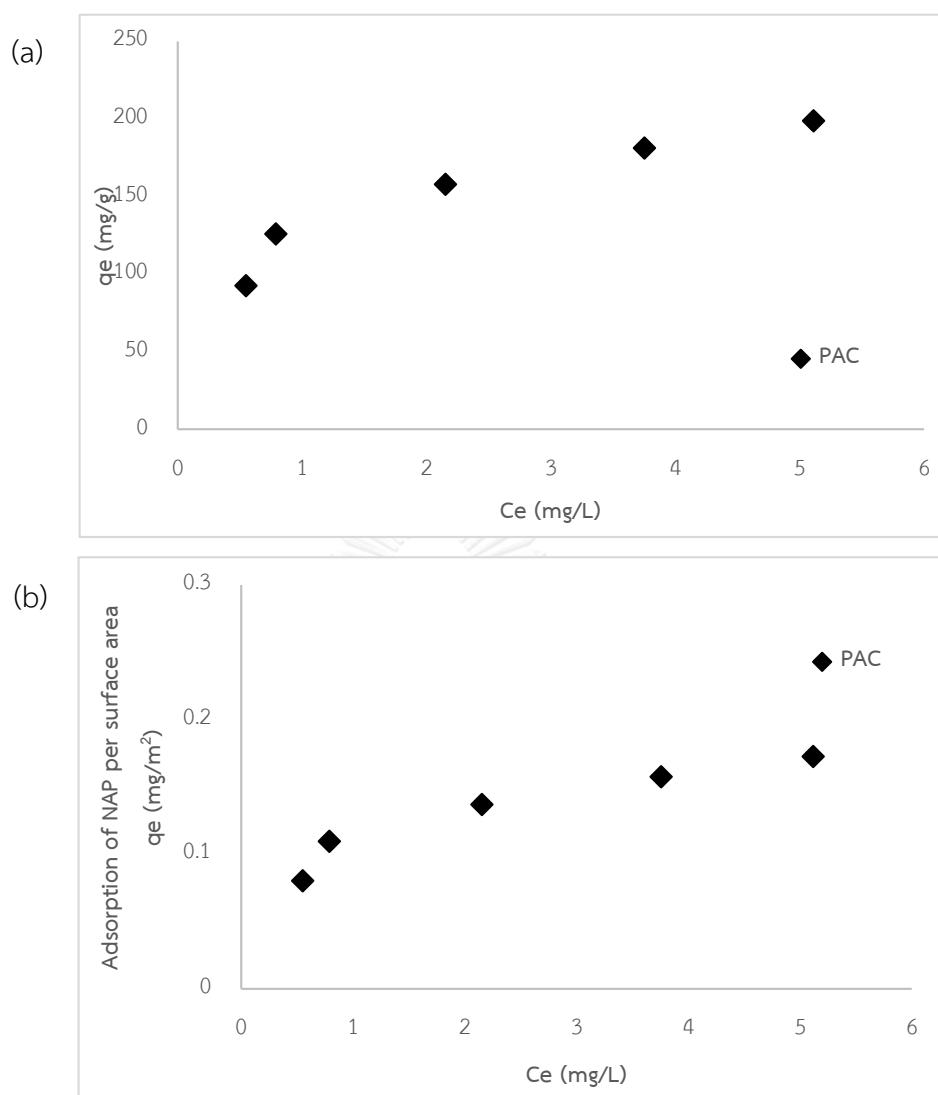


Figure 4.30 Adsorption isotherm of NAP on PAC a) per g of adsorbent and b) per m² of surface area

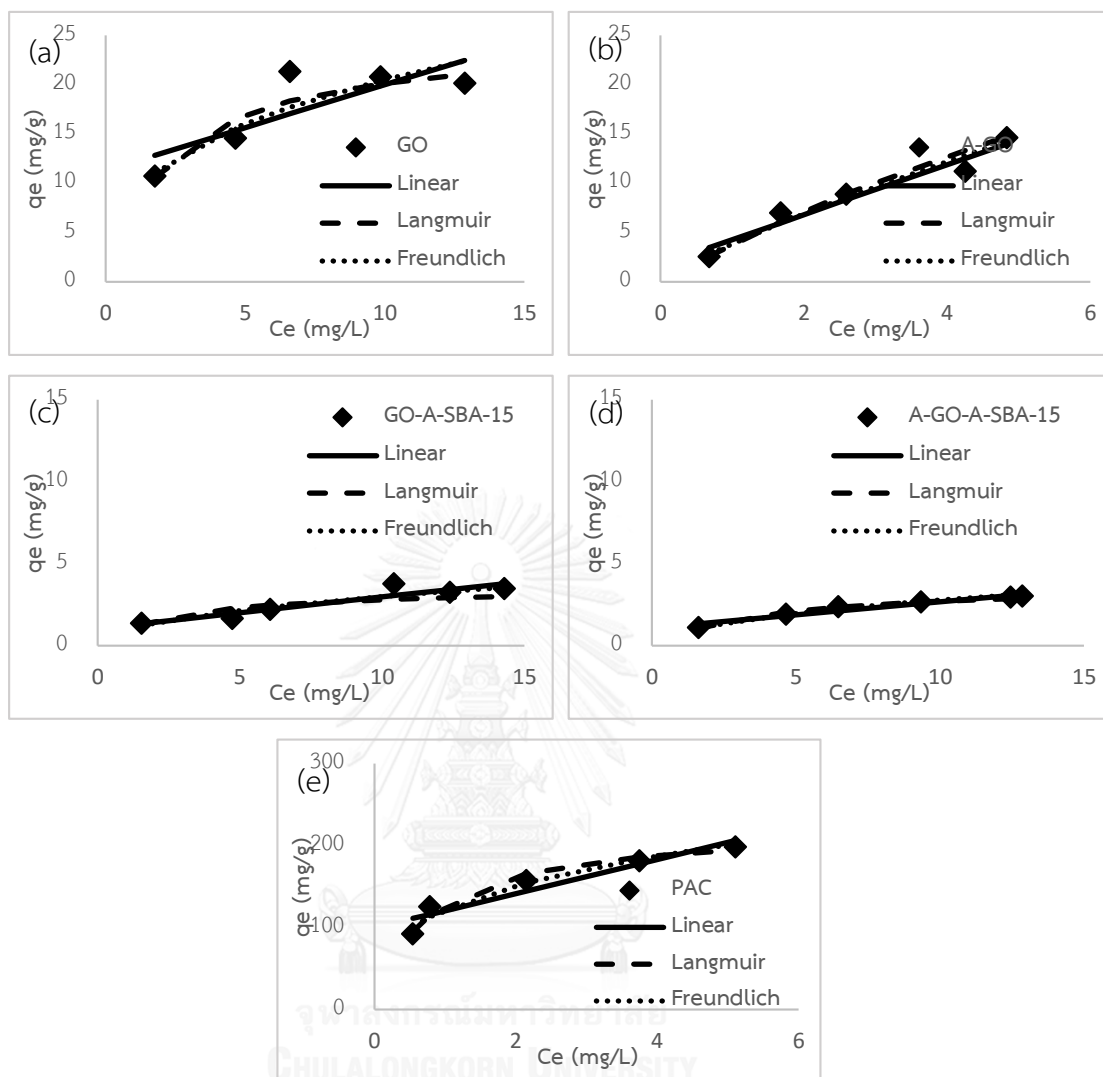


Figure 4.31 The adsorption isotherm of NAP on a) GO, b) A-GO, c) GO-A-SBA-15, d) A-GO-A-SBA-15, and e) PAC

Table 4.13 The adsorption isotherm parameters of NAP on GO, A-GO, GO-A-SBA-15, A-GO-A-SBA-15 and PAC at pH 7 after fitting with Linear, Langmuir, and Freundlich isotherm model.

Adsorbent	Linear			Langmuir			Freundlich		
	$K_p(\text{L/mg})$	c	R^2	$K_L(\text{L/mg})$	$q_m(\text{mg/g})$	R^2	n	K_{fr}	R^2
GO	0.8684	11.3150	0.6555	0.4234	24.9377	0.9153	2.8225	9.0684	0.8507
A-GO	2.5351	1.7465	0.9472	0.0685	59.1716	0.9897	1.2137	3.8954	0.9690
GO-A-SBA-15	0.1921	1.0482	0.8575	0.3741	3.5600	0.7613	2.1093	1.0033	0.8647
A-GO-A-SBA-15	0.1588	1.0935	0.9334	0.2497	3.7951	0.9960	2.0165	0.8885	0.9889
PAC	20.8180	99.8100	0.9060	1.3636	222.2222	0.9701	3.2352	122.1073	0.9466

In short, the adsorption isotherm of NAP were reported as order PAC >> GO > A-GO >> GO-A-SBA-15 > A-GO-A-SBA-15. PAC had the highest adsorption isotherm by the same reason as reported in CFA section due to the variety suitable functional group and more specific surface area. Moreover, amine group grafted on GO (A-GO) did not show the significantly change in NAP adsorption capacity (until equilibrium concentration at 5 ppm.). One possible reason might relate to the affinity via π - π interaction between NAP and aromatic ring of GO and A-GO. And this π - π interaction might not be affected by the modification of amine group on A-GO. Moreover, A-GO showed the adsorption isotherm nearly with GO, although A-GO had the folding of A-GO sheet and losing some surface area. It can be suggested that the adsorption capacity of NAP on GO and A-GO were not high enough to show the effect from folding phenomena.

4.2.3.7 Comparison of adsorption isotherms for NAP on GO-A-SBA-15, and 3N-HMS at high concentration

In order to compare the adsorption isotherm of NAP on synthesized GO-A-SBA-15 with other adsorbents, the adsorption isotherm data of P-HMS-SP from (Ruangtrakul 2010) was used to investigate. The results showed that phenol group grafted HMS-SP was reported the slightly higher adsorption isotherm than GO-A-SBA-15 as shown in Figure 4.32.

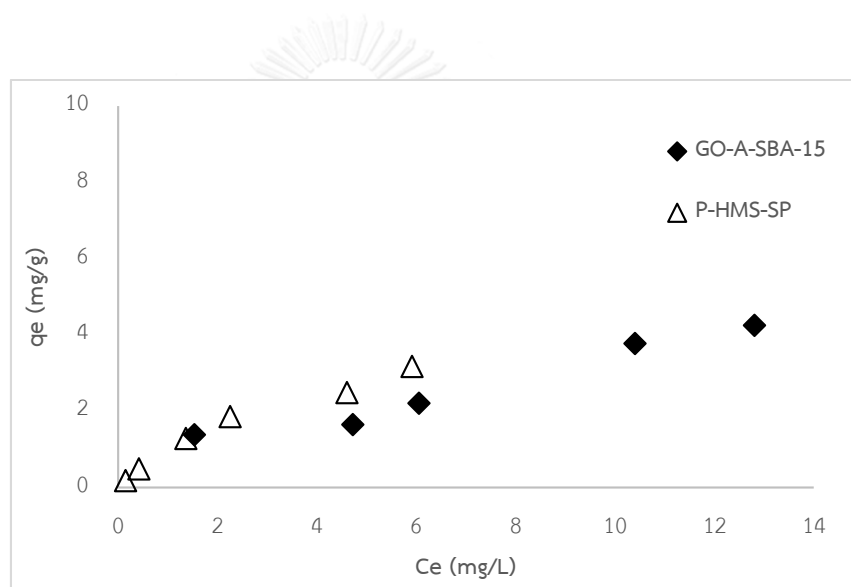


Figure 4.32 The comparison of GO-A-SBA-15, and P-HMS-SP adsorption for NAP at high concentration

4.2.3.8 Adsorption isotherms of NAP on GO-A-SBA-15 at high concentration in pH 5-9 (single solute)

The NAP adsorption isotherms were investigated under batch experiment in controlling of phosphate buffer 0.01 M, pH 5, 7 and 9 at 25°C on GO-A-SBA-15. GO-A-SBA-15 was chosen to study the effect of pH because of highest adsorption capacity

of NAP comparing with all synthesized adsorbents. Moreover, adsorption isotherm data were fitted using linear model, Langmuir model, and Freundlich model.

Adsorption isotherms of NAP on GO-A-SBA-15 in pH 5, 7 and 9 were showed as Figure 4.33. At pH 5, 7 and 9, the adsorption capacity was reported around 5.8, 2.8 and 0.7 mg/g, respectively at the equilibrium concentration around 2 ppm. The PZC of GO-A-SBA-15 was an important factor to describe adsorptive phenomena. In this experiment, NAP showed negative charge in all pH because pK_a equals 4.15 (as Table 4.15). Besides, pH 5, 7, and 9 were less than PZC, hence the surface of GO-A-SBA-15 presented positive charge (as Table 4.16). The electrostatic attractive between NAP and GO-A-SBA-15 can be occurred. Moreover, as same as the obtained results from the case of CFA and A-GO-A-SBA-15, the adsorption capacity of NAP on GO-A-SBA-15 in lower pH was more than higher pH. It could be described that the surface of adsorbent in lower pH was protonated more than higher pH due to lots of protons in the solution. Thus lower pH can drive the electrostatic interaction to be stronger than higher pH; in other words, the surface of adsorbent in lower pH has more positive charge density than in higher pH.

Therefore, it could be clear that electrostatic interaction had the crucial impact in the adsorption of NAP on GO-A-SBA-15.

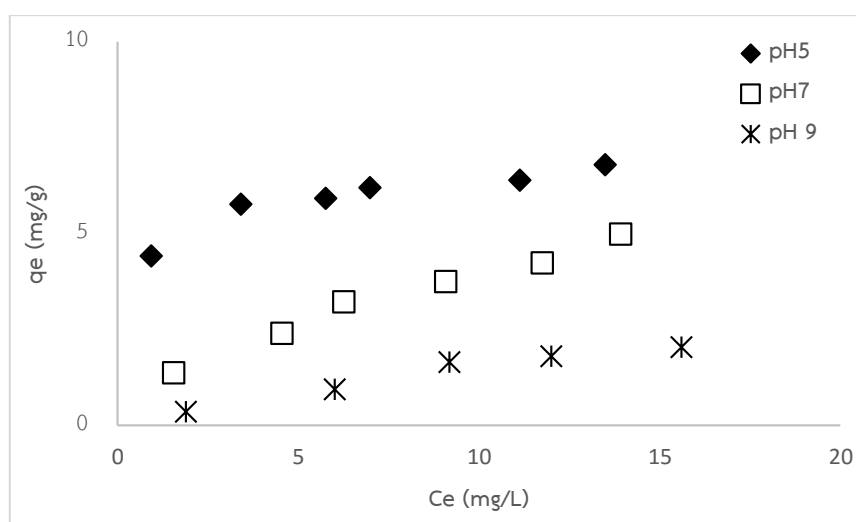


Figure 4.33 Effect of pH on GO-A-SBA-15 adsorbent materials in adsorption capacity of NAP

4.2.3.9 Adsorption isotherms of NAP on GO-A-SBA-15 at low concentration in pH 7 (single solute)

To stimulate the real concentration of NAP in the real practice, the adsorption isotherm of NAP on GO-A-SBA-15 in ppb level was conducted. GO-A-SBA-15 was chosen as a model in this study because of its highest adsorption capacity of NAP comparing with all synthesized adsorbents. The result of adsorption capacity and equilibrium concentration were showed in the unit of $\mu\text{g/g}$ and $\mu\text{g/L}$, respectively. Moreover, the adsorption isotherm of NAP at low concentration on GO-A-SBA-15 had the best fit with Langmuir isotherm model as shown in Table 4.14. However, the plot of adsorption capacity (as Figure 4.34) shows the shape of linear line. It might be clear that linear line always occurs in the beginning part of many adsorption isotherms.

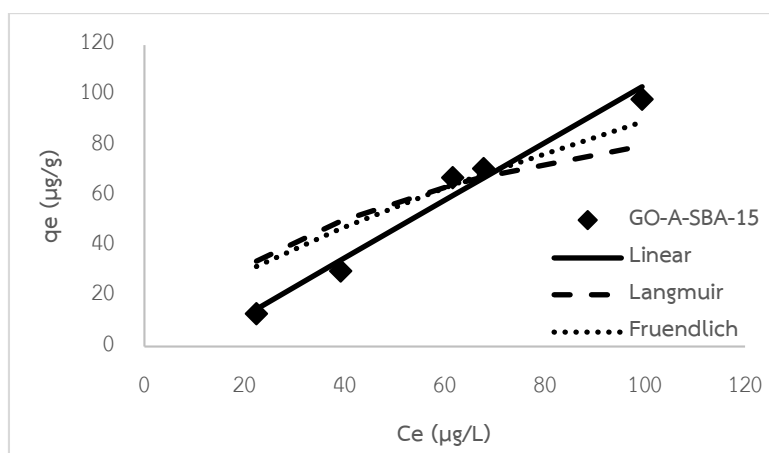


Figure 4.34 Adsorption isotherm of CFA on A-GO-A-SBA-15 at low concentration

Table 4.14 The adsorption isotherm parameters of NAP on GO-A-SBA-15 at low concentration after fitting with Linear, Langmuir, and Freundlich isotherm model.

Adsorbent	Linear			Langmuir			Freundlich		
	$K_p(L/\mu g)$	c	R^2	$K_L(L/\mu g)$	$q_m(\mu g/g)$	R^2	n	K_{fr}	R^2
GO-A-SBA-15	1.1492	-10.8340	0.9756	268.3642	131.5789	0.9850	1.4466	3.7143	0.9804

Table 4.15 The charge present, and pKa of CFA

Pharmaceutic	pKa	pH 7
CFA	2.84	Negative charge
NAP	4.15	Negative charge

Table 4.16 The charge present, and PZC of SBA-15, A-SBA-15, GO, A-GO, GO-A-SBA-15, and A-GO-A-SBA-15 at pH 7

Adsorbents	PZC	pH 7
SBA-15	5.26	Negative charge
A-SBA-15	9.60	Positive charge
GO	3.19	Negative charge
A-GO	7.63	Positive charge
GO-A-SBA-15	9.24	Positive charge
A-GO-A-SBA-15	9.35	Positive charge
PAC	9.50 ^a	Positive charge

^a(Prarat 2011)

4.2.4 Adsorption selectivity

In order to study the mechanism of selective adsorption on synthesized adsorbents which showed the highest adsorption capacity for both CFA and NAP. In this study, the adsorption selectivity was performed in the multi-solute of CFA and NAP comparing with the results of adsorption capacity in single solute.

4.2.4.1 Adsorption selectivity on GO-A-SBA-15 at high concentration in multi-solute

GO-A-SBA-15 was selected because this adsorbent showed the highest adsorption capacity of NAP comparing with all synthesized adsorbents. The adsorption selectivity on GO-A-SBA-15 was conducted by varying concentration of NAP between 2-13 ppm and fix concentration of CFA at 7 ppm. And then, the concentration CFA was varied between 10-20 ppm and fixed concentration of NAP at 15 ppm in controlling of phosphate buffer 0.01M at pH 7.

Obtained results showed that in the vary concentration of NAP between 2-13 ppm and fix CFA concentraion at 7 ppm on GO-A-SBA-15 exhibited the decrease of adsorption capacity of both NAP and CFA as shown in Figure 4.35. However, the adsorption capacity of CFA was reduced from the single solute around 28.98% but the concentration of NAP was exhibited the reduction around 39.39% as Table 4.17. Therefore, the adsorption of NAP on GO-A-SBA-15 might be easily disturbed by the existence of CFA.

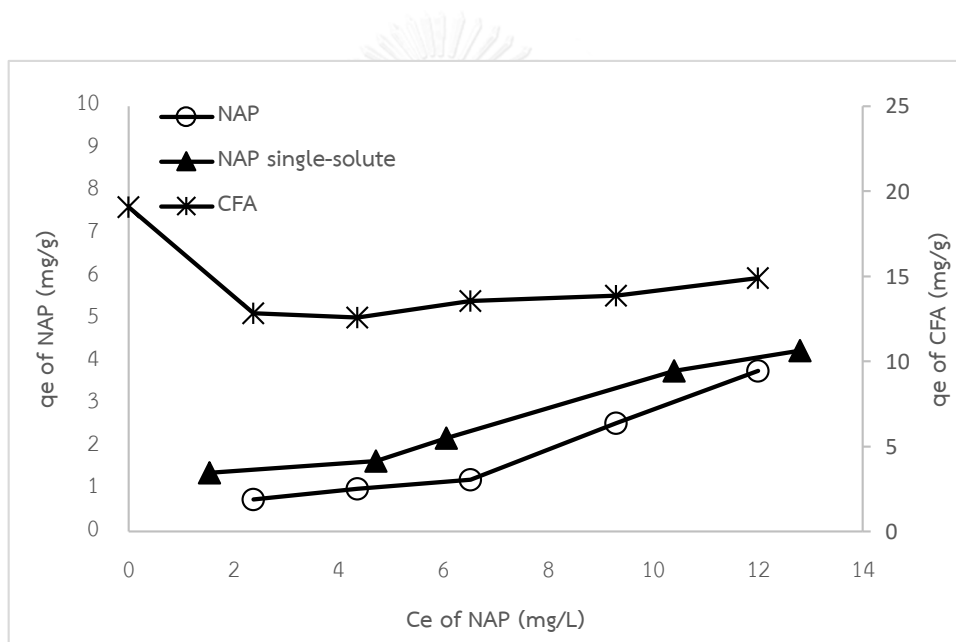


Figure 4.35 Adsorption isotherm of vary NAP and CFA on GO-A-SBA-15 in multi-solute

Table 4.17 The adsorption isotherm data of vary NAP and CFA on GO-A-SBA-15 in multi-solute.

C_e of NAP (Single solute)	q_e of NAP (Single solute)	C_e of NAP (Multi-solute)	q_e of NAP (Multi-solute)	q_e of CFA (Multi-solute)
-	-	0	-	19.08517
1.540382	1.380785	2.381983	0.74941	12.83019
4.720316	1.650939	4.356723	1.003521	12.56604
6.060092	2.201746	6.523122	1.223176	13.54717
10.41036	3.777028	9.296802	2.545411	13.84906
12.80804	4.247416	12.00588	3.781508	14.90566
% Reduction			39.39%	28.98%

Whereas, the results of varying concentration of CFA between 10-20 ppm and fix concentration of NAP at 15 ppm on GO-A-SBA-15 also showed the significantly decline of adsorption capacity of both CFA and NAP as Figure 4.36. The adsorption capacity of CFA was dropped from the single solute around 26.07%. And for NAP, the adsorption capacity was showed the decrease around 38.82% (as Table 4.18). The obtained results exhibited the same as shown in the varying concentration of NAP between 2-13 ppm and fix CFA concentration at 7 ppm on GO-A-SBA-15. Thus the adsorption of CFA on GO-A-SBA-15 might be also interrupted by the presence of NAP.

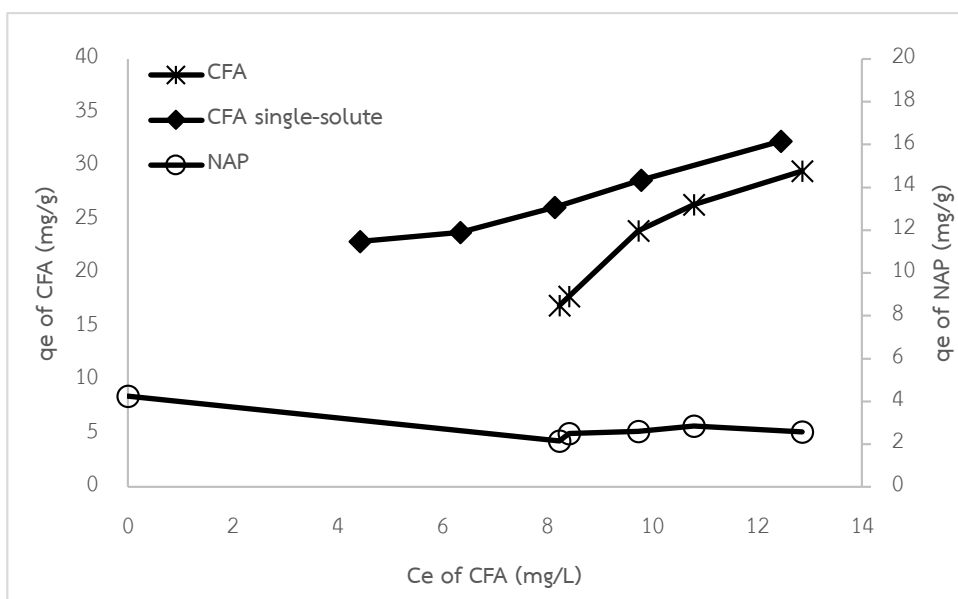


Figure 4.36 Adsorption isotherm of vary CFA and NAP on GO-A-SBA-15 in multi-solute

Table 4.18 The adsorption isotherm data of vary CFA and NAP on GO-A-SBA-15 in multi-solute.

C _e of CFA (Single solute)	q _e of CFA (Single solute)	C _e of CFA (Multi-solute)	q _e of CFA (Multi-solute)	q _e of NAP (Multi-solute)
-	-	0	-	4.247416
4.427071	22.97206	8.226415	16.98113	2.162092
6.331741	23.7842	8.415094	17.81132	2.510956
8.139727	26.14329	9.735849	23.96226	2.610016
9.783351	28.65706	10.79245	26.37736	2.846898
12.45182	32.33105	12.85849	29.50943	2.579867
% Reduction			26.07%	38.82%

4.2.4.2 Adsorption selectivity on A-GO-A-SBA-15 at high concentration in multi-solute

A-GO-A-SBA-15 was chosen because its highest adsorption capacity for CFA comparing with all synthesized adsorbents. The adsorption selectivity on A-GO-A-SBA-15 was preformed by varying concentration of CFA between 10-20 ppm and fix NAP concentration at 15 ppm. And then, vary concentration of NAP between 2-13 ppm and fix concentration of CFA at 7 ppm under the control of phosphate buffer 0.01M at pH 7.

The results obtained from varying concentration of CFA between 10-20 ppm and fixing NAP concentration at 15 ppm on A-GO-A-SBA-15 illustrated slightly decrease of adsorption capacity of CFA and dramatically reducing of NAP adsorption capacity (as Figure 4.37). Moreover, the adsorption capacity of CFA was a little bit reduced from the single solute around 5.49% but the capacity of NAP was reported the decrease around 60.07% (as Table 4.19). In summary, the adsorption of CFA on A-GO-A-SBA-15 might be hardly interrupted by the presence of NAP.

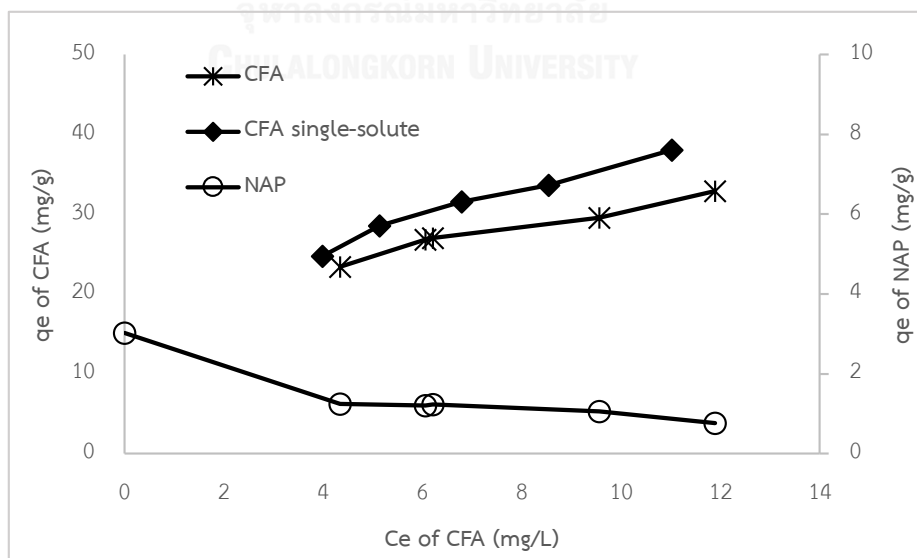


Figure 4.37 Adsorption isotherm of vary CFA and NAP on A-GO-A-SBA-15 in multi-solute

Table 4.19 The adsorption isotherm data of vary CFA and NAP on A-GO-A-SBA-15 in multi-solute.

C_e of CFA (Single solute)	q_e of CFA (Single solute)	C_e of CFA (Multi-solute)	q_e of CFA (Multi-solute)	q_e of NAP (Multi-solute)
-	-	0	-	3.028921
3.982326	24.75104	4.339623	23.39623	1.249017
5.132863	28.57972	6.056604	26.79245	1.210255
6.786155	31.55758	6.207547	27.0566	1.23179
8.536131	33.64594	9.556604	29.54717	1.068125
11.0209	38.05472	11.88679	32.90566	0.770945
% Reduction			5.49%	60.07%

The results obtained from the varying concentration of NAP between 2-13 ppm and fixing concentration of CFA at 7 ppm on A-GO-A-SBA-15 were reported in Figure 4.38. The decrease of adsorption capacity of CFA and strongly decrease of NAP can be investigated. The concentration of CFA was moderately reduced from the single solute around 7.62% On contrary, the concentration of NAP exhibited the decrease around 60.07% (as Table 4.20). In conclusion, the adsorption of NAP on A-GO-A-SBA-15 might be easily reduced by the existence of CFA.

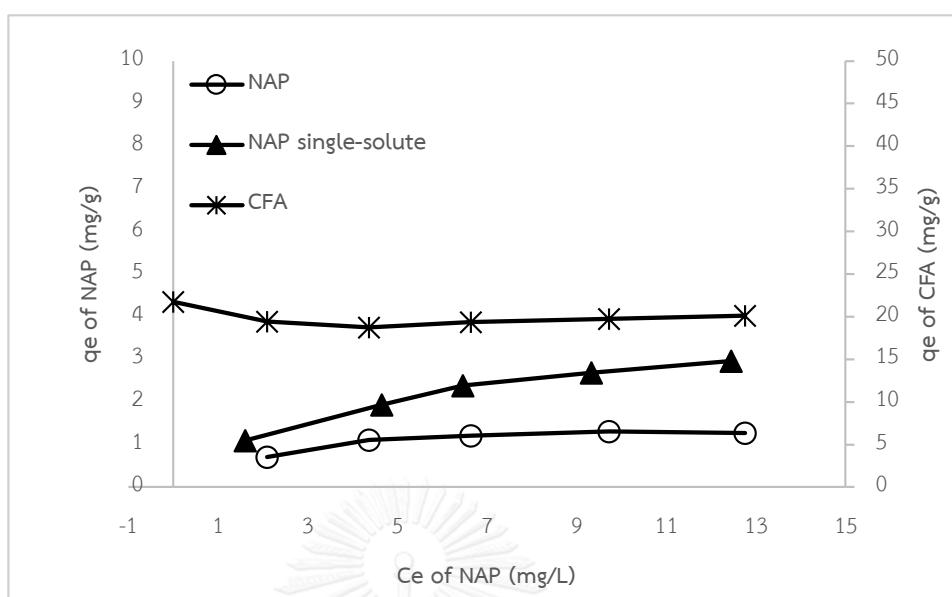


Figure 4.38 Adsorption isotherm of vary NAP and CFA on A-GO-A-SBA-15 in multi-solute

Table 4.20 The adsorption isotherm data of vary NAP and CFA on A-GO-A-SBA-15 in multi-solute.

C _e of NAP (Single solute)	q _e of NAP (Single solute)	C _e of NAP (Multi-solute)	q _e of NAP (Multi-solute)	q _e of CFA (Multi-solute)
-	-	0	-	21.77322
1.611673	1.095623	2.094494	0.706341	19.43396
4.649025	1.936101	4.37072	1.106888	18.75472
6.461306	2.378853	6.64587	1.201641	19.35849
9.333565	2.686528	9.726421	1.309315	19.73585
12.44637	2.955935	12.7639	1.270552	20.11321
% Reduction			56.95%	7.62%

Overall, the adsorption selectivities on GO-A-SBA-15 and A-GO-A-SBA-15 in multi-solute of CFA and NAP were investigated. On both adsorbents, NAP was easily disturbed on both adsorbents. However, CFA was slightly interrupted on A-GO-A-SBA-15.

CHAPTER V

CONCLUSION AND RECOMMENDATIONS

5.1 CONCLUSION

The objectives in this study are to synthesize and characterize GO modified SBA-15, to study the adsorptive information of CFA and NAP on GO modified SBA-15 by batch experiment, and to investigate selective adsorption of CFA and NAP on GO modified SBA-15. SBA-15, amine functional group modified SBA-15 (A-SBA-15), GO, amine functional group modified GO (A-GO), GO modified SBA-15 (GO-A-SBA-15) and amine functional group on GO modified SBA-15 (A-GO-A-SBA-15) were synthesized to investigate the adsorption efficiency of CFA and NAP comparing with powder activated carbon (PAC). All synthesized adsorbents were characterized and studied the adsorptive information such as the adsorption kinetic, the adsorption isotherm, and the adsorption selectivity were studied under batch experiments.

From the characterization of all synthesized adsorbents, the structure of A-SBA-15, GO, and GO-A-SBA-15 were confirmed by characteristic peaks in XRD pattern. The pore size and pore volume of SBA-15 and A-SBA-15 were analyzed using N₂ adsorption-desorption isotherm. Additionally, the functional groups on the surface of adsorbents were detected by FTIR spectra and XPS. SEM and TEM were used to study the external and internal morphologies, respectively.

In addition, the adsorption kinetic was studied using the pseudo-first order, the pseudo-second order, and the Ritchie-second order models. The adsorption kinetic of CFA and NAP on all adsorbents including PAC were reported the best fit with the pseudo-second order model. Intraparticle diffusion mechanism of CFA and NAP exhibited that amine functional group could reduce the rate of adsorption by stearic

effect as well as the contrast of hydrophilic-hydrophobic like. The pore size was showed the involvedness in adsorption of CFA; however, no significant was occurred in adsorption of NAP because the size of NAP was bigger than the pore size of synthesized adsorbents.

For adsorption isotherm, there is no doubt that the presence of GO, and amine functional group could affect the adsorption efficiency of CFA and NAP. The results of GO modified SBA-15 were reported as follow; A-GO-A-SBA-15 showed better adsorption efficiency for CFA and GO-A-SBA-15 also showed better results for NAP than all synthesized adsorbents. Likewise, Langmuir model was reported the highest R^2 for the adsorption isotherm of CFA on A-GO-A-SBA-15. While, Freundlich model gave the best fitting for the adsorption isotherm of NAP on GO-A-SBA-15. The adsorption capacities of CFA on A-GO-A-SBA-15 and NAP on GO-A-SBA-15 were higher in lower pH due to attractive electrostatic interaction. In low concentration, the adsorptions of CFA on A-GO-A-SBA-15 and NAP on GO-A-SBA-15 were fitted with Linear model.

Besides, adsorption selectivity was studied in multi-solute of CFA and NAP. The results demonstrated that the adsorption of NAP was easily disturbed by CFA on GO-A-SBA-15 and A-GO-A-SBA-15. The adsorption of CFA showed slightly effect on A-GO-A-SBA-15 but on GO-A-SBA-15 was exhibited the strongly effect indicating that amine functional group might decrease the effect of competitive molecule.

5.2 RECOMMENDATIONS

1. GO modified SBA-15 should be developed to increase the quantity of GO attached on silicate materials.
2. The amine functional group on adsorbent should be improved the stability.
3. The regeneration method should be studied.
4. Dispersion of GO might affect the adsorption efficiency.
5. TOC level should be improved.



REFERENCES

- Albadarin, A. B., et al. (2012). "Kinetic and thermodynamics of chromium ions adsorption onto low-cost dolomite adsorbent." Chemical Engineering Journal **179**: 193-202.
- Andreozzi, R., et al. (2003). "Ozonation and H₂O₂/UV treatment of clofibrilic acid in water: a kinetic investigation." Journal of Hazardous Materials **103**(3): 233-246.
- Asgharinezhad, A. A. and H. Ebrahimzadeh (2016). "Poly(2-aminobenzothiazole)-coated graphene oxide/magnetite nanoparticles composite as an efficient sorbent for determination of non-steroidal anti-inflammatory drugs in urine sample." J Chromatogr A **1435**: 18-29.
- Babić, B. M., et al. (1999). "Point of zero charge and intrinsic equilibrium constants of activated carbon cloth." Carbon **37**(3): 477-481.
- Benotti, M. J., et al. (2009). "Pharmaceuticals and Endocrine Disrupting Compounds in U.S. Drinking Water." Environmental Science & Technology **43**(3): 597-603.
- Boyd, G. R., et al. (2003). "Pharmaceuticals and personal care products (PPCPs) in surface and treated waters of Louisiana, USA and Ontario, Canada." Science of The Total Environment **311**(1-3): 135-149.
- Brown, K. D., et al. (2006). "Occurrence of antibiotics in hospital, residential, and dairy effluent, municipal wastewater, and the Rio Grande in New Mexico." Sci Total Environ **366**(2-3): 772-783.
- Bui, T. X. and H. Choi (2009). "Adsorptive removal of selected pharmaceuticals by mesoporous silica SBA-15." J Hazard Mater **168**(2-3): 602-608.

Bui, T. X., et al. (2013). "Adsorption of pharmaceuticals onto trimethylsilylated mesoporous SBA-15." J Hazard Mater **254-255**: 345-353.

Buser, H.-R., et al. (1998). "Occurrence of the Pharmaceutical Drug Clofibric Acid and the Herbicide Mecoprop in Various Swiss Lakes and in the North Sea." Environmental Science & Technology **32**(1): 188-192.

Cabrera-Lafaurie, W. A., et al. (2012). "Transition metal modified and partially calcined inorganic-organic pillared clays for the adsorption of salicylic acid, clofibric acid, carbamazepine, and caffeine from water." J Colloid Interface Sci **386**(1): 381-391.

Carmona, E., et al. (2014). "Occurrence of acidic pharmaceuticals and personal care products in Turia River Basin: from waste to drinking water." Sci Total Environ **484**: 53-63.

Carrara, C., et al. (2008). "Fate of Pharmaceutical and Trace Organic Compounds in Three Septic System Plumes, Ontario, Canada." Environmental Science & Technology **42**(8): 2805-2811.

Cheng, T., et al. (2015). "Transition-metal-functionalized ordered mesoporous silicas: an overview of sustainable chiral catalysts for enantioselective transformations." Green Chem. **17**(4): 2100-2122.

Chowdhury, S. and R. Balasubramanian (2014). "Recent advances in the use of graphene-family nanoadsorbents for removal of toxic pollutants from wastewater." Adv Colloid Interface Sci **204**: 35-56.

Coimbra, A. M., et al. (2015). "Chronic effects of clofibric acid in zebrafish (*Danio rerio*): a multigenerational study." *Aquat Toxicol* **160**: 76-86.

de Jesus Gaffney, V., et al. (2015). "Occurrence of pharmaceuticals in a water supply system and related human health risk assessment." *Water Res* **72**: 199-208.

de Villiers, M. M., et al. (2008). *Nanotechnology in Drug Delivery*, Springer New York.

Faust, S. D. and O. M. Aly (1987). *Adsorption processes for water treatment*, Butterworth.

Ferrari, B. t., et al. (2003). "Ecotoxicological impact of pharmaceuticals found in treated wastewaters: study of carbamazepine, clofibric acid, and diclofenac." *Ecotoxicology and Environmental Safety* **55**(3): 359-370.

Grenni, P., et al. (2013). "Degradation of Gemfibrozil and Naproxen in a river water ecosystem." *Microchemical Journal* **107**: 158-164.

Hasan, Z., et al. (2013). "Adsorption of naproxen and clofibric acid over a metal-organic framework MIL-101 functionalized with acidic and basic groups." *Chemical Engineering Journal* **219**: 537-544.

Hasan, Z., et al. (2012). "Adsorptive removal of naproxen and clofibric acid from water using metal-organic frameworks." *Journal of Hazardous Materials* **209-210**: 151-157.

Heberer, T., et al. (2004). "Field Studies on the Fate and Transport of Pharmaceutical Residues in Bank Filtration." *Ground Water Monitoring & Remediation* **24**(2): 70-77.

Heberer, T. and H. J. Stan (1997). *Int. J. Environ. Anal. Chem.* **67**(1-4): 113.

Heberer, T. and H. J. Stan (1997). "Determination of Clofibric Acid and N-(Phenylsulfonyl)-Sarcosine in Sewage, River and Drinking Water." International Journal of Environmental Analytical Chemistry **67**(1-4): 113-124.

Hoffmann, F., et al. (2006). "Silica-based mesoporous organic-inorganic hybrid materials." Angew Chem Int Ed Engl **45**(20): 3216-3251.

Huang, Y.-L., et al. (2011). "Effect of extended polymer chains on properties of transparent graphene nanosheets conductive film." Journal of Materials Chemistry **21**(45): 18236-18241.

Hummers, W. S. and R. E. Offeman (1958). "Preparation of Graphitic Oxide." J Am Chem Soc **80**(6): 1339-1339.

Isidori, M., et al. (2005). "Ecotoxicity of naproxen and its phototransformation products." Sci Total Environ **348**(1-3): 93-101.

Jácome-Acatitla, G., et al. (2014). "Photodegradation of sodium naproxen and oxytetracycline hydrochloride in aqueous medium using as photocatalysts Mg-Al calcined hydrotalcites." Journal of Photochemistry and Photobiology A: Chemistry **277**: 82-89.

Jallouli, N., et al. (2016). "UV and solar photo-degradation of naproxen: TiO₂ catalyst effect, reaction kinetics, products identification and toxicity assessment." J Hazard Mater **304**: 329-336.

Janssen, A. H., et al. (2002). "A 3D-TEM study of the shape of mesopores in SBA-15 and modified SBA-15 materials." Chemical Communications(15): 1632-1633.

Kanakaraju, D., et al. (2015). "TiO₂ photocatalysis of naproxen: effect of the water matrix, anions and diclofenac on degradation rates." Chemosphere **139**: 579-588.

Kanamori, K. and K. Nakanishi (2011). "Controlled pore formation in organotrialkoxysilane-derived hybrids: from aerogels to hierarchically porous monoliths." Chemical Society Reviews **40**(2): 754-770.

Kaosaiphun, J. (2013). Application of functionalized superparamagnetic mesoporous silicates adsorbent's on clofibric acid removal in wastewater. Program in Environmental Management (Interdisciplinary Program), Graduate School, Chulalongkorn University. Master of Science: 106.

Kim, I., et al. (2009). "Performance of UV and UV/H₂O₂ processes for the removal of pharmaceuticals detected in secondary effluent of a sewage treatment plant in Japan." J Hazard Mater **166**(2-3): 1134-1140.

Kim, I., et al. (2009). "Photodegradation of pharmaceuticals and personal care products during UV and UV/H₂O₂ treatments." Chemosphere **77**(4): 518-525.

Lai, L., et al. (2011). "One-step synthesis of NH₂-graphene from in situ graphene-oxide reduction and its improved electrochemical properties." Carbon **49**(10): 3250-3257.

Lautier, J., et al. (1986). "Comparative hypolipidemic effects of clofibric acid and itanoxone on the metabolism and the distribution of lipids in the crab *Pachygrapsus marmoratus* (Decapoda, Brachyura)." Comparative Biochemistry and Physiology Part C: Comparative Pharmacology **85**(2): 269-274.

Lewinsky, A. A. (2007). Hazardous Materials and Wastewater: Treatment, Removal and Analysis, Nova Science Publishers.

Li, W., et al. (2009). "Photo-degradation of clofibric acid by ultraviolet light irradiation at 185 nm." Water Sci Technol **60**(11): 2983-2989.

Li, W., et al. (2010). "Clofibric acid degradation in UV254/H₂O₂ process: effect of temperature." J Hazard Mater **176**(1-3): 1051-1057.

Li, X., et al. (2015). "Preparation, characterization, and application of mesoporous silica-grafted graphene oxide for highly selective lead adsorption." Chemical Engineering Journal **273**: 630-637.

Lindqvist, N., et al. (2005). "Occurrence of acidic pharmaceuticals in raw and treated sewages and in receiving waters." Water Res **39**(11): 2219-2228.

Liu, Z., et al. (2013). "Biosorption of clofibric acid and carbamazepine in aqueous solution by agricultural waste rice straw." Journal of Environmental Sciences **25**(12): 2384-2395.

Marco-Urrea, E., et al. (2010). "Biodegradation of the analgesic naproxen by *Trametes versicolor* and identification of intermediates using HPLC-DAD-MS and NMR." Bioresour Technol **101**(7): 2159-2166.

Marco-Urrea, E., et al. (2010). "Oxidation of atenolol, propranolol, carbamazepine and clofibric acid by a biological Fenton-like system mediated by the white-rot fungus *Trametes versicolor*." Water Res **44**(2): 521-532.

Metcalfe, C. D., et al. (2003). "Occurrence of neutral and acidic drugs in the effluents of Canadian sewage treatment plants." Environ Toxicol Chem **22**(12): 2872-2880.

Mompelat, S., et al. (2009). "Occurrence and fate of pharmaceutical products and by-products, from resource to drinking water." Environ Int **35**(5): 803-814.

Myoung-Jun, K. and C. Gyu-Hoon (2012). "Study on the PV Driven Dehumidifying System with Oyster Shell and Thermoelectric Device." Journal of the Korean Society of Marine Environment and Safety **18**(3): 287-293.

Nie, Y., et al. (2014). "Removal of clofibric acid from aqueous solution by polyethylenimine-modified chitosan beads." Frontiers of Environmental Science & Engineering **8**(5): 675-682.

Permrunguang, J. (2013). Effects of surface functional groups and natural organic matter on clofibric acid adsorption by mesoporous silicate SBA-15. Program in Environmental Management (Interdisciplinary Program), Graduate School, Chulalongkorn University, Bangkok, Thailand. Master of Science: 127.

Prarat, P. (2011). Removal of haloacetonitriles by adsorption on modified inorganic porous materials. Program in Environmental Management (Interdisciplinary Program), Graduate School, Chulalongkorn University. Doctor of Philosophy: 200.

Pulido, A., et al. (2012). "Reconstruction of the carbon sp² network in graphene oxide by low-temperature reaction with CO." Journal of Materials Chemistry **22**(1): 51-56.

Rabiet, M., et al. (2006). "Consequences of treated water recycling as regards pharmaceuticals and drugs in surface and ground waters of a medium-sized Mediterranean catchment." Environ Sci Technol **40**(17): 5282-5288.

Reynel-Avila, H. E., et al. (2015). "Assessment of naproxen adsorption on bone char in aqueous solutions using batch and fixed-bed processes." Journal of Molecular Liquids **209**: 187-195.

Richert, L., et al. (2003). "Effects of clofibric acid on mRNA expression profiles in primary cultures of rat, mouse and human hepatocytes." Toxicology and Applied Pharmacology **191**(2): 130-146.

Rosal, R., et al. (2009). "Identification of intermediates and assessment of ecotoxicity in the oxidation products generated during the ozonation of clofibric acid." J Hazard Mater **172**(2-3): 1061-1068.

Rosal, R., et al. (2009). "Ozonation of clofibric acid catalyzed by titanium dioxide." J Hazard Mater **169**(1-3): 411-418.

Rosal, R., et al. (2008). "Catalytic ozonation of naproxen and carbamazepine on titanium dioxide." Applied Catalysis B: Environmental **84**(1-2): 48-57.

Ruangtrakul, W. (2010). Application of superparamagnetic mesoporous silicates on naproxen removal. Program in Environmental Management (Interdisciplinary Program), Graduate School, Chulalongkorn University. **Master of Science**: 103.

Sable, S. S., et al. (2014). "Clofibric acid degradation by catalytic ozonation using hydrotalcite-derived catalysts." Applied Catalysis B: Environmental **150-151**: 30-36.

Salgado, R., et al. (2012). "Biodegradation of clofibric acid and identification of its metabolites." J Hazard Mater **241-242**: 182-189.

Sim, W. J., et al. (2010). "Occurrence and fate of pharmaceuticals in wastewater treatment plants and rivers in Korea." Environ Pollut **158**(5): 1938-1947.

Sing, K. S. W. (1982). "Reporting physisorption data for gas/solid systems with special reference to the determination of surface area and porosity (Provisional)." Pure and Applied Chemistry **54**(11).

Solomons, T. W. G. and C. B. Fryhle (2011). Organic Chemistry, Wiley.

Sovadinova, I., et al. (2014). "Effects of clofibrac acid alone and in combination with 17beta-estradiol on mRNA abundance in primary hepatocytes isolated from rainbow trout." Toxicol In Vitro **28**(6): 1106-1116.

Stancova, V., et al. (2015). "Effects of the non-steroidal anti-inflammatory drug(NSAID) naproxen on gene expression of antioxidant enzymes in zebrafish (Danio rerio)." Environ Toxicol Pharmacol **40**(2): 343-348.

Stein, A., et al. (2000). "Hybrid Inorganic–Organic Mesoporous Silicates—Nanosopic Reactors Coming of Age." Advanced Materials **12**(19): 1403-1419.

Suriyanon, N., et al. (2015). "Selective adsorption mechanisms of antilipidemic and non-steroidal anti-inflammatory drug residues on functionalized silica-based porous materials in a mixed solute." Chemosphere **136**: 222-231.

Tanev, P. T., et al. (1994). "Titanium-containing mesoporous molecular sieves for catalytic oxidation of aromatic compounds." Nature **368**(6469): 321-323.

Teng, C.-C., et al. (2011). "Thermal conductivity and structure of non-covalent functionalized graphene/epoxy composites." Carbon **49**(15): 5107-5116.

Ternes, T. A. (1998). "Occurrence of drugs in German sewage treatment plants and rivers1." Water Research **32**(11): 3245-3260.

Tixier, C., et al. (2003). "Occurrence and Fate of Carbamazepine, Clofibric Acid, Diclofenac, Ibuprofen, Ketoprofen, and Naproxen in Surface Waters." Environ Sci Technol **37**(6): 1061-1068.

Trelle, S., et al. (2011). "Cardiovascular safety of non-steroidal anti-inflammatory drugs: network meta-analysis." BMJ **342**: c7086.

Verenitch, S. S., et al. (2006). "Determination of acidic drugs and caffeine in municipal wastewaters and receiving waters by gas chromatography-ion trap tandem mass spectrometry." J Chromatogr A **1116**(1-2): 193-203.

Winkler, M., et al. (2001). "Selective degradation of ibuprofen and clofibric acid in two model river biofilm systems." Water Res **35**(13): 3197-3205.

Wojcieszynska, D., et al. (2014). "Bacterial degradation of naproxen--undisclosed pollutant in the environment." J Environ Manage **145**: 157-161.

Xu, Y., et al. (2008). "Flexible graphene films via the filtration of water-soluble noncovalent functionalized graphene sheets." J Am Chem Soc **130**(18): 5856-5857.

Yang, A., et al. (2015). "One-step amine modification of graphene oxide to get a green trifunctional metal-free catalyst." Applied Surface Science **346**: 443-450.

Yang, D. Q., et al. (2005). "Spectroscopic evidence for pi-pi interaction between poly(diallyl dimethylammonium) chloride and multiwalled carbon nanotubes." J Phys Chem B **109**(10): 4481-4484.

Yu, Z., et al. (2008). "Adsorption characteristics of selected pharmaceuticals and an endocrine disrupting compound-Naproxen, carbamazepine and nonylphenol-on activated carbon." Water Res **42**(12): 2873-2882.

Zhang, Y.-L., et al. (2014). "Adsorption of Clofibric Acid from Aqueous Solution by Graphene Oxide and the Effect of Environmental Factors." Water, Air, & Soil Pollution **225**(8).

Zhang, Y., et al. (2012). "Heterogeneous oxidation of naproxen in the presence of α -MnO₂ nanostructures with different morphologies." Applied Catalysis B: Environmental **127**: 182-189.

Zhao, D., et al. (1998). "Triblock copolymer syntheses of mesoporous silica with periodic 50 to 300 angstrom pores." Science **279**(5350): 548-552.



APPENDIX A

Information for Physiochemical Characterization of Adsorbents

จุฬาลงกรณ์มหาวิทยาลัย
CHULALONGKORN UNIVERSITY

A.1 Point of Zero Charge

Table A.1 Data from pH meter of SBA-15

Initial pH	Final pH
3.24	3.26
4.51	4.87
6.3	5.8
8.61	7.72
10.48	9.11

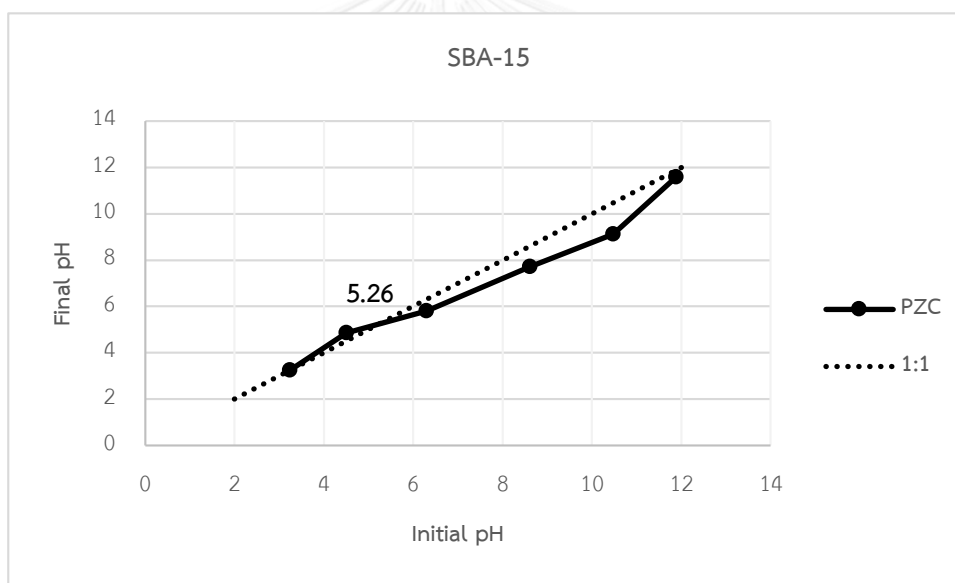


Figure A.1 PZC of SBA-15

Table A.2 Data from pH meter of A-SBA-15

Initial pH	Final pH
4.16	7.71
6.87	9.3
8.37	9.3
9.03	9.42
10.96	10.04

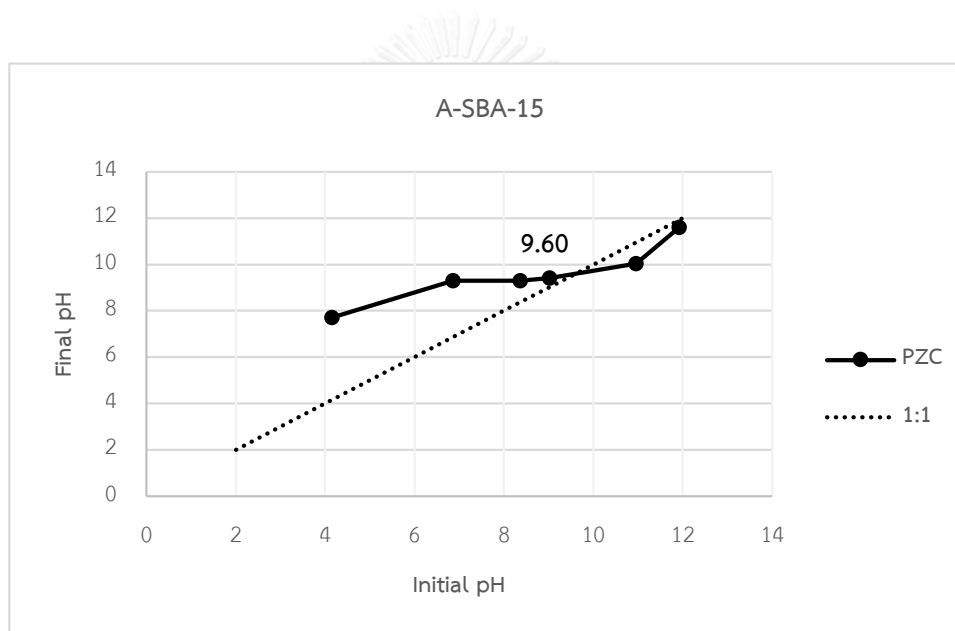


Figure A.2 PZC of A-SBA-15

Table A.3 Data from pH meter of GO

Initial pH	Final pH
3.2	3.19
3.71	3.89
3.75	3.9
3.93	4.09
10.48	10.55

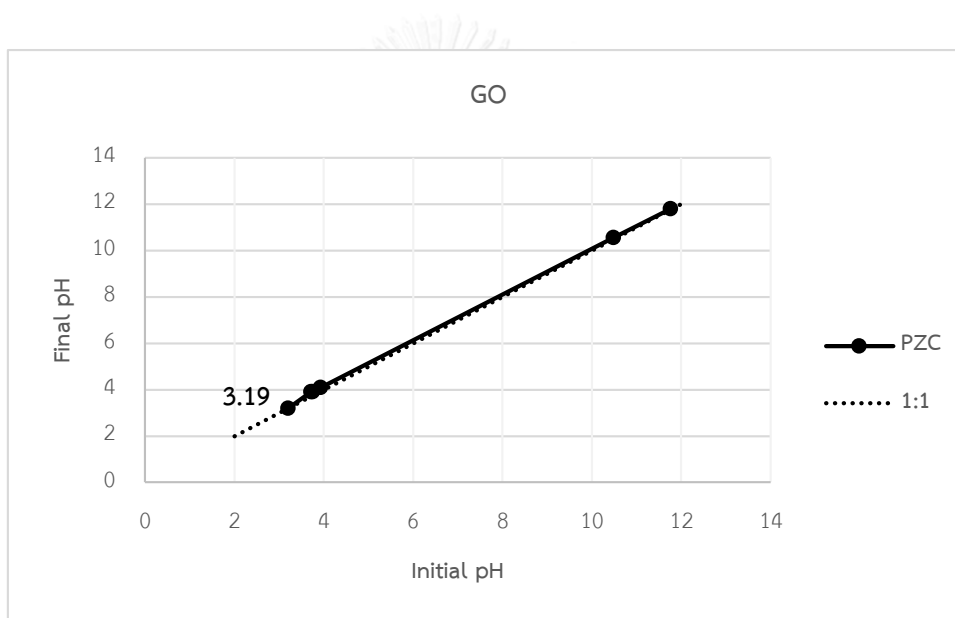


Figure A.3 PZC of GO

Table A.4 Data from pH meter of A-GO

Initial pH	Final pH
3.38	3.58
5.25	7.16
7.63	7.51
10.71	10.17
11.93	11.8

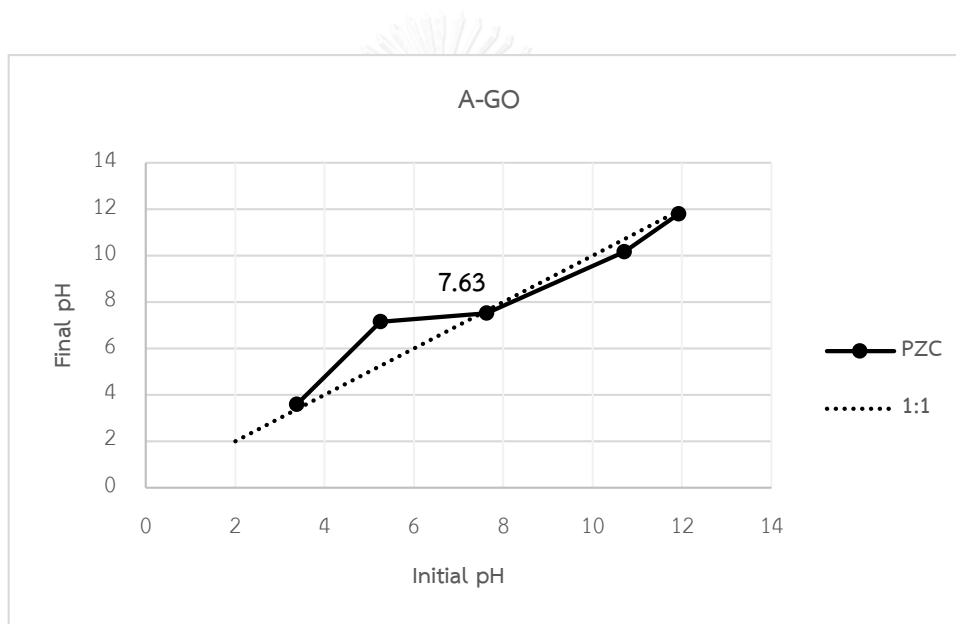


Figure A.4 PZC of A-GO

Table A.5 Data from pH meter of GO-A-SBA-15

Initial pH	Final pH
3.36	3.5
5.61	8.56
8.02	8.71
10.92	9.97
11.97	11.63

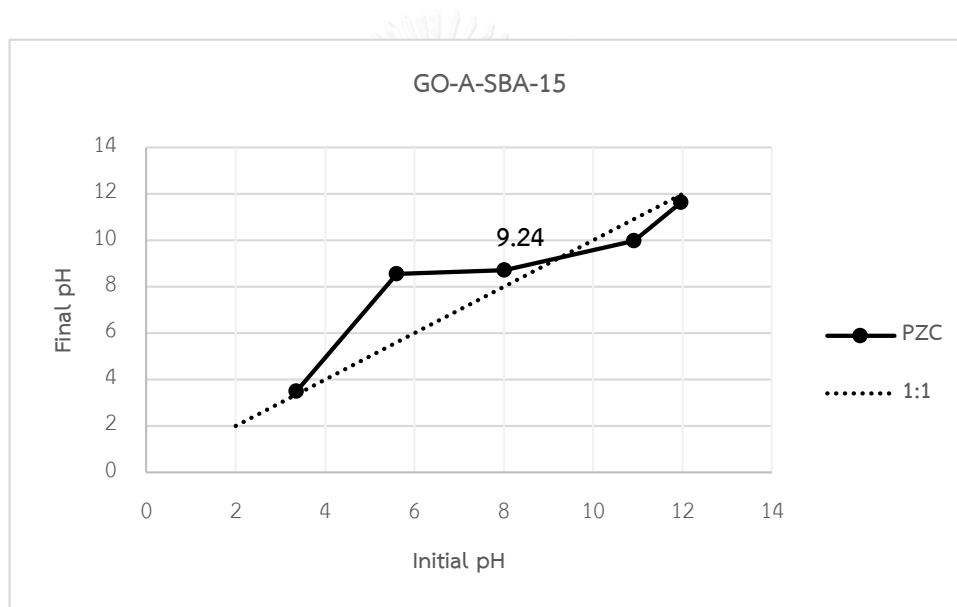


Figure A.5 PZC of GO-A-SBA-15

Table A.6 Data from pH meter of A-GO-A-SBA-15

Initial pH	Final pH
3.39	3.58
5.71	8.46
6.07	8.88
8.22	8.91
10.92	9.96

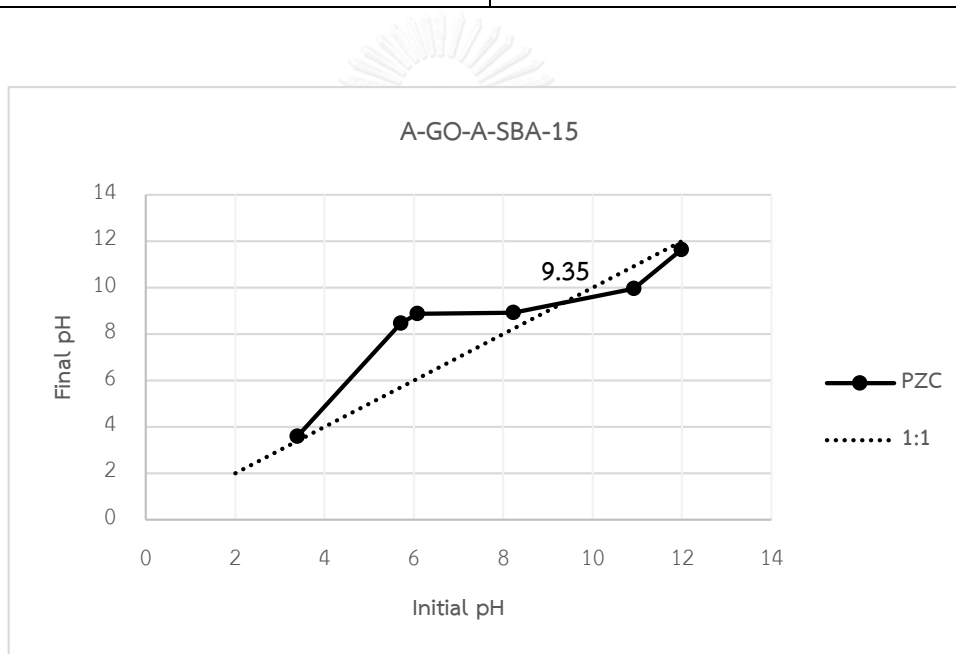
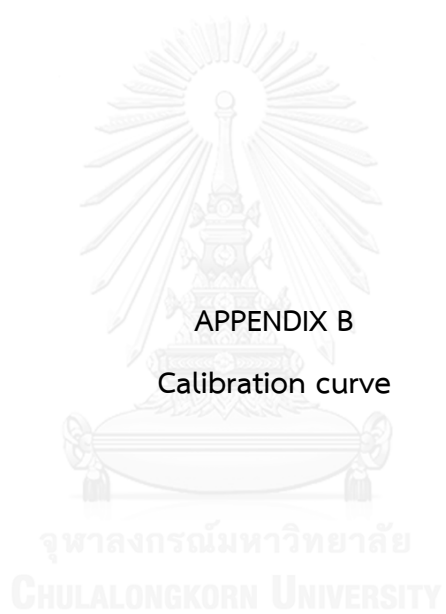


Figure A.6 PZC of GO-A-SBA-15



Information of analyze CFA and NAP concentration by High Performance Liquid Chromatography (HPLC) with diode array detector (DAD) at high and low concentration.

Laboratory equipment and chemical reagent

1. High Performance Liquid Chromatography (HPLC) with diode array detector (DAD), Agilent 1100 series.
2. Stock solution of CFA and NAP at concentration 20,000 ppm
3. Methanol (MeOH)
4. Phosphate buffer
5. 5Volumetric flask
6. Micropipette
7. Deionized water (DI water)

Preparation of CFA and NAP stock solution at 20,000 ppm

Table B.1 The preparation of CFA and NAP stock solution at 20,000 ppm

Pharmaceutics	Amount of pharmaceutics (g)	Total volume (mL)
CFA	0.1	5
NAP	0.1	5

Pharmaceutics 0.1 g were dissolved in MeOH using micropipette to adjust volume. Then dilute the stock of 20,000 ppm to 2, 5, 7, 10, 13, and 15 ppm for NAP and 7, 10, 13, 15, 17, and 20 ppm for CFA with DI water as equation B1;

$$C_1V_1 = C_2V_2$$

Example Preparation for 2 ppm of NAP from stock solution 20,000 mg/L in 100 mL of volumetric flask.

$$C_1V_1 = C_2V_2$$

$$20,000 \text{ mg/L} \times V_1 = 2 \text{ mg/L} \times 100 \text{ mL}$$

$$V_1 = 0.01 \text{ mL}$$

After that, 0.01 mL of stock solution was pipetted and added into 100 mL of volumetric flask and adjusted volume to 100 mL with condition of 10 mM phosphate buffer as Table B.2.

Table B.2 Volume of 20,000 ppm stock solution to prepare the standard concentration for high concentration in ppm unit.

Concentration of pharmaceuticals (ppm)	Volume of 20,000 stock solution (mL)
2	0.010
5	0.025
7	0.035
10	0.050
13	0.065
15	0.075
17	0.085
20	0.100

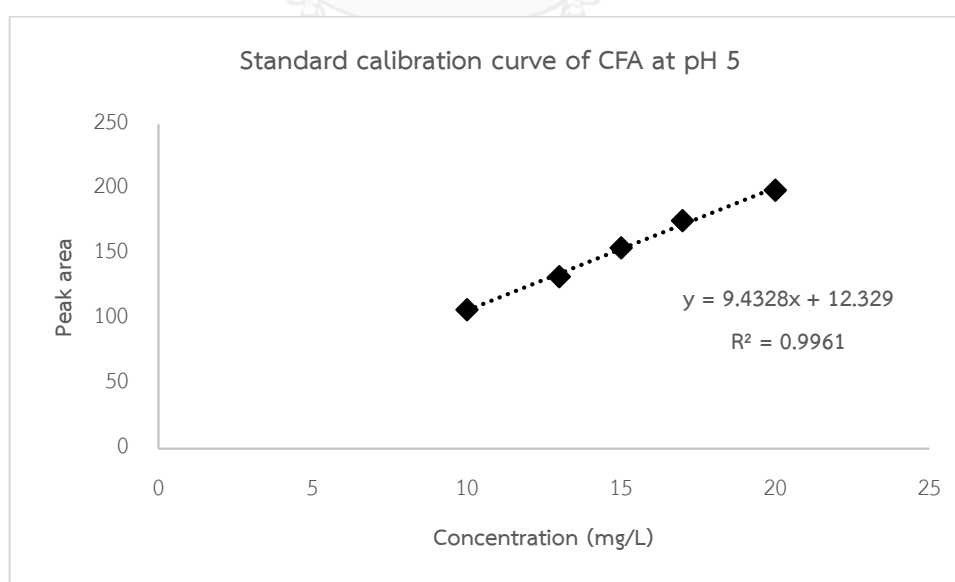
Next, preparation of CFA and NAP standard concentration in low concentration in ppb unit using the dilution of 10 ppm stock solution for both CFA and NAP in 25 mL of volumetric flask by the calculation from equation B1 as Table B.3

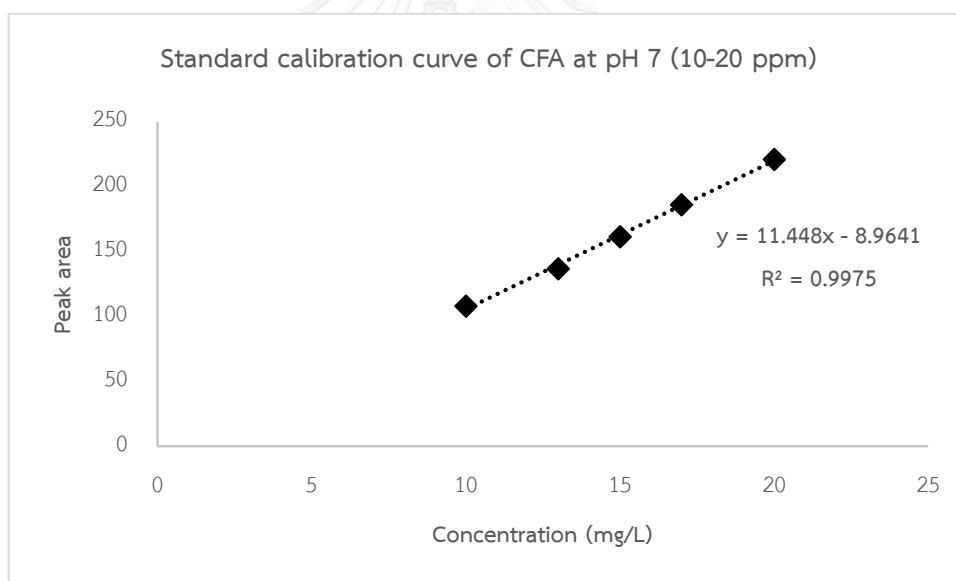
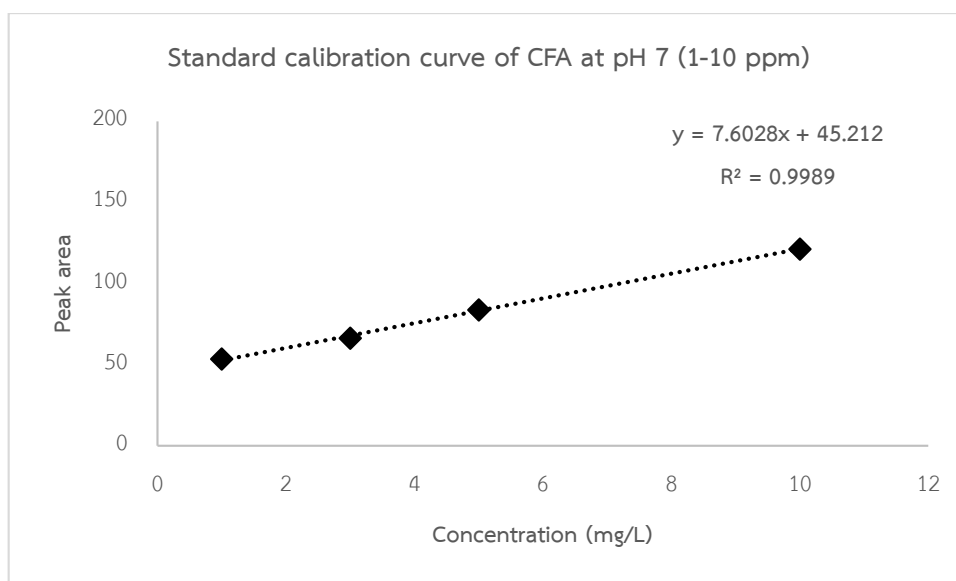
Table B.3 Volume of 10 ppm stock solution to prepare the standard concentration for low concentration in ppb unit.

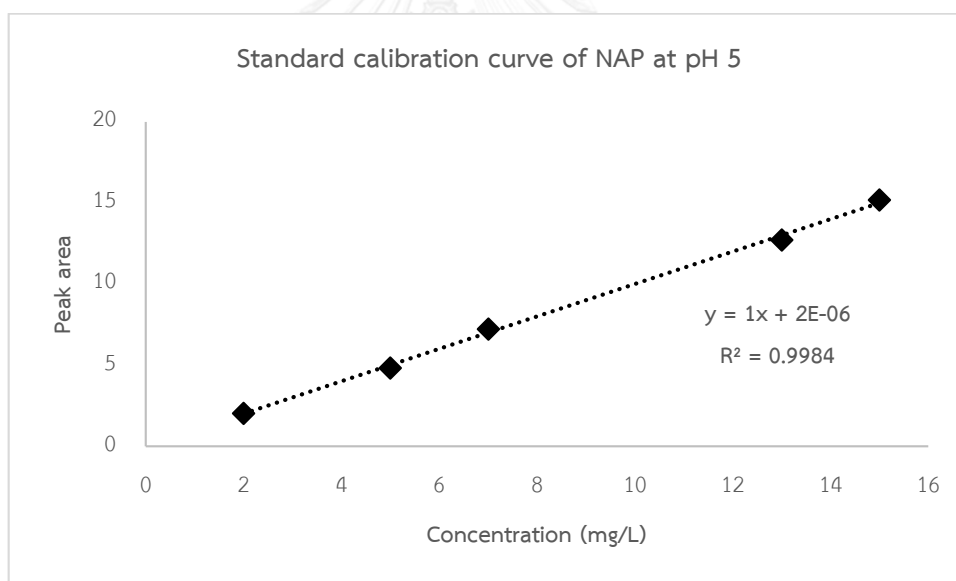
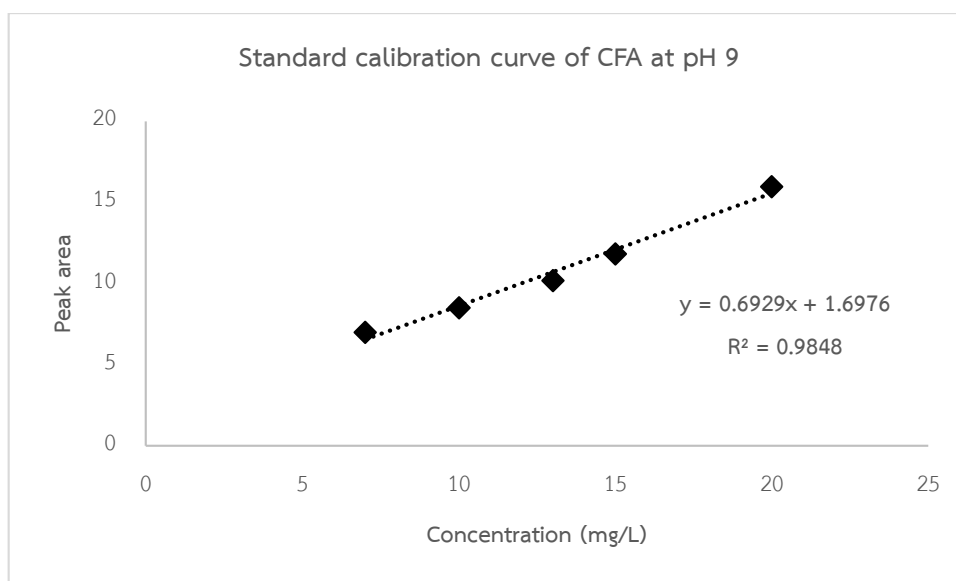
Concentration of pharmaceuticals (ppb)	Volume of 10 stock solution (mL)
25	0.010
50	0.025
75	0.035
100	0.050
125	0.065

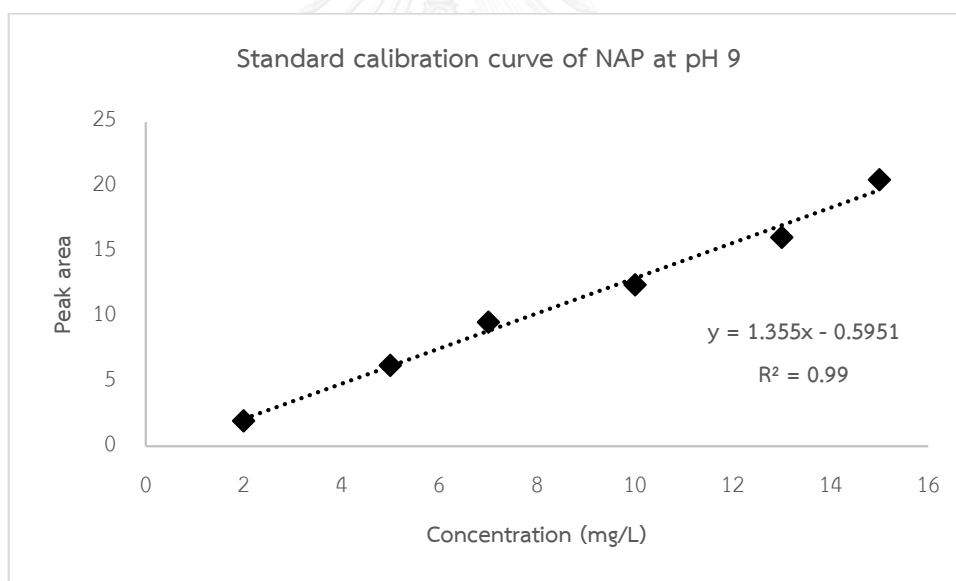
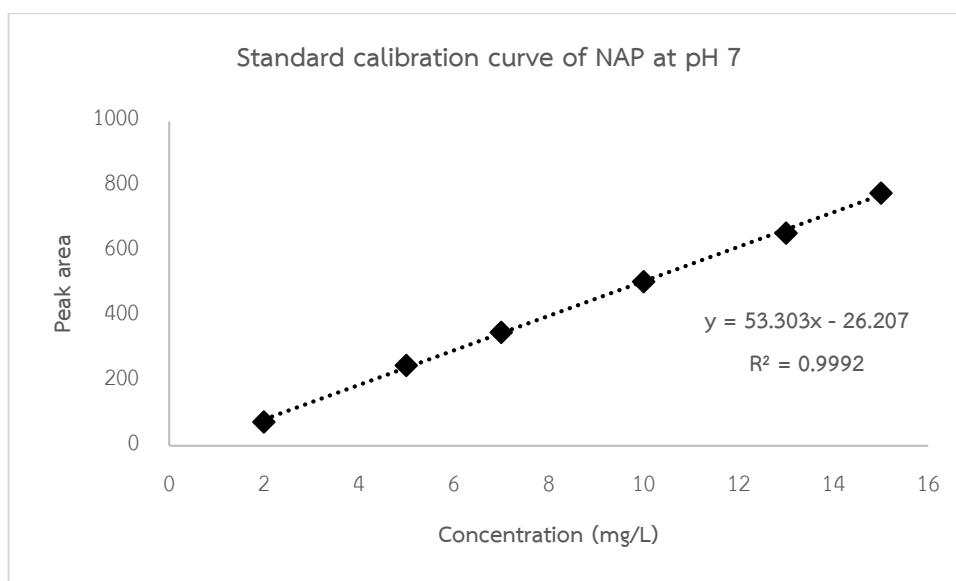
Standard calibration curve at high concentration

The concentration of standard solution of CFA and NAP were analyzed using HPLC/DAD with C18 hypersil ODS column at 254 nm. Standard calibration curves were plotted by the relationship of concentration of standard solution and peak area.



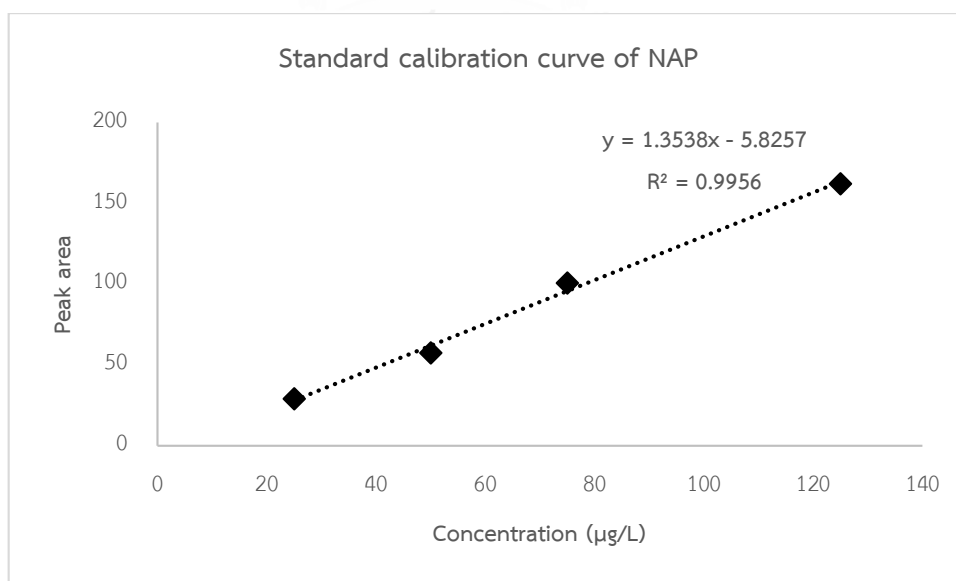
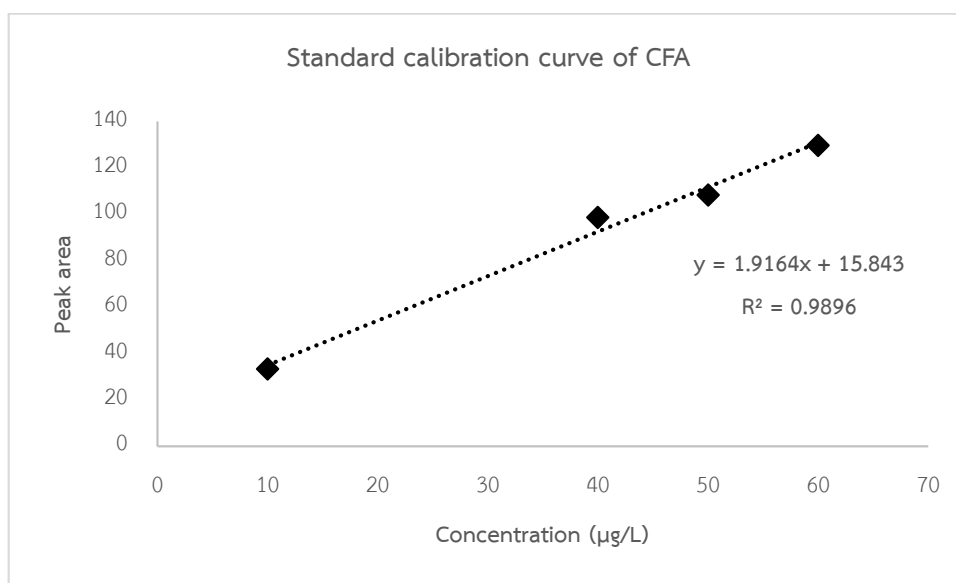






Standard calibration curve at low concentration

The concentration of standard solution of CFA and NAP were analyzed using HPLC/DAD with C18 hypersil ODS column at 230 nm. Standard calibration curves were plotted by the relationship of concentration of standard solution and peak area.





C.1 Adsorption kinetic study

Table C.1 Data of adsorption kinetic for CFA and NAP on SBA-15 at pH 7 and IS 0.01

M

CFA		NAP	
Time (min)	q_t (mg/g)	Time (min)	q_t (mg/g)
0.25	1.720971	0.233333	0
0.5	2.223726	0.533333	0
1	2.281736	1	0
10	2.301073	2	0
120	2.088369	5	0
180	2.339747	10	0
240	2.165716	15	0
		30	0
		60	0
		120	0
		180	0
		240	0
		300	0
		360	0
		420	0
		480	0
		540	0
		600	0

Table C.2 Data of adsorption kinetic for CFA and NAP on A-SBA-15 at pH 7 and IS 0.01

M

CFA		NAP	
Time (min)	q_t (mg/g)	Time (min)	q_t (mg/g)
0.25	2.318044	0.266667	0
0.5	2.193388	0.516667	0
1	2.66708	1	0
2	2.741873	2	0
5	4.43719	5	0
10	5.33471	10	0
15	5.459366	15	0
30	5.409504	30	0
60	5.658815	60	0
120	5.658815	120	0
180	5.459366	180	0
240	5.608953	240	0
300	5.509228	300	0
360	5.608953	360	0
		420	0
		480	0
		540	0
		600	0

Table C.3 Data of adsorption kinetic for CFA and NAP on GO at pH 7 and IS 0.01 M

CFA		NAP	
Time (min)	q_t (mg/g)	Time (min)	q_t (mg/g)
0.5	28.93863	1	8.700747
1	41.42196	2	17.90513
2	96.1784	5	15.49115
5	92.20643	10	20.84011
10	98.44809	15	14.50125
60	112.6337	60	19.225
240	129.9401	120	19.53761
420	121.1451	240	28.01259
480	118.3079	300	24.33083
		360	25.1297
		480	22.92412
		660	22.97623

Table C.4 Data of adsorption kinetic for CFA and NAP on A-GO at pH 7 and IS 0.01 M

CFA		NAP	
Time (min)	q_t (mg/g)	Time (min)	q_t (mg/g)
0.25	21.65716	0.2485	1.178623
2	27.99961	0.562333	1.39233
10	36.7785	0.996667	1.813266
30	45.05463	1.9905	2.269821
60	46.2535	4.967667	2.583904
180	47.06565	10.43767	2.982175
300	47.49106	14.59767	3.40635
		29.60767	3.616818
		60.68767	3.814335
		119.8077	3.859666
		239.3977	3.866142
		440.6312	3.947092
		609.8677	3.963282

Table C.5 Data of adsorption kinetic for CFA and NAP on GO-A-SBA-15 at pH 7 and IS 0.01 M

CFA		NAP	
Time (min)	q_t (mg/g)	Time (min)	q_t (mg/g)
0.25	20.22624	0.25	1.240732
0.5	25.60186	0.5	1.145912
2	27.07145	1	1.295204
10	28.85043	2	1.303273
15	28.96645	5	1.430373
60	29.00512	10	1.480809
120	29.73992	15	1.587734
300	28.19298	30	1.763252
420	29.85594	60	1.940788
		120	1.987189
		180	2.029556
		360	2.156655
		480	2.16876
		540	2.154638
		600	2.180864
		660	2.14455

Table C.6 Data of adsorption kinetic for CFA and NAP on A-GO-A-SBA-15 at pH 7 and IS 0.01 M

CFA		NAP	
Time (min)	q_t (mg/g)	Time (min)	q_t (mg/g)
0.25	19.91685	0.25	1.129773
0.5	21.69583	2	1.190296
1	29.73992	15	1.194331
2	31.40288	30	1.252837
60	35.54095	120	1.414233
120	34.53543	180	1.545367
180	35.54095	240	1.841933
240	35.23156	360	2.142533
420	35.96635	420	2.281737
		540	2.475412
		600	2.489534
		660	2.515761
		720	2.527866

Table C.7 Data of adsorption kinetic for CFA and NAP on PAC at pH 7 and IS 0.01 M

CFA		NAP	
Time (min)	q_t (mg/g)	Time (min)	q_t (mg/g)
0.25	136.1307	0.25	21.50603
2	160.8818	0.5	20.13416
5	176.1578	1	28.8899
10	175.3843	2	33.67126
30	172.2904	5	49.06441
60	177.5114	10	62.05679
120	179.0583	15	67.28199
180	176.5445	30	80.55682
		60	106.8846
		120	118.263
		180	125.9091
		240	128.3301
		300	131.8808
		360	134.7859
		420	135.5525
		480	136.7025
		540	138.3366
		600	138.1954
		660	136.9042
		720	139.8094
		780	139.9304
		840	141.2821
		900	141.3426
		1080	141.6049

		1260	142.2706
		1440	143.7837
		1500	143.0776
		1560	143.6627
		1620	142.7347



C.2 Adsorption isotherm in single solute at high concentration and pH 7

Table C.8 Data of adsorption isotherm for CFA and NAP on SBA-15 at pH 7 and IS 0.01 in single solute and high concentration.

CFA			NAP		
C_0 (mg/L)	C_e (mg/L)	q_e (mg/g)	C_0 (mg/L)	C_e (mg/L)	q_e (mg/g)
1.611843	1.358987	0.486262	2.244648	2.244648	0
5.28975	4.048456	2.387103	4.818205	4.818205	0
7.358573	7.128704	0.425684	7.07483	7.07483	0
9.933108	8.829736	2.12187	9.668195	9.668195	0
12.80647	12.59959	0.362951	12.84819	12.84819	0
			15.34556	15.34556	0

Table C.9 Data of adsorption isotherm for CFA and NAP on A-SBA-15 at pH 7 and IS 0.01 in single solute and high concentration.

CFA			NAP		
C_0 (mg/L)	C_e (mg/L)	q_e (mg/g)	C_0 (mg/L)	C_e (mg/L)	q_e (mg/g)
1.611843	0.692366	1.585305	2.244648	2.244648	0
5.28975	2.393398	5.081319	4.818205	4.818205	0
7.358573	4.324299	6.068547	7.07483	7.07483	0
9.933108	6.737926	6.265063	9.668195	9.668195	0
12.80647	9.657265	6.298416	12.84819	12.84819	0
			15.34556	15.34556	0

Table C.10 Data of adsorption isotherm for CFA and NAP on GO at pH 7 and IS 0.01 in single solute and high concentration.

CFA			NAP		
C_0 (mg/L)	C_e (mg/L)	q_e (mg/g)	C_0 (mg/L)	C_e (mg/L)	q_e (mg/g)
5.233998	0.334146	94.22792	1.969363	1.754443	10.74597
7.385152	1.7802	107.7875	4.935555	4.644423	14.5566
8.651943	2.604809	116.291	7.02073	6.59394	21.33951
13.65935	7.528563	117.8998	10.26129	9.845144	20.80731
15.06955	8.628041	123.8752	13.25339	12.85099	20.12011

Table C.11 Data of adsorption isotherm for CFA and NAP on A-GO at pH 7 and IS 0.01 in single solute and high concentration.

CFA			NAP		
C_0 (mg/L)	C_e (mg/L)	q_e (mg/g)	C_0 (mg/L)	C_e (mg/L)	q_e (mg/g)
10.17009	1.787605	33.52992	2.007821	0.673044	2.566879
12.27779	3.141178	36.54646	5.162161	1.670087	6.984148
14.67555	4.813806	39.44697	7.039898	2.592796	8.894204
16.94762	5.790312	44.62922	9.843576	4.250764	11.18562
20.53458	8.023707	50.04351	12.36931	4.830891	14.63771

Table C.13 Data of adsorption isotherm for CFA and NAP on GO-A-SBA-15 at pH 7 and IS 0.01 in single solute and high concentration.

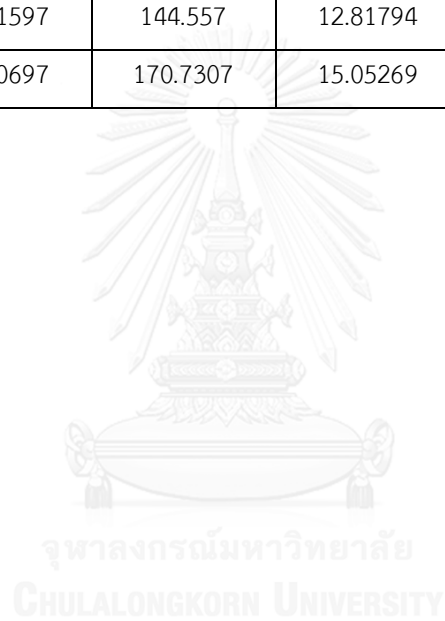
CFA			NAP		
C_0 (mg/L)	C_e (mg/L)	q_e (mg/g)	C_0 (mg/L)	C_e (mg/L)	q_e (mg/g)
6.345482	1.57419	19.08517	1.885579	1.540382	1.380785
10.17009	4.427071	22.97206	5.133051	4.720316	1.650939
12.27779	6.331741	23.7842	6.610528	6.060092	2.201746
14.67555	8.139727	26.14329	11.35462	10.41036	3.777028
16.94762	9.783351	28.65706	11.74619	12.80804	4.247416
20.53458	12.45182	32.33105			

Table C.14 Data of adsorption isotherm for CFA and NAP on A-GO-A-SBA-15 at pH 7 and IS 0.01 in single solute and high concentration.

CFA			NAP		
C_0 (mg/L)	C_e (mg/L)	q_e (mg/g)	C_0 (mg/L)	C_e (mg/L)	q_e (mg/g)
6.345482	0.902177	21.77322	1.885579	1.611673	1.095623
10.17009	3.982326	24.75104	5.133051	4.649025	1.936101
12.27779	5.132863	28.57972	7.056019	6.461306	2.378853
14.67555	6.786155	31.55758	10.0052	9.333565	2.686528
16.94762	8.536131	33.64594	13.18535	12.44637	2.955935
20.53458	11.0209	38.05472	13.60806	12.85083	3.028921

Table C.15 Data of adsorption isotherm for CFA and NAP on PAC at pH 7 and IS 0.01 in single solute and high concentration.

CFA			NAP		
C_0 (mg/L)	C_e (mg/L)	q_e (mg/g)	C_0 (mg/L)	C_e (mg/L)	q_e (mg/g)
10.73648	4.470458	125.3205	5.176607	0.549889	92.53437
12.51679	5.9436	131.4638	7.08771	0.790318	125.9478
14.95299	8.127006	136.5198	10.04376	2.15275	157.8201
15.74945	8.521597	144.557	12.81794	3.754069	181.2774
21.04351	12.50697	170.7307	15.05269	5.113418	198.7855



C.3 Adsorption isotherm in single solute at high concentration and vary pH

Table C.16 Data of adsorption isotherm for CFA on A-GO-A-SBA-15 at pH 5, 7, and 9 in single solute and high concentration.

pH 5			pH 7			pH 9		
C_0 (mg/L)	C_e (mg/L)	q_e (mg/g)	C_0 (mg/L)	C_e (mg/L)	q_e (mg/g)	C_0 (mg/L)	C_e (mg/L)	q_e (mg/g)
			6.345482	0.902177	21.77322	7.007758	4.053426	11.81733
9.686871	0.195747	37.96449	10.17009	3.982326	24.75104	8.515913	5.0141	14.00725
13.05968	3.153852	39.62331	12.27779	5.132863	28.57972	10.18935	6.377638	15.24683
15.01934	4.633882	41.54183	14.67555	6.786155	31.55758	11.84212	7.896123	15.78398
17.37815	6.746747	42.5256	16.94762	8.536131	33.64594	15.14766	10.9021	16.98224
19.81735	8.730969	44.34554	20.53458	11.0209	38.05472	15.97405	11.30497	18.67634

Table C.17 Data of adsorption isotherm for NAP on GO-A-SBA-15 at pH 5, 7, and 9 in single solute and high concentration.

pH 5			pH 7			pH 9		
C_0 (mg/L)	C_e (mg/L)	q_e (mg/g)	C_0 (mg/L)	C_e (mg/L)	q_e (mg/g)	C_0 (mg/L)	C_e (mg/L)	q_e (mg/g)
2.025922	0.920727	4.420781	1.885579	1.540382	1.380785	1.973486	1.883403	0.360331
4.838658	3.397332	5.765301	5.133051	4.720316	1.650939	6.245025	6.00839	0.946542
7.229214	5.750242	5.915887	6.610528	6.060092	2.201746	9.586157	9.1707	1.661826
8.519953	6.969721	6.200925	11.35462	10.41036	3.777028	12.44461	11.99285	1.807035
12.72158	11.1216	6.399914	11.74619	12.80804	4.247416	16.10439	15.59213	2.049048
15.18474	13.48526	6.797892				20.53593	19.58535	3.802302

C.4 Adsorption isotherm in multi-solute at high concentration and pH 7

Table C.18 Data of adsorption isotherm for multi-solute of vary CFA and fixed NAP on GO-A-SBA-15 at pH 7 in high concentration.

Single solute			Multi-solute			
C_0 of CFA (mg/L)	C_e of CFA (mg/L)	q_e of CFA (mg/g)	C_0 of CFA (mg/L)	C_e of CFA (mg/L)	q_e of CFA (mg/g)	q_e of NAP (mg/g)
6.345482	1.57419	19.08517		0		4.247416
10.17009	4.427071	22.97206	12.4717	8.226415	16.98113	2.162092
12.27779	6.331741	23.7842	12.86792	8.415094	17.81132	2.510956
14.67555	8.139727	26.14329	15.72642	9.735849	23.96226	2.610016
16.94762	9.783351	28.65706	17.38679	10.79245	26.37736	2.846898
20.53458	12.45182	32.33105	20.23585	12.85849	29.50943	2.579867

Table C.19 Data of adsorption isotherm for multi-solute of vary NAP and fixed CFA on GO-A-SBA-15 at pH 7 in high concentration.

Single solute			Multi-solute			
C_0 of NAP (mg/L)	C_e of NAP (mg/L)	q_e of NAP (mg/g)	C_0 of NAP (mg/L)	C_e of NAP (mg/L)	q_e of NAP (mg/g)	q_e of CFA (mg/g)
1.885579	1.540382	1.380785		0		19.08517
5.133051	4.720316	1.650939	2.569336	2.381983	0.74941	12.83019
6.610528	6.060092	2.201746	4.607603	4.356723	1.003521	12.56604
11.35462	10.41036	3.777028	6.828916	6.523122	1.223176	13.54717
11.74619	12.80804	4.247416	9.933155	9.296802	2.545411	13.84906
15.15688	14.28263	3.496989	12.95125	12.00588	3.781508	14.90566

Table C.20 Data of adsorption isotherm for multi-solute of vary CFA and fixed NAP on A-GO-A-SBA-15 at pH 7 in high concentration.

Single solute			Multi-solute			
C_0 of NAP (mg/L)	C_e of NAP (mg/L)	q_e of NAP (mg/g)	C_0 of NAP (mg/L)	C_e of NAP (mg/L)	q_e of NAP (mg/g)	q_e of CFA (mg/g)
6.345482	0.902177	21.77322		0		3.028921
10.17009	3.982326	24.75104	10.18868	4.339623	23.39623	1.249017
12.27779	5.132863	28.57972	12.75472	6.056604	26.79245	1.210255
14.67555	6.786155	31.55758	12.9717	6.207547	27.0566	1.23179
16.94762	8.536131	33.64594	16.9434	9.556604	29.54717	1.068125
20.53458	11.0209	38.05472	20.11321	11.88679	32.90566	0.770945

Table C.21 Data of adsorption isotherm for multi-solute of vary NAP and fixed CFA on A-GO-A-SBA-15 at pH 7 in high concentration.

Single solute			Multi-solute			
C_0 of NAP (mg/L)	C_e of NAP (mg/L)	q_e of NAP (mg/g)	C_0 of NAP (mg/L)	C_e of NAP (mg/L)	q_e of NAP (mg/g)	q_e of CFA (mg/g)
1.885579	1.611673	1.095623		0		21.77322
5.133051	4.649025	1.936101	2.271079	2.094494	0.706341	19.43396
7.056019	6.461306	2.378853	4.647442	4.37072	1.106888	18.75472
10.0052	9.333565	2.686528	6.94628	6.64587	1.201641	19.35849
13.18535	12.44637	2.955935	10.05375	9.726421	1.309315	19.73585
13.60806	12.85083	3.028921	13.08154	12.7639	1.270552	20.11321

C.5 Adsorption isotherm in single solute at low concentration and pH 7

Table C.22 Data of adsorption isotherm for CFA on A-GO-A-SBA-15 and NAP on GO-A-SBA-15 at pH 7 in single solute and low concentration.

CFA on A-GO-A-SBA-15			NAP on GO-A-SBA-15		
C_0 ($\mu\text{g/L}$)	C_e ($\mu\text{g/L}$)	q_e ($\mu\text{g/g}$)	C_0 ($\mu\text{g/L}$)	C_e ($\mu\text{g/L}$)	q_e ($\mu\text{g/g}$)
506.2229	14.11866	1968.417	25.65054	22.40043	13.00044
732.1667	40.31361	2767.412	46.77626	39.24191	30.13739
748.4547	42.13995	2825.259	78.53871	61.69722	67.36593
857.8767	64.57785	3173.195	85.55599	67.82811	70.91151
1229.577	92.39042	4548.748	124.0403	99.44283	98.38972
1515.662	124.7427	5563.675			

VITA

Miss Wanchalach Sathienthamanee was born on January 27, 1992 in Bangkok province. She graduated Bachelor's degree of Science majoring in Chemistry from Department of Chemistry, Faculty of Science, Chulalongkorn University in 2013. She pursued her Master's degree in International Program in Hazardous Substance and Environmental Management, Graduate School, Chulalongkorn University in 2014 and finished her Master's degree in 2015.

